Deeply implanted medical device based on a novel ultrasonic telemetry technology

THÈSE N^{O} 5730 (2013)

PRÉSENTÉE LE 17 MAI 2013

À LA FACULTÉ DES SCIENCES ET TECHNIQUES DE L'INGÉNIEUR
LABORATOIRE DE PRODUCTION MICROTECHNIQUE 2
PROGRAMME DOCTORAL EN SYSTÈMES DE PRODUCTION ET ROBOTIQUE

ÉCOLE POLYTECHNIQUE FÉDÉRALE DE LAUSANNE

POUR L'OBTENTION DU GRADE DE DOCTEUR ÈS SCIENCES

PAR

Michela PEISINO

acceptée sur proposition du jury:

Prof. H. Bleuler, président du jury
Prof. P. Ryser, directeur de thèse
Dr C. Dehollain, rapporteur
Prof. L. Pourcelot, rapporteur
Dr R. Receveur, rapporteur

ÉCOLE POLYTECHNIQUE
FÉDÉRALE DE LAUSANNE

Suisse
2013

Résumé

Les dispositifs médicaux ont connu des gros progrès depuis leur apparition. Durant les dernières décennies, on observe une tendance en direction des dispositifs implantables. Les avancées technologiques ont permis de concevoir des dispositifs à plus long terme et moins invasifs. Aujourd'hui, plusieurs dispositifs sont disponibles tant pour la détection de paramètres physiologiques que pour des actions thérapeutiques. Ils facilitent la prise en charge du patient, tout en préservant sa qualité de vie.

Le but ultime d'un implant médical serait de conjuguer à la fois des mesures et des actions dans un cycle d'asservissement, afin d'optimiser la thérapie. Un certain nombre de défis technologiques restent à surmonter pour atteindre ce but, notamment dans le domaine de l'approvisionnement en énergie et dans la miniaturisation. Le dépassement de ces limites pourrait ouvrir des horizons encore inexplorés et permettre des applications dont on ne rêve pas encore : des mesures plus fréquentes et à long terme permettraient des diagnostics plus détaillés dans des nombreux cas ; par exemple, des implants plus petits et profonds permettraient la formation d'un réseau de capteurs et actionneurs. Des populations à risque souffrant de certaines maladies pourraient être mieux suivies et prises en charge. De plus, des implants minimalement invasifs sur le corps pourraient améliorer sensiblement la recherche médicale, grâce à une observation et une compréhension plus précises des phénomènes physiologiques.

Ce travail de thèse décrit la contribution de son auteur au développement d'une nouvelle stratégie pour un dispositif médical implantable, développé dans le cadre du projet européen FP7 ULTRAsponder. L'auteur a œuvré à tous les niveaux de l'intégration du dispositif : l'établissement du cahier des charges du système, l'identification des composants commerciaux adaptés, le placement et la fixation des circuits dans le boîtier, le choix d'un matériau approprié pour l'enveloppe de protection et l'analyse de son effet sur la transmission d'énergie.

Le but du projet est la conception d'un nœud générique dans un réseau de dispositifs (*Body Sensor Network*), qui soit implantable à n'importe quel endroit, qui agisse sur le long terme et en autonomie. Les principales caractéristiques du système proposé sont la télé-alimentation et la possibilité de communiquer avec une unité de contrôle externe à travers une modulation par rétro-diffusion. A la fois l'énergie et les données échangées sont véhiculées par une onde ultrasonique plutôt que par des vecteurs plus usuels, telles que les ondes électromagnétiques. Ceci à cause de la compatibilité intrinsèque des ultrasons avec l'imagerie par résonance magnétique, et pour éviter les interférences avec les émetteurs d'ondes électromagnétiques présents dans l'environnement du patient, tels que téléphones portables ou instruments électroniques. Aussi, les ultrasons ont démontré une meilleure efficacité que les émissions radiofréquences ou l'induction magnétique dans le cas de dispositifs petits par rapport à la profondeur d'implantation.

Les exigences de l'utilisateur et les contraintes techniques liées à son application ont été évaluées et ont mené à la définition du cahier des charges du dispositif. Des composants commerciaux, ainsi que des technologies émergentes, ont été identifiés pour mettre en œuvre le concept.

L'intérêt de ce travail consiste dans l'intégration de différentes technologies, composants et approches scientifiques dans un dispositif novateur. En particulier, le défi spécifique de la transmission d'ultrasons à travers un boîtier médical standard, composé de titane, a été abordé. L'excellente biocompatibilité du titane en fait le matériau de référence pour la protection des dispositifs médicaux. Néanmoins, il interfère lourdement avec la propagation d'ondes mécaniques telles que les ultrasons. La combinaison d'une

transmission à ultrasons et d'un boîtier en titane constitue un point essentiel dans l'industrialisation et commercialisation du dispositif développé.

Des démonstrateurs du dispositif implantable et de son unité de contrôle ont étés fabriqués, en se focalisant sur la transmission d'énergie, le traitement du signal et la communication des données. Un boîtier commercial a été exploité, pour prouver la compatibilité du système avec des matériaux et procédés industriels.

Le concept de transmission d'énergie et de données entre le dispositif et son unité de contrôle, ainsi que l'interface utilisateur, ont été validés par des essais *in vitro*. Des tests *in vivo* pratiqués sur des cochons ont ensuite permis d'évaluer le système en conditions réelles. Sa fonctionnalité a été prouvée, bien qu'à une distance de transmission réduite.

Le travail futur consiste à optimiser la transmission acoustique, à intégrer le capteur proprement dit, et à miniaturiser les dispositifs.

Mots clés : Dispositifs médicaux implantés, Génie biomédical, Réseau de capteurs, Ultrasons, Modulation par diffusion, Titane, Télémétrie, Récupération d'énergie.

Riassunto

I dispositivi medici si sono evoluti considerevolmente rispetto ai loro albori. Negli ultimi decenni si è potuta osservare una chiara tendenza verso i sistemi impiantabili. I progressi tecnologici hanno permesso lo sviluppo di dispositivi a più lunga durata e meno invasivi per il paziente. Al giorno d'oggi, disponiamo di una moltitudine di dispositivi utilizzati sia per il monitoraggio di parametri fisiologici che a scopo terapeutico. Essi permettono una migliore gestione della cura, pur preservando la qualità di vita del paziente.

L'obiettivo a lungo termine di un tale impianto medico è il connubio tra sensori e attuatori in un ciclo di retroazione, in modo da ottimizzare la terapia. Per raggiungere tale scopo, alcune sfide tecnologiche devono essere affrontate, in particolare nell'ambito dell'alimentazione e della miniaturizzazione del sistema. Dare risposta a tali problemi apre la strada ad applicazioni ancora inesplorate dei sistemi medici impiantabili: la possibilità di misurare frequentemente e a lungo termine dei parametri fisiologici permetterebbe in molti casi diagnosi più precise; dispositivi più piccoli e impiantati più in profondità sarebbero la base per una rete di sensori ed attuatori. Si potrebbero analizzare e trattare più efficacemente le popolazioni a rischio per una certa malattia. Inoltre, degli impianti a basso impatto sul corpo (minimamente invasivi) potrebbero migliorare sensibilmente la ricerca medica attraverso una più precisa osservazione e la comprensione di specifici fenomeni fisiologici.

Questa tesi descrive il contributo dell'autrice allo sviluppo di una nuova strategia per un dispositivo medico impiantabile, sviluppato nell'ambito del progetto europeo FP7 ULTRAsponder. L'autrice si è concentrata sugli aspetti di integrazione nella progettazione e nella produzione del sistema proposto: in particolare, si è occupata della definizione delle specifiche tecniche, della selezione di componenti commerciali idonei, del loro posizionamento sul circuito stampato, della scelta di un materiale adatto per l'involucro dell'impianto e dell'analisi del suo effetto sulla trasmissione di energia.

Lo scopo del progetto è lo sviluppo di un generico nodo in una rete di dispositivi (Body Sensor Network), che sia impiantabile ovunque, che agisca a lungo termine e in autonomia. Le caratteristiche principali del sistema proposto sono l'alimentazione a distanza e la capacità di comunicare con una unità di controllo esterna attraverso una modulazione a radiazione di ritorno (backscattering). Sia l'energia che i dati scambiati sono trasmessi tramite onde ultrasoniche, anziché tramite le più comuni onde elettromagnetiche. La ragione risiede nella compatibilità intrinseca degli ultrasuoni con le tecniche di risonanza magnetica e per evitare interferenze con gli emettitori di onde elettromagnetiche nell'ambiente del paziente, come telefoni cellulari o strumenti elettronici. Inoltre, nel caso di dispositivi di piccole dimensioni rispetto alla profondità di impianto, gli ultrasuoni si sono dimostrati più efficienti delle tecniche a radiofrequenza o dell'induzione magnetica.

Le esigenze del paziente ed i vincoli tecnici alla loro applicazione sono stati valutati e ciò ha portato alla definizione delle specifiche di un dispositivo di nuova generazione. Adeguati componenti commerciali e tecnologie emergenti sono stati individuati per permettere la realizzazione di un prototipo che rispondesse a tali caratteristiche e servisse da verifica del concetto.

L'originalità di questo lavoro consiste nell'integrazione di diverse tecnologie, componenti e approcci scientifici in un dispositivo innovativo. In particolare, è stato affrontato il problema specifico della trasmissione degli ultrasuoni attraverso un involucro di titanio omologato per impianti medici: la biocompatibilità del titanio lo rende il materiale di riferimento per la protezione di dispositivi impiantabili.

Tuttavia, esso interferisce pesantemente con la propagazione di onde meccaniche, come gli ultrasuoni. La combinazione della trasmissione tramite ultrasuoni e di un rivestimento in titanio è un punto fondamentale per l'industrializzazione e la commercializzazione del dispositivo sviluppato.

Si sono realizzati prototipi dell'impianto e della sua unità di controllo, con particolare attenzione alla trasmissione di energia, elaborazione dei segnali e comunicazione dei dati. Un involucro commerciale è stato sfruttato per dimostrare la compatibilità del sistema proposto con materiali e processi industriali.

In una prima fase, la trasmissione di energia e la comunicazione tra l'impianto e l'unità di controllo sono stati dimostrati tramite test *in vitro*. Successivamente, test *in vivo*, eseguiti su maiali, sono stati utilizzati per valutare il sistema in condizioni reali. La sua funzionalità è stata dimostrata, anche se ad una distanza di trasmissione ridotta.

Il lavoro futuro sull'impianto comprende l'ottimizzazione della trasmissione acustica, l'integrazione del sensore vero e proprio nell'impianto e la miniaturizzazione del dispositivo.

Parole chiave: Impianto medico, Ingegneria biomedica, Body Sensor Network, Ultrasuoni, Backscattering, Titanio, Alimentazione a distanza, Energy Harvesting.

Zusammenfassung

Die Medizintechnik hat einen langen Weg zurückgelegt hin zu immer häufiger genutzten und komplexeren implantierbaren Systemen. Dank des technologischen Fortschritt verfügt man heute über die notwendigen Kenntnisse und Technologien für die Entwicklung und Herstellung beständiger und weniger invasiven Implantaten. Mehrere implantierbare Geräte für die Messung physiologischer Größen sowie zur therapeutischen Behandlung sind heute bereits im Handel erhaältlich. Sie vereinfachen die Überwachung des Therapieverlaufs und erhöhen so die Lebensqualität des Patienten. Ein ideales Implantat würde sowohl Sensoren als auch Aktoren in einer Regelschleife integrieren, um eine optimale Therapie zu gewährleisten. Um dieses Ziel zu erreichen, müssen einige technische Herausforderungen bewältigt werden – insbesondere hinsichtlich Stromversorgung und Miniaturisierung.

Die Lösung dieser Probleme würde Anwendungen ermöglichen, die heute in dieser Form noch nicht realisierbar sind: bessere Diagnosen könnten für jene Behandlungsfälle erzielt werden, für die eine kontinuierliche, langfristige Überwachung von physiologischen Größen unter realen Bedingungen erforderlich ist. Die Qualität der dazu nötigen Messungen könnte durch den Einsatz eines Netzwerks aus mehreren kleineren und tiefer implantierten Geräten verbessert werden. Außer zu Therapiezwecken könnten diese Implantate auch zur Überwachung von Risikopatienten eingesetzt werden. Darüber hinaus würden minimalinvasive Implantate die medizinische Forschung voranbringen, indem physiologische Mechanismen genauer beobachtet werden könnten.

Diese Arbeit beschreibt den Beitrag der Autorin zur Entwicklung eines neuartigen Körpersensornetzwerkkonzeptes, welches innerhalb des Europäischen FP7-Projektes ULTRAsponder vorgeschlagen wurde. Die Autorin hat sich auf die Aspekte des Entwurfs und der Fertigung dieser neuen implantierbaren Plattform konzentriert: Festlegung der technischen Spezifikationen, Auswahl der kommerziellen Bauelemente, Einpassung der Leiterplatte in das Gehäuse, Wahl eines geeigneten Gehäusematerials und Beurteilung dessen Einflusses auf die Energieübertragung.

Das Ziel war einen generischen und autonom arbeitenden Netzwerkknoten für ein Körpersensornetzwerk zu entwickeln, welcher vorbehaltslos implantiert und langfristig genutzt werden kann. Hauptmerkmale des vorgeschlagenen Systems sind die drahtlose Energieversorung des implantierten Gerätes und die bidirektionale Kommunikation über den Energieübertragungskanals durch Modulierung der rückgestreuten Wellen (*backscatter modulation*). Für die Übertragung wurden Ultraschall- anstatt elektromagnetischer Wellen gewählt, da diese die Kombatibilität mit wichtigen medizinischen bildgebenden Verfahren, wie z.B. de Kernspintomographie, sicherstellen und Interferenzen mit anderen elektronischen Geräten, wie z.B. Mobiltelefonen, vermieden werden. Ultraschall als Übertragungsmedium erwies sich als effizienter als Radiowellen oder magnetische Induktion für den Fall, dass die Implantate tief im Körper sitzen oder klein sind.

Die Nutzungsszenarien und technischen Randbedingungen für ein optimales Implantat wurden analysiert, um darauf aufbauend die Eigenschaften unseres neuen Systems festzulegen. Daran schloss sich die Auswahl passender kommerziell erhältlicher Bauelemente sowie neuer Technologien an, die die Entwicklung des Gerätes ermöglichten.

Die Neuheit dieser Arbeit liegt in der Integration verschiedener Technologien, Komponenten und wissenschaftlicher Ansätze in einem neuen, viel versprechenden implantierbaren Gerät. Ein Augenmerk lag insbesondere auf der Etablierung einer zuverlässigen Ultraschallverbindung durch ein medizintechnisch

konformes Titangehäuse. Titan ist das Standardmaterial für biokompatible Gehäuse in der Medizintechnik, wirkt sich allerdings negativ auf die Übertragung von Ultraschallwellen aus. Der im Rahmen dieser Doktorarbeit erbrachte Nachweis der Realisierbarkeit einer sicheren Ultraschallübertragung zu einem in Titan gekapselten Implantat ist die Voraussetzung für die medizintechnische Nutzung dieser neuen Technologie.

Prototypen des Implantates und des externen Steuergerät wurden wurden hergestellt, um die Energieübertragung, Signalverarbeitung und Ultraschallrückstreuung zu untersuchen. Ein Titanstandardgehäuse für medizinische Implantate wurde genutzt, um die mögliche Kommerzialisierung dieser neuen Technologie zu demonstrieren.

Die Energieübertragung und Kommunikation zwischen Implantat und Steuergerät wurde durch automatisierte *in-vitro* Tests validiert. Die Funktionalität unter realen Bedingungen wurde durch *in-vivo* Tests an Schweinen nachgewiesen. Allerdings konnten nur kürzere Übertragunslängen realisiert werden.

Weiterführende Arbeiten könnten sich auf die Optimierung der Ultraschallübertragung, die Integration eines Sensors sowie die Miniaturisierung der Elektronik konzentrieren.

Stichpunkte: Medizinisches Implantat, Medizintechnik, Körpersensornetzwerk, Ultraschall, Rückstreumodulierung, Titan, Fernsteuerung, Drahtlose Energieversorgung.

Resumo

Medicinaj aparatoj multe evoluis ekde ilia naskiĝo. Dum la lastaj jardekoj, la tendenco estis al enplantitaj aparatoj – *Implanted Medical Devices (IMDs)*. La teknologia evoluado havigis la necesajn ilojn por longa daŭro, malpli invasivaj aparatoj. Pluraj aranĝaĵoj por malkaŝo kaj ekzekuto estas komerce haveblaj kaj plibonigas terapian demarŝon, konservante la kvalito de vivo de la paciento.

Ideala enplantaĵo ebligus ambaŭ malkaŝadon kaj ekzekutadon en fermita maŝo, tiel ke oni atingu optimuman terapion. Por atingi tiun celon, pluraj defioj estas, ĉefe pri energia nutrado kaj miniaturigo. Solvante ĉi tiuj temoj devus malfermi novajn eblecojn kaj permesi aplikojn kiuj ankoraŭ ne eblas: oni povus atingi plej bonan diagnozon kien ajn estas bezonata kontinua, longtempa monitorado de fiziologiaj parametroj en reala vivo kondiĉoj. Ekzemple, pli malgrandaj kaj pli profunde enplantitaj aranĝaĵoj permesus disfaldi plurajn aparatojn en la korpo, sukcesante reton de sensiloj kaj agiloj – *Body Sensor Networks (BSNs)*. Apud terapio, oni povus uzi enplantaĵoj pro diagnozo en homoj riskantaj malsanojn. Krome, minimume invasivaj enplantaĵoj povus multe plibonigi medicinan esploron, pro tio ke ili permesas pli proksiman observadon, tiel helpante kompreni fiziologiajn mekanismojn.

Ĉi tiu tezo priskribas la aŭtorinan kontribuon al la disvolviĝo de nova IMD koncepto, proponita ene de la Eŭropa FP7 projekto ULTRAsponder. La aŭtorino plej laboris pri la integriĝaj aspektoj en la dezajno kaj la fabrikado de la nova enplantinda mekanismo: ŝi difinis la teknikajn specifojn; ŝi pritaksis taŭgajn komercajn komponantojn kaj la geometrian lokigon de la stampita cirkvito ene de la ŝelo; ŝi elektis taŭgan uja materialon, kaj pritaksis ĝian efikon sur la energia transdono.

La celo estas ĝenerala reta nodo, kiu povas esti enplantita kien ajn, kiu longe daŭras, kaj kiu povas funkcii aŭtonome. Gravaj trajtoj de la sistemo proponita inkluzivas foran energian donadon a la enplantita mekanismo kaj komunikadon kun ekstera komandilo pere de reflekta modulado - *Backscattering*. Por ambaŭ energio kaj transporto de datumoj, oni preferas ultrasonajn ol elektromagnetaj ondoj, ĉar ultrasonoj estas kongruaj kun magneta resono kaj ne malhelpas elektromagnetajn elsendilojn kiel poŝtelefonoj kaj elektronika ekipaĵo. Ĝi ankaŭ pli efikas ol radiofrekvencaj ondoj aŭ magneta indukto kiam atingante profundan enplantaĵon kaj kiam uzante malgrandajn sentilojn.

La uzantaj postuloj kaj la teknikaj limigoj al optimuma enplantaĵo estis taksitaj kaj la trajtoj de la sistemo estis difinita. Taŭgaj komercaj komponantoj kaj aperantaj teknologioj estis identigitaj, kiu permesis disvolviĝi la aparaton.

La originaleco de tiu verko trovas en la integriĝo de malsamaj teknologioj, komponantoj kaj sciencaj aliroj en nova, promesanta IMD. Krom tio, la defio de sukcese uzi ultrasonoj tra ŝelo farita de norma medicina titano estis studita. Titanaj ŝeloj estas la nuna normo por aparatoj kongruaj kun la viva korpo, sed ili forte influas al la ultrasona transporto. Sukcesa integriĝo de ultrasona transdono kun titanaj ŝeloj certigas ke oni povas fabriki la proponitan aparaton industrie kaj vendi ĝin.

Facsimilaj enplantaĵo kaj ekstera komandilo estis fabrikitaj, montrante la transdonon de energio, la signalan traktadon, kaj la reflektan moduladon. Komerce havebla, sufiĉe granda ŝelo estis uzita, pro pruvi la industrian uzeblecon de la aparato.

In vitro esplorado validigis la transdonon de energio kaj la komunikadon inter komandilo kaj enplantaĵo, tiel kiel la uzantinterfacon. Taksado en realaj kondiĉoj estis atingita pere de *in viva* provojn sur porkoj. Funkcio estis pruvita, tamen je multe pli malgranda distanco ol oni intencis.

Estonteca laboro inkludas optimumigo de la ultrasona transporto, integriĝo de la sensila cirkvito, kaj miniaturigo de la rezultanta aparato.

Gravaj vortoj: Medicina aparato, Biomedicina inĝenierio, Reto de sensiloj, Ultrasono, Reflekta modulado, Titano, Defora energia transdono, Rikolto de Energio.

Abstract

Medical devices have gone a long way since their beginning. In the last decades, the trend has been towards Implanted Medical Devices (IMDs). The technology evolution has provided the necessary tools for longer-term, less invasive devices. Several devices for sensing and actuation are commercially available and ease therapy management, while preserving the patient's life quality.

An ideal implant would integrate both sensing and actuating possibilities in a feedback loop, thus achieving optimum therapy. To reach this goal, several challenges remain, in particular concerning power supply and miniaturization. Solving these issues would open new possibilities and allow applications which are not possible yet: better diagnosis could be achieved wherever a continuous, long-term monitoring of physiological parameters in real life conditions is required. For instance, smaller and deeper implanted devices would allow deploying several IMDs in the body, achieving a Body Sensor Network (BSN). Beside therapy, implants could be used for diagnosis in populations at risk. Furthermore, minimal invasive implants would greatly improve medical research, by allowing closer observation, thus helping to understand physiological mechanisms.

This thesis describes the author's contribution to the development of a novel IMD concept, proposed within the European FP7 project ULTRAsponder. The author focused on the integration aspects in the design and manufacturing process of the novel implantable device platform: definition of the technical specifications, assessment of appropriate commercial components, geometrical placement of the Printed Circuit Boards (PCBs) inside the casing, choice of a suitable housing material, and assessment of its effect on the energy transmission.

The target is a generic BSN node, which can be implanted wherever needed on a long-term basis and which can operate autonomously. Key features of the proposed system include remote powering of the implanted device and communication with an external Control Unit (CU) by backscattering modulation. For both energy and data transfer, an ultrasonic carrier is used instead of Electromagnetic (EM) waves because it is compatible with Magnetic Resonance Imaging (MRI) and does not interfere with EM emitters like mobile phones and electronic equipment. It also proved to be more efficient than the use of Radio Frequency (RF) waves or magnetic induction to reach deep implants and when using small transducers.

The user requirements and the technical constraints towards an optimal implant were evaluated and the characteristics of the proposed system were defined. Appropriate commercial components and emerging technologies were identified, which allowed the development of the device.

The originality of this work lies in the integration of different technologies, components and scientific approaches into a novel, promising IMD. In particular, the challenge of achieving an ultrasonic link through a standard medical grade titanium casing is addressed. Titanium casings are the golden standard for biocompatible device housing, but they have a strong influence on ultrasonic energy transfer. Successful integration of ultrasonic transmission and titanium casing ensures the ability of the proposed device to be industrially exploited and commercialized.

A demonstrator implant and an external CU have been manufactured, focusing on energy transfer, signal treatment, and backscattering. A commercial, rather large housing was used, in order to demonstrate the industrial viability of the device.

Abstract

In vitro tests validated the energy transfer and the communication between the CU and the Transponder (TR), as well as the user interface. Assessment in real conditions is achieved by *in vivo* tests on pigs. Functionality was proved, however at a much smaller distance than intended.

Future work includes optimization of the ultrasonic transfer, integration of the sensing circuitry, and miniaturization of the resulting device.

Keywords: Implanted Medical Device, Biomedical Engineering, Body Sensor Network, Ultrasound, Backscattering modulation, Titanium, Telemetry, Energy Harvesting.

Acknowledgements

Achieving a PhD degree is a journey requiring not only personal conviction, but also many external factors to fit. I would like to take the opportunity to acknowledge some people who made this journey possible, safe, and inspiring.

I would like to thank my thesis director, Prof. Peter Ryser, for giving me the opportunity to work in the Laboratoire de Production Microtechnique (LPM). I am very grateful to my supervisor, Eric Meurville, who acted by all means as a thesis co-director, by having provided a stable and enriching work environment, both in terms of fund harvesting and guidance. His precise evaluation of my work and skills are a precious help for my future career. Thanks to my thesis jury for carefully evaluating my research work and asking many good questions: Prof. Léandre Pourcelot (Université de Tours), Dr Rogier Receveur (Medtronic Bakken Research Center), MER Dr Catherine Dehollain (EPFL), as well as the jury president, Prof. Hannes Bleuer (EPFL). It was a honor discussing with you my research results.

Good research is done in a team. I had the opportunity to be part of a European consortium, which allowed me to experience very different work styles, both in industry and academia. I am particularly grateful to Dr Jean Martial Mari for his extensive cooperation on a publication and for all his support. The research described in this thesis was funded by the European Commission within the project Ultrasponder (grant agreement number 224009). I was lucky to be part of the LPM laboratory, with its good rhythm of small social gatherings. Among the many colleagues encountered during these years, I would like to remember and thank Nathalie, as my only fellow PhD girl; Léandre, for introducing me to LabVIEW; Frédéric and Karim, who politely heard all my stories during lunch; Louis, Davide, Romain, Christophe B., Christophe C., and Simon, who shared the office and their best practices with me; and finally Matteo, who was my office mate, lunch fellow, Italian grammar guide... and a friend. I also would like to acknowledge Fragkiskos Koufogiannis, a brilliant student I had the chance to welcome for an internship. All the best for his own PhD degree! The quality of my thesis manuscript improved significantly due to the proofreading and extensive feedback of Marco Peisino and Dr Torsten Mähne. They, together with my supervisors, helped me clarify the content. Thanks as well to Maurizio Peisino for some last-minute image editing. On the administrative side, I am grateful to Karine Genoud, Morgane Katz, and Clémence Birbaum from LPM; Claire Chabanel and Corinne Lebet from the Ecole Doctorale de Production et Robotique (EDPR); Marie Halm from the Ecole Doctorale de Microsystèmes et Microélectronique (EDMI), who started my application file at EPFL and became a friend in the last years. I would also like to express my unconditioned gratitude to the EDOC team and to the ACIDE Association of Researcher at EPFL. Their efforts in representing PhD students, their collaborative attitude, and their sincere listening are the most valuable tool for making the best out of the PhD experience. It has been an honor collaborating with them. A very particular thought to Wajd Zimmermann, who devoted to ACIDE her energy far beyond office hours: my warmest thank for your work and friendship.

Thesis or not, growing from twenty-five to thirty is another very significant journey. Many more people as I could possibly remember were present along the path, and deserve my thanks.

To all my friends back in Italy and around the world, which I too often forgot to stay in touch with. To the scuba diving team, and particularly Pouli, Philippe, Murielle, and Torsten: making bubbles with you was intense in many ways. To my fellow members of ACIDE, and particularly Sylvie, Maya,

Tobias, Nicolas, Grégoire, Florent, Sébastien, Ludger, and Torsten: thanks for devoting time to the EPFL community. To my engaged Swiss friends Adrien, Arnaud, Benoît, Charlotte, Lara, Samuel, and the whole Jeunesse Socialiste: thank you for making Switzerland an even better place to live and work. To my Italian friends at EPFL, who didn't let me forget about how speaking, cooking, and behaving got to be. Particular thanks to Matteo, Cristina, Ivan, Ludovica, Camilla, Andrea, Jacopo, Massimo, and Anna. To my flatmates Ben, "little" Andrea, Michele, and Lucia! Thanks for the food, the laughters, and most importantly for having rounded the sometimes edgy cleaning maniac I seem to be. I'll miss our big flat and our Sunday breakfasts. You are great! Relaxed thanks to my fellow sauna-likers: to Torsten, who introduced me to this world; to Pam, Vera, Anja, Carmen, who shared the Wednesday routine. It was a nice moment to balance work and regain a clear view. Thanks to Anna, Enrico, Elisa, and Mattia for all the nice evenings spent questioning around God and Society, with lots of humor. Many other friends shaped my stay here in Lausanne, both inside and outside EPFL. In order of appearance, thanks to Estelle & Sylvain, Chiara & Nicolas, Anja & Dominique and the beautiful Florentin & Valentin, Camille & Sébastien & little Mathias, Elena, Neil, Miloš, Virginie, Vincent, Aristeidis & Yadira & little Nikolaos, Sébastien & Gaëlle, Carly & Michael, Vlasta, Yüksel & Selma, and all the others I keep in my heart.

I am mostly indebted to my several, wonderful "families". First of all, of course, to my parents Lucia and Marco: your moral integrity, welcoming attitude, and curiosity towards the world shaped me. One thank is not enough... Thanks for supporting and encouraging so many of my choices, even when it meant to have so little from me; thanks for your enthusiastic interest in my studies, my friends, and my discoveries; and thanks for every trip you had to make in Europe to pick me up! I'm proud to be your daughter. To my brother Maurizio, who best got to know the dark side of this engineer... Thanks for loving your little sister beyond her "caterpillar" behavior and for teasing her down when she takes life too seriously. To my strong grandmothers Nonna Sabina and Nonna Caterina and in memory of my lovely grandfathers Nonno Piero and Nonno Francesco. Everything has a root. I'll never know what I would be without you.

Beside my "real" family, I would like to acknowledge the importance of family Schneider and family Demond: they welcomed me as a teenager during my exchange year in Germany and contributed to make me what I am. I am very grateful to have had a privileged insight into different family styles. Thanks for being in touch with me through so many years and kilometers, thanks for giving me German brothers and sisters! Since some years now, I have the opportunity to increasingly know family Mähne. Thank you – especially Gabi and Manfred – for the warm welcome and care you reserve to me every single time. It is a privilege for me to share with you some moments.

Last, but in no way least, multiple acknowledgments and my whole gratitude go to Torsten Mähne. Thanks for being part of so many aspects in my Swiss experience, for your technical help and advices in all possible domains. Most importantly though, thanks for being my caring boyfriend. You hold the one end of the steering wheel towards our future. Let's drive!

Lausanne, 25/04/2013

Michela Peisino

Contents

Résumé i

Riassunto iii

Zusammenfassung v

Resumo vii

Abstract ix

Acknowledgements xi

1 Introduction 1
- 1.1 Motivation . . . 1
- 1.2 Scope of the work . . . 2
- 1.3 Thesis outline . . . 3

2 State of the art 5
- 2.1 Introduction . . . 5
- 2.2 Commercial Medical Devices . . . 5
- 2.3 Device packaging . . . 7
- 2.4 Minimally invasive implantation . . . 9
- 2.5 Power supply . . . 10
  - 2.5.1 Energy harvesting from human body . . . 10
  - 2.5.2 Electromagnetic waves . . . 11
  - 2.5.3 Mechanical waves . . . 13
- 2.6 Data communication . . . 14
- 2.7 Applications of Ultrasound . . . 15
- 2.8 Conclusion . . . 16

3 Towards a new generation of IMDs 19
- 3.1 Introduction . . . 19
- 3.2 Implant requirements . . . 20
  - 3.2.1 Body Sensor Network . . . 20
  - 3.2.2 Implantability . . . 20
  - 3.2.3 Deep Implantation . . . 21
  - 3.2.4 Size . . . 21
  - 3.2.5 Long-Term Implantation . . . 22
  - 3.2.6 Biocompatibility . . . 23
  - 3.2.7 Autonomy . . . 24

3.2.8 Connection to a Control Unit . . . 24
3.2.9 Ultra-low power consumption . . . 25
3.2.10 Cost . . . 26
3.3 Gap between the state of the art and the ideal implant . . . 27
3.3.1 Energy and communication carrier . . . 27
3.3.1.1 Carrier type . . . 27
3.3.1.2 Carrier frequency range . . . 29
3.3.2 Ultra-low power consumption . . . 29
3.3.3 Casing . . . 29
3.3.4 Choice of electronic components . . . 30
3.4 Scientific and Technological impact . . . 31
3.5 Conclusion . . . 32

4 Physics of Ultrasound 35
4.1 Introduction . . . 35
4.2 Definition . . . 35
4.3 Mathematical description . . . 35
4.3.1 Ultrasonic wave in fluids . . . 36
4.3.2 Ultrasonic wave in solids . . . 38
4.3.3 Wave energy and intensity . . . 41
4.3.4 Acoustical Impedance . . . 42
4.3.5 Piezoelectric materials . . . 44
4.3.5.1 Composites and multiple elements . . . 45
4.3.5.2 Network notation . . . 46
4.3.5.3 Reflection and transmission . . . 48
4.3.6 Attenuation . . . 50
4.4 Biological effects . . . 50
4.4.1 Thermal effects . . . 50
4.4.2 Cavitation . . . 51
4.4.3 Radiation force . . . 52
4.5 System Modeling . . . 52
4.5.1 Acoustic propagation . . . 52
4.5.2 Transducers . . . 54
4.5.2.1 Impedance matching layers . . . 55
4.6 Simulations and parameters chosen . . . 56
4.6.1 Working frequency . . . 56
4.6.2 Location . . . 57
4.6.3 Titanium thickness . . . 57
4.6.3.1 Characteristics of the Transponder materials . . . 58
4.6.3.2 Results . . . 59
4.7 Conclusion . . . 60

5 ULTRAsponder project 63
5.1 Introduction . . . 63
5.2 Functional Demonstrator . . . 63
5.2.1 Application . . . 64

5.2.2 Carrier choice and implantation location . . . 66
5.3 Algorithm . . . 66
5.3.1 Backscattering . . . 68
5.3.2 Connection to the Analog-to-Digital Converter . . . 69
5.3.3 Graphical User Interface . . . 69
5.4 Materials and components . . . 69
5.4.1 Casing . . . 71
5.4.2 Transducers . . . 73
5.4.2.1 Transponder transducer . . . 73
5.4.2.2 Control Unit transducer . . . 74
5.4.3 Power storage . . . 74
5.4.4 Digital Signal Processor . . . 75
5.4.5 Memory . . . 75
5.4.6 Sensor . . . 76
5.4.7 Backscattering modulation switch . . . 76
5.4.7.1 Subcarrier generator . . . 76
5.4.8 Phantom material . . . 77
5.5 Means of verification . . . 77
5.6 Conclusion . . . 78

6 Demonstrators produced **81**
6.1 Introduction . . . 81
6.2 Testbed . . . 81
6.3 Housing . . . 81
6.3.1 Aluminium casing for electronics development . . . 81
6.3.2 Titanium casing for *in vivo* measurements . . . 82
6.3.2.1 Casing thinning . . . 82
6.3.2.2 Connection to electronics . . . 83
6.3.2.3 Sealing method . . . 83
6.4 Characterization of the TR transducer array . . . 84
6.4.1 Method . . . 84
6.4.2 Results . . . 86
6.5 First proof of concept . . . 88
6.5.1 Electronics description . . . 88
6.5.1.1 CU baseboard . . . 88
6.5.1.2 CU receiver and filter . . . 90
6.5.1.3 TR baseboard . . . 90
6.5.2 Test performed . . . 91
6.5.2.1 Functional test of the CU baseboard . . . 91
6.5.2.2 Functional test of the TR baseboard . . . 91
6.5.2.3 *In vitro* energization . . . 92
6.5.2.4 Functional test of the CU receiver . . . 92
6.5.2.5 *In vitro* backscattering . . . 92
6.5.3 Results . . . 92
6.5.3.1 Functional test of the CU baseboard . . . 93
6.5.3.2 Functional test of the TR baseboard . . . 94

6.5.3.3 *In vitro* energization . . . 95
6.5.3.4 Misalignment . . . 96
6.5.3.5 Functional test of the CU receiver . . . 96
6.5.3.6 *In vitro* backscattering . . . 98
6.5.3.7 Misalignment . . . 98
6.6 Final electronics . . . 99
6.6.1 Electronics description . . . 99
6.6.2 Tests performed . . . 101
6.6.2.1 *In vitro* test . . . 101
6.6.2.2 *In vivo* test . . . 101
6.6.3 Results . . . 102
6.7 Discussion . . . 107
6.7.1 Energization simulation and *in vitro* assessment . . . 107
6.7.2 *In vivo* energization and communication . . . 107
6.8 Conclusion . . . 107

7 Conclusions **109**

Bibliography **111**

Curriculum Vitæ **121**

List of Figures

1.1 Author's contribution to the system. . . . 3

2.1 Types and examples of medical devices. . . . 6
2.2 Evolution in pacemaker devices. . . . 6
2.3 Rendering of a generic active sensor IMD. . . . 8
2.4 Power supply methods in IMDs. . . . 10
2.5 Spectrum of electromagnetic waves. . . . 11
2.6 Piezocomposite structure 1-3. . . . 14
2.7 Concept of Backscattering with RF waves. . . . 15

3.1 Concept of Body Sensor Network. . . . 21
3.2 Thin electronics concept. . . . 22
3.3 Example of an algorithm for an implanted sensor device. . . . 25
3.4 Chronograph of a possible sensor. . . . 26

4.1 Effect of a mechanical wave on a fluid element. . . . 37
4.2 Effect of a mechanical wave on a solid element 39
4.3 Deformation of a 2-dimension shape. . . . 40
4.4 Set of stresses on an element of infinitesimal volume. . . . 41
4.5 Schematics and equation of an acoustic transmission line. . . . 46
4.6 Schematics and equations for cascading of two quadrupoles. . . . 46
4.7 Schematic and equation of a piezoelectric element. . . . 47
4.8 Equivalent KLM model of a piezoelectric element. . . . 47
4.9 Wave propagation between two materials of different acoustic impedance. . . . 49
4.10 Schematics of the system to be modeled. . . . 53
4.11 Generic transducer layers and acoustic power at different locations. . . . 54
4.12 Wave propagation between three materials of different acoustic impedance. . . . 55
4.13 Transducer structure taken into account in the simulation. . . . 59
4.14 Simulation: Sweep titanium thickness 61
4.15 Simulation: Sweep piezo thickness 62

5.1 Overview of the proposed system. . . . 64
5.2 Proposed application: heart impedance measurement. . . . 65
5.3 Compression of a Electrocardiography signal 67
5.4 Message produced by the microprocessor 68
5.5 Conversion by the custom ADC of a Direct Current (DC) voltage. . . . 69
5.6 Concept of the transponder electronics. . . . 70
5.7 Demonstrator housing (Kinetra® casing). . . . 71
5.8 Assembly of the transponder device. . . . 72
5.9 Thinning result on a titanium sheet. . . . 73

5.10 Transducers exploited in the final demonstrator (not to scale). 74
5.11 Resulting signal of a subcarrier at 100 kHz and a modulating signal at 5 kHz. 77
5.12 Phantom material mimicking a soft tissue and ribs. 78

6.1 Testbed developed for the demonstrator assessment. 82
6.2 Aluminium demonstrator casing. 83
6.3 Geometrical plans for the thinning of a region on the Kinetra® housing. 84
6.4 Connection strategy in the Kinetra® housing. 85
6.5 Kinetra® casing with modified leads. 86
6.6 Frequency spectrum of a single flat array element in emission-reception. 87
6.7 Directivity of the TR transducer in emission. 87
6.8 Directivity of the TR transducer in reception. 88
6.9 Block diagram of the first demonstrator. 89
6.10 First system demonstrator. 89
6.11 Detail of CU_base. 90
6.12 Functional test of CU_base. 93
6.13 Crosstalk on CU element #4 dedicated to energization. 93
6.14 Crosstalk on CU element #8 dedicated to backscattering. 94
6.15 Linear increase in power consumed with respect to the amount of elements. 94
6.16 Functional test of TRANS. 95
6.17 *In vitro* energization. 96
6.18 Displacement of TR from optimal point. 97
6.19 Effect of the amount of CU elements emitting on the rectified voltage in the TR. 97
6.20 Setup schematics for the functional test of CU_RX. 97
6.21 Modulated signal at the output of CU_RX. 98
6.22 Effect of side displacement on data communication. 99
6.23 Final CU and TR electronics. 100
6.24 *In vivo* test of the final demonstrator. 102
6.25 Acoustic pulse received on transducer element. 102
6.26 Treatment of the incoming voltage into a DC level. 103
6.27 Battery charging using different sets of piezoelectric elements. 104
6.28 Backscattering of a fixed message. 105
6.29 Backscattering and demodulation of a message. 106
6.30 Energy harvesting *in vivo* at subcutaneous distance. 106
6.31 Backscattered acoustic signal from subcutaneous implant. 107

List of Tables

2.1 State of the art of technologies and materials for IMDs. 17

3.1 Attenuation comparison of ultrasound, RF, and magnetic induction. 27
3.2 Technical challenges towards a new generation of IMDs. 33

4.1 Acoustic characteristics of various materials. 44
4.2 Parameters of a piezoelectric material. 48
4.3 Characteristics of the piezoelectric layer. 58

5.1 Command summary for the Graphical User Interface. 70
5.2 Main characteristics of the icyflex microprocessor. 76

6.1 Electrical impedance, sensitivity, and central frequency of TR transducer. 86
6.2 Voltage levels on TRANS when supplying a sinusoidal wave at 1 MHz. 95
6.3 Efficiency of the CU_RX. 98

List of Acronyms

AC Alternating Current

ADC Analog-to-Digital Converter

ASTM American Society for Testing and Materials

BHTE BioHeat Transfer Equation

BSN Body Sensor Network

CAD Computer Aided Design

CHF Congestive Heart Failure

CMOS Complementary MOS

COM COMmunication port

CRT Cardiac Resynchronization Therapy

CSEM Centre Suisse d'Électronique et de Microtechnique SA

CU Control Unit

DC Direct Current

DPCM Differential Pulse-Code Modulation

DSP Digital Signal Processing

ECG Electrocardiography

EEPROM Electrically Erasable Programmable Read-Only Memory

EM Electromagnetic

FDA Food and Drug Administration

FES Functional Electrical Stimulation

FM Frequency Modulation

FRAM Ferroelectric Random Access Memory

GPIO General Purpose Input/Output

GSM™ Global System for Mobile communications: *originally from Groupe Spécial Mobile*

GUI Graphical User Interface

HIFU High Intensity Focused Ultrasound

IC Integrated Circuit

IEE Institution of Electrical Engineers

IEEE Institute of Electrical and Electronics Engineers

I^2C Inter-Integrated Circuit bus

IMD Implanted Medical Device

INSERM Institut National de la Santé Et de la Recherche Médicale

IP Internet Protocol

IPAH Idiopathic Pulmonary Arterial Hypertension

IPS Infinite Power Solutions

KLM Krimholtz Leedom Matthaei model

LAP Left Atrial Pressure

LaRC-SI Langley Research Center - Soluble Imide

LIPUS Low-Intensity Pulsed UltraSound

MEMS Micro-Electro-Mechanical System

MI Mechanical Index

MICS Medical Implant Communication Service

MRI Magnetic Resonance Imaging

PCB Printed Circuit Board

PC Personal Computer

PEEK PolyEther Ether Ketone

PMMA Poly(Methyl MethAcrylate)

POTS Plain Old Telephone Service

PTFE PolyTetraFluoroEthylene

PZT Lead Zirconate Titanate $Pb(Zr_{1-x}Ti_x)O_3$

RAM Random Access Memory

RF Radio Frequency

RFID Radio Frequency IDentification

RoHS Restriction of Hazardous Substances directive

ROM Read-Only Memory

RSSI Received Signal Strength Indication

RTC Real-Time Clock

RX Receiver

SI Système International d'unités

SoC System on a Chip

SOI Silicon On Insulator

SPI Serial Peripheral Interface

TTL Transistor-Transistor Logic

TR Transponder

TX Transmitter

UMTS Universal Mobile Telecommunications System

USB Universal Serial Bus

WLAN Wireless Local Area Network

1 Introduction

1.1 Motivation

The technology evolution in the last decades has promoted the development of new sensing and monitoring devices for health-care. Several promising prototypes for monitoring or treating patients with chronic diseases are commercial reality or under development. Most common examples are pacemakers, glucose monitor systems, and neurostimulators. The trend is towards Implanted Medical Devices (IMDs), which show promising characteristics in continuous monitoring of physiological indicators, while preserving the autonomy of the patient.

In particular, following categories may greatly benefit from IMDs:

- **Patients suffering from chronic diseases**. Early diagnosis in populations at risk and regular monitoring of physiological parameters is a common goal for treating many diseases, in order to prevent long-term complications. In many cases, an implanted system which would autonomously measure relevant parameters and possibly raise an alert in case of need, would be a great improvement for the patients. An IMD could also integrate an actuator to form a closed feedback loop, that is able to autonomously deliver therapy (e.g., drugs, electrical stimulation) and monitor the patient's response to the treatment.

- **Hospital patients**. At present, hospitalized patients are monitored intermittently, intensively, or continuously (e.g., in intensive care units). This monitoring consists in vital sign measurements (e.g., blood pressure, heart rate, ECG, respiratory rate, and temperature), visual appearance, and verbal response. The monitoring tends to be very labor-intensive. It requires manual measurement, documentation, and it is prone to human error. The automation of this process would be therefore advantageous for both the health-care provider and the patient in terms of costs, precision, and patient's quality of life.

- **Elderly patients**. The proposed monitoring system would also be of benefit to populations at risk, such as the elderly whose life expectancy is continuously increasing. Identifying ways of surveying in a minimally invasive manner this aging population in their domestic environment is very important, especially during months of non-temperate weather. This would allow earlier detection of any degradation in their condition, without requiring frequent visits at the hospital.

The development of IMDs gave rise to the creation of standards and best practices in the field. As a relevant example for this work, titanium and its alloys are by far the most used casing materials, because of their long-term biocompatibility and their lack of interaction with the Magnetic Resonance Imaging (MRI) equipment.

However, a certain amount of technological challenges still need to be overcome. Limitations of the currently commercial devices include their size and possible adverse interaction with the external world (e.g., compatibility with MRI, interference with mobile phones and medical equipment).

A technological gap has to be filled in order to obtain smaller, longer term, deeper implantable devices working in an autonomous way. Particular design issues for deeply implanted devices (5 to 10 cm)

concern miniaturization and power consumption. In order to combine small size and long term, the power required for the IMD operation must be minimized and the device must be able to be recharged from the external world, through a Control Unit (CU). A transmission strategy able to reach the implant at deep locations is required. Furthermore, the device must be as small as possible to fit the implantation site, in order to be minimally invasive, minimize the implantation risks, and minimize possible discomfort to the patient.

Current contact-less rechargeable devices rely on electromagnetic waves for the energy transfer, either in the form of RF techniques or magnetic induction. Both strategies may not provide efficient communication with deeply implanted devices, because of the dielectric nature of the body. To be able to recharge the device wherever it is implanted, the nature of the source should be different.

Another important concern, always associated with radio communication, is the electromagnetic compatibility. It is becoming more and more difficult to ensure a radio communication characterized by a high immunity to external emitters. The ever increasing number of wireless hotspots associated with the wide frequency spectrum of modern radio devices, render the use of electromagnetic waves for energy transfer difficult.

1.2 Scope of the work

The European project ULTRAsponder, to which the author of this thesis work contributed, aims to achieve a new generation of IMDs. To this end it proposes:

- The exploitation of ultrasonic (mechanical) waves as a carrier for energy and data transfer,
- A data communication based on backscattering technique, similar to Radio Frequency IDentification (RFID),
- A design suitable for industrial mass-manufacturing, complying with current standards and safety regulations.

Within the project, several technologies towards a novel IMD were developed and integrated into a demonstrator.

The specific contribution of the author concerned the integration of the different parts manufactured into a coherent device. This ranged from the definition of technical specifications in the early stage of the product design to the choice of appropriate commercial components, e.g., for compatibility with MRI, long operation life, and small device size. Further tasks were the geometrical placement of the Printed Circuit Boards (PCBs) inside the casing, the choice of a suitable housing material, and the optimization of the housing for good energy transfer to the transducer.

In view of this choice, the scientific challenge of the project, to which this thesis work tries to answer, is the propagation of an ultrasonic wave through a titanium casing and in such a way that the adverse bioeffects on the surrounding tissues are minimum.

To this end, the effect of the titanium barrier is simulated at several thicknesses and for slightly different configurations of the implanted transducer.

Figure 1.1 schematically shows the target overall system. The contribution treated in this thesis work is highlighted in blue.

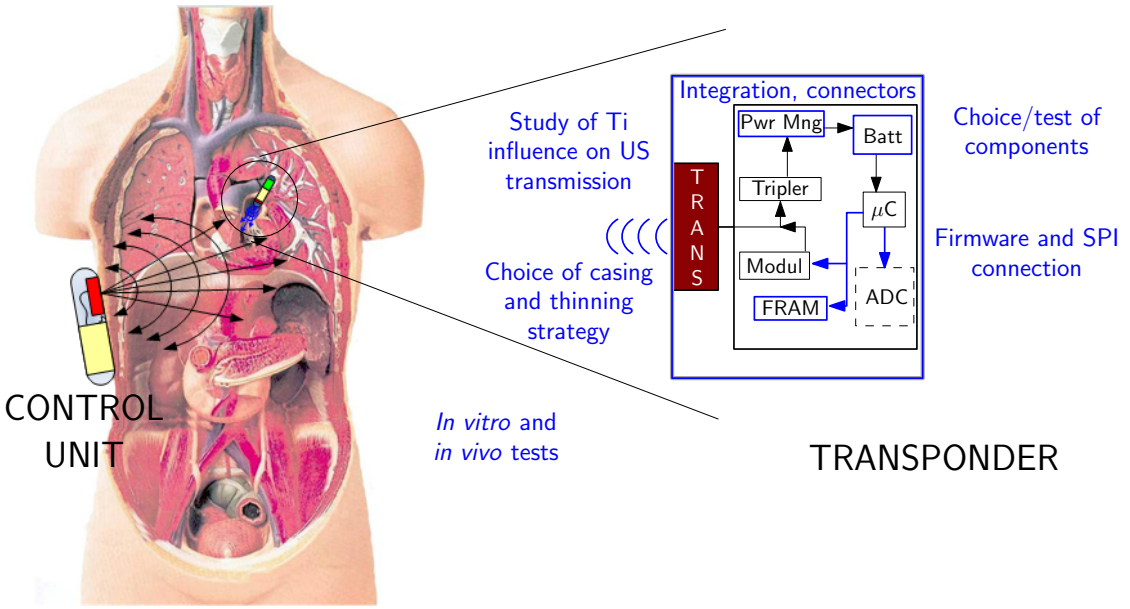

Figure 1.1: Author's contribution to the system proposed within the ULTRAsponder project.

1.3 Thesis outline

This thesis work is structured as follows.
Chapter 2 presents the state of the art in IMDs and in medical applications of ultrasound. The limitations of the available devices are identified in Chapter 3, where a generic device concept is proposed, which would address the challenges towards a new generation of IMDs. Chapter 5 relates on the device designed within the ULTRAsponder project, based on that ideal device. The required technological tools and the choices made in the conception of the product are described. Finally, the manufactured demonstrators are presented in Chapter 6. The protocol and the results of *in vitro* and *in vivo* tests are detailed.
Chapter 4 shows the necessary theoretical tools to describe mechanical waves, and in particular ultrasound, towards the goal of modeling the transmission of the energy and data carrier. In particular, the effect of the titanium casing in the received transducer is addressed through simulation.
Conclusions and outlook are discussed in Chapter 7.

2 State of the art

2.1 Introduction

Medical devices are man-made instruments aiming to replace, support, or enhance a biological structure. This chapter reports on the state of the art in active, implantable medical devices. Special focus is put on the IMD power source, on the encapsulation and implantation strategy, as well as on the communication with the external world.

The packaging exploited in commercial devices are for the most part titanium-based casings, because of the excellent characteristics of this material [60].

Implantation methods are tending towards minimally invasive techniques, which is increasingly possible because of the small size of the implants [31, 46, 84, 109]. Vice-versa, the planned implantation technique influences the device design.

Autonomous power supply is a major challenge for IMDs. Wireless recharge of a local power storage from an external unit is advantageous. Two main strategies are identified: magnetic induction and ultrasonic energy transfer. This second method, known for years but still at its infancy, proved most efficient for small and deep implants [22].

Besides, ultrasound is already widely used in medical domain for imaging and manipulation at cell level, thus its exploitation as energy carrier is very promising.

2.2 Commercial Medical Devices

Medical devices are formally defined by the European Commission as follows [32]:

> *Medical Device means any instrument, apparatus, appliance, material or other article, whether used alone or in combination, together with any accessories or software for its proper functioning, intended by the manufacturer to be used for human beings in the:*
>
> - *diagnosis, prevention, monitoring, treatment or alleviation of disease or injury,*
> - *investigation, replacement or modification of the anatomy or of a physiological process,*
> - *control of conception,*
>
> *and which does not achieve its principal intended action by pharmacological, chemical, immunological, or metabolic means, but which may be assisted in its function by such means;*

Medical devices range from extra-body machinery (such as glucose monitors, external insulin pumps) to implanted devices. There again, IMDs can be divided into passive and active. The main example of passive IMDs are implanted prostheses, such as knee or hips replacements. Active IMDs contain electronics and are able to sense a particular parameter or deliver a treatment. Pacemakers, cochlear implants, neurostimulators fall in this category. Figure 2.1 shows the different divisions in the medical device family, and cites some examples of devices. An extensive review of commercial IMDs was performed by Receveur *et al.* in 2007 [82].

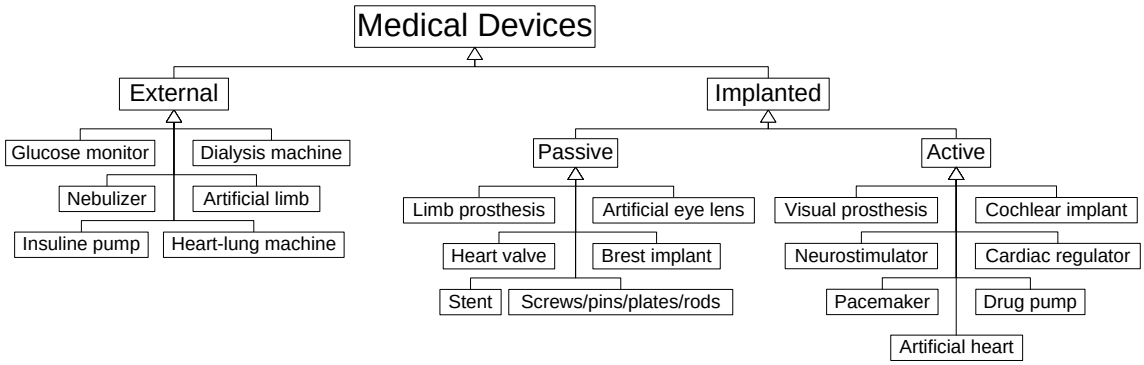

Figure 2.1: Types and examples of medical devices.

(a) First pacemaker prototype (around 1940) © *Canadian Heritage Information Network [16].*

(b) First implanted pacemaker (1958). © *Professor Marko Turina, University Hospital, Zurich [105].*

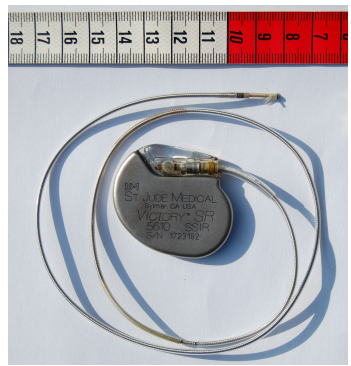

(c) Victory™ SR 5610 device (present). © *Steven Fruitsmaak [39].*

Figure 2.2: Evolution in pacemaker devices.

Evolution of medical devices is well depicted by the treatment of heart anomalies. Artificial pacemakers are devices that deliver electrical impulses in order to regulates the heart beating. They are employed when the cells responsible for beat initiation (natural pacemaker) are not working properly, or when the heart electrical propagation system is damaged, thus blocking the beating impulse. The concept of artificial pacemaking is known since the beginning of the 20th century [64]. The first prototype was a 30 cm large machinery worn by the patient and connecting with the heart through wires coming out of the skin. It was developed in the 1940s by Canadian surgeons Dr. Wilfred G. Bigelow and Dr. John C. Callaghan at the Banting Institute in Toronto [8]. The tendency in the last decades has been to implant medical devices, in order to avoid wires. Progress in microtechnology allowed the first implantable pacemaker to be exploited in 1958 in Sweden. It had the size of a hockey puck (about 7.5 cm diameter and 2.5 cm thick). Today pacemaker devices are much smaller, similar to Victory™ SR model 5610 (St. Jude Medical Inc., St. Paul, MN, USA), which has a size of 4.3 cm × 4.4 cm × 0.6 cm, and a device life of ten years is standard for cardiac implants. In addition to resynchronization functionality, many cardiac implants nowadays contain a cardioverter-defibrillator: this device intervenes in case of cardiac arrhythmia (possibly leading to sudden cardiac death) and restores the normal rate and sequence of contraction. Figure 2.2 shows the different evolution steps.

Implanted Medical Devices make possible to sense more precisely, act where it is needed, and deliver drugs on the exact spot to be treated, thus reducing the quantity of drug needed. The closer feedback allows the adaption of the therapy to the patient reactions. Several promising prototypes for managing patients (with acute diabetes, for treatment of epilepsy and other debilitating neurological disorders) and for monitoring patients with chronic diseases have been developed. On medical research level, IMDs allow monitoring unexplored mechanisms, such as long-term variations of a given parameter (e.g., glucose concentration or blood pressure).

Important examples of IMDs are neural prostheses, such as cochlear implants, which translate the sounds from the external world into an electrical stimulus, thus compensating for damaged hair cells in the cochlea [113]; spinal cord simulators, based on the fact that pain transmission can be blocked by stimulating large portions of nerves [57]; visual prostheses, that can create a sense of vision by electrically stimulating neural cells in the visual system where photoreceptive cells fail to translate photons into neural signal [112]. Functional Electrical Stimulation (FES), a particular type of neurostimulation which aims to restore motion in people with disabilities, by injecting electrical currents to activate nerves innervating extremities affected by paralysis, could greatly benefit from IMDs, allowing several stimulation and sensing locations in the body [91]. Also, several devices have been developed to treat heart anomalies, like the already mentioned pacemaker.
Commercial devices include for example the ACTIVA® PC neurostimulator (Medtronic, Minneapolis, MN, USA) [1], the cochlear implant HIRES 90K™ (Advanced Bionics AG, Stäfa, Switzerland) [2], or the pacemaker ALTRUA™ (Boston Scientific, Natick, MA, USA) [3]. Pacemakers and implanted defibrillators are well assessed and implanted in about 200'000 persons every year in Europe [30].

IMDs can also be used to identify a patient and ease retrieving important medical information. VeriChip (PositiveID, Delray Beach, FL, USA), achieves this exploiting a RFID tag and it is to date the only microchip approved by the Food and Drug Administration (FDA) for implantation in humans.

This thesis work is focused on active, implanted, long-term medical devices. Figure 2.3 shows the general schematics of an active IMD. A sensor/actuator block carries the functionality of the IMD. The data sensed are kept in a non-volatile memory. A local power storage and an optional energy harvesting block provide the required electrical energy to run the implant. A telemetry block allows communication with the external world. Finally, a microprocessor is the core of the implant, as it manages the other blocks.
Challenges in the product design are in particular related to device packaging and power supply [112]. Therefore, following sections will particularly detail the state of the art concerning those parameters.

2.3 Device packaging

To ensure long-term implant activity and safety for the patient, encapsulation of the electronics is necessary, and several specifications must be met [56]. Main characteristic for the implant casing is biocompatibility, which means the property of not eliciting immune response from the body. Conversely, the implant should be resistant to corrosion, coming from the contact with body fluids. Indeed, in order to avoid short circuits, major dysfunction, and injuries, the body fluids should not get in touch with the electronics during the whole implant life. According to the application, the casing material should

[1] http://professional.medtronic.com/pt/neuro/dbs-md/prod/activa-pc/
[2] http://www.advancedbionics.com/com/en/products/hires_90k_implant.html
[3] http://www.bostonscientific.com/Device.bsci?page=HCP_Overview&navRelId=1000.1003&method=DevDetailHCP&id=10103841&pageDisclaimer=Disclaimer.ProductPage

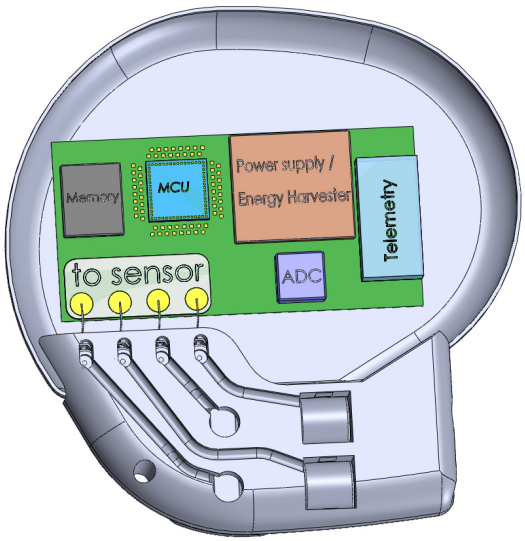

Figure 2.3: Rendering of a generic active sensor IMD.

integrate in different ways with the surrounding tissues. For example, for hip or knee replacement, the integration of the implant to the bones is very important, while for drug delivery systems the encapsulation of the implant in a fibrotic, inert tissue needs to be avoided. The casing also protects the device electronics from mechanical stress, which can be more or less important depending on the implant site. The device needs to undergo sterilization before implantation. This requires a casing resistant to the standard sterilization methods, including steam sterilization, Ethylene Oxide, or gamma rays [59, 73]. Finally, the entire above characteristic set should be maintained through the whole life of the implant. Materials for IMDs are subject to different regulations in different countries. The biocompatibility of the device components is a milestone for IMD development. Several materials used in Micro-Electro-Mechanical Systems (MEMSs) were considered by Kotzar *et al.* [53], in order to assess their exploitability in medical devices.

Several encapsulation methods are currently used for IMDs. The natural choice for long-term implants is titanium, because of its excellent biocompatibility and interesting mechanical properties. At room temperature titanium is resistant to tarnishing. Oxydation may occur at higher temperatures, but this layer of titanium oxide will prevent further corrosion. Thus, titanium can be considered to be inert to body tissues. It has a very low electrical and thermal conductivity, and it is paramagnetic. Medical grade titanium, a 99% pure alloy, is widely used for medical prostheses [60] and instruments [58]. Through coating with polymers [103], it is possible to encourage its reaction with bones (osseointegration), thus making titanium an excellent candidate for orthopedics and dental implants. The biocompatibility of titanium and its alloys is assessed by several standards and publications of the American Society for Testing and Materials (ASTM) [2, 4, 7, 54]. Indeed, currently manufactured IMDs are almost exclusively made of titanium and titanium alloys. Alternative materials are some polymers, such as PolyTetraFluoroEthylene (PTFE), PolyEther Ether Ketone (PEEK), Poly(Methyl MethAcrylate) (PMMA), polyethylene, and silicones. They are non-toxic, may be degradation resistant, and provide good fatigue strength and wear resistance [80]. Nevertheless, they have tendency to be colonized by microbes, thus requiring special treatment in order to be suited for long-term implantation [97, 107].

Furthermore, polymers do not provide electrical shielding and strong mechanical protection for the implanted electronics, as metals do.

In case of allergies against titanium, Medtronic applies a special coating of medical silicone or parylene on its implant housings, and the device is then treated as a custom-made piece, to be followed-up in particular ways.

Polymers may also be required for some parts of a specific device. As a recent and media-covered example, Medtronic exploits Langley Research Center - Soluble Imide (LaRC-SI), developed by NASA, to insulate thin metal wires on its Cardiac Resynchronization Therapy (CRT) devices [14].

The casing will have an influence on the energy and data transmission, which has to be taken into account. Titanium is MRI compatible because of its paramagnetic properties. The specific issue of heat production in the tissue surrounding the device is addressed by exploiting heat-absorbing materials, which change state depending on the temperature [89]; they can be coupled with an internal algorithm to further reduce the power supply and thus the heating produced.

2.4 Minimally invasive implantation

The goal is to reduce as much as possible adverse effects of the implantation, thus improving recovery of the patient and reducing costs. Without complications, a patient undergoing minimally invasive implantation can leave the hospital within 24 hours and visit the medical facility for follow-up [46].

This translates into minimizing damage of biological tissues at the point of entrance of the instruments. Incisions will be as small as possible, and anatomical openings will be exploited to access the implantation site.

A great step towards minimally invasive implantation techniques has been the development of the catheter-delivered stent for angioplasty [27]. The motto of its inventor, which well resumes the aim of minimally invasive implantation, is: "*What can be accomplished without operative exposure should be.*" (*cit.* Dr Charles T. Dotter, 1969).

Since then, percutaneous approaches (through the skin) are widespread [31, 84, 109]. This involves a needle catheter getting access to a blood vessel, followed by the introduction of a guidewire through the lumen (pathway) of the needle. It is over this wire that surgeons can place other catheters into the blood vessel, or implant a medical device. This technique is most used for implantation of stents in the blood vessels, placement of artificial heart valves or heart pumps. For larger implants, more traditional methods must be employed. As an example, pacemakers and cardiac devices in general are usually inserted in the left shoulder area where an incision is made below the collar bone creating a small pocket. Once the implant is in place, the leads are inserted through a large vein into the heart, and their insertion is monitored using real-time X-Ray imaging (fluoroscopy).

In order to reduce the risk of infections, standard procedures require that the IMD is kept in a sterile container or sterilized prior to introduction to the sterile implantation environment. In addition, drugs may be administrated on the implantation site. Two methods for local drug elution have been disclosed by Bischoff [9, 10]. The author proposes either to cover the device housing with a polymer layer impregnated with drugs, or to insert a temporary, dedicated element next to the main implant. This second method has the advantage to separate the actual IMD, which can have a long shelf life, from the drug-impregnated element, which undergoes quicker deterioration.

Ideally, IMDs would be implanted through catheterization or similar transcutaneous implantation techniques, in order to reduce the pain of the patient, avoid infections and save money. This influences

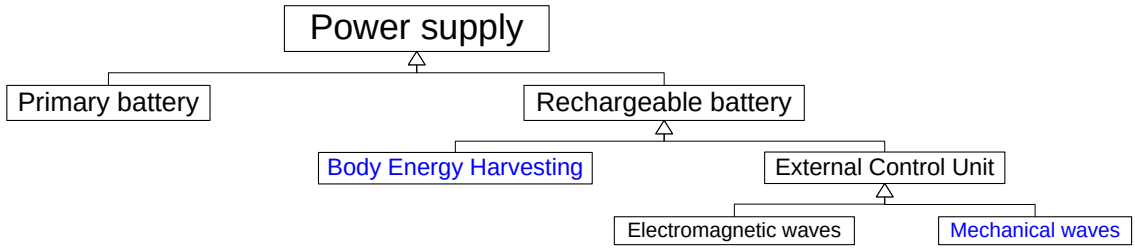

Figure 2.4: Characterization of IMDs according to power supply method. Blue categories are not yet commercial technologies.

the maximum size of the device: blood vessels range in diameter between 25 mm to some μm, while the maximum size of currently used catheters is 14 F (about 4.5 mm diameter) [74].

2.5 Power supply

Active IMDs need an internal power supply, allowing autonomous operation over a certain amount of time. Figure 2.4 resumes the different options for supplying the energy.

A first option is to use primary cell batteries as the source of energy of the IMD. This can be effective for low power applications, such as pacing devices. However, high capacity batteries must be used in order to supply the power required on a long term. The device size devoted to batteries can become very large. Once the battery is depleted, the device needs to be explanted and re-implanted. This is not very appealing to the patient, and it incurs costs to the hospital. For this reason, and given the trend towards long-term implants, rechargeable batteries are increasingly used.

2.5.1 Energy harvesting from human body

An approach to reduce the need of energizing the implants from outside the body is based on the observation that the human body produces a substantial amount of energy. It can take different forms such as dissipated heat, inertia, muscle contraction, joint movement or heel strike. Several microsystems are under development to harvest part of it. A piezoelectric energy harvesting system could potentially power active IMDs [24]: a piezoelectric diaphragm could be placed in a blood vessel and translate the mechanical quasi-static deflection caused by the blood pressure variation (about 2 Hz frequency) into electrical energy. An alternative is to use the human body as a natural source of chemical and physical energy [19]. Chemical energy could be extracted by implantable micro fuel cells (for example from glucose); MEMSs could transform physical energy, such as body heat, blood pressure, breathing, and body motions into electrical power.

Nevertheless, despite dynamic research and promising results in this field [6, 48, 62], body energy harvesting is to date not ready to be used as a steady, reliable power source for IMDs [68].

A more developed approach consists in having an external power source, which transcutaneously delivers energy. Wireless energy transfer is preferred: having electrical wires which perforate the skin is disadvantageous due, in part, to the considerably elevated risk of infection. Both electromagnetic and mechanical waves can be considered as wireless energy carriers.

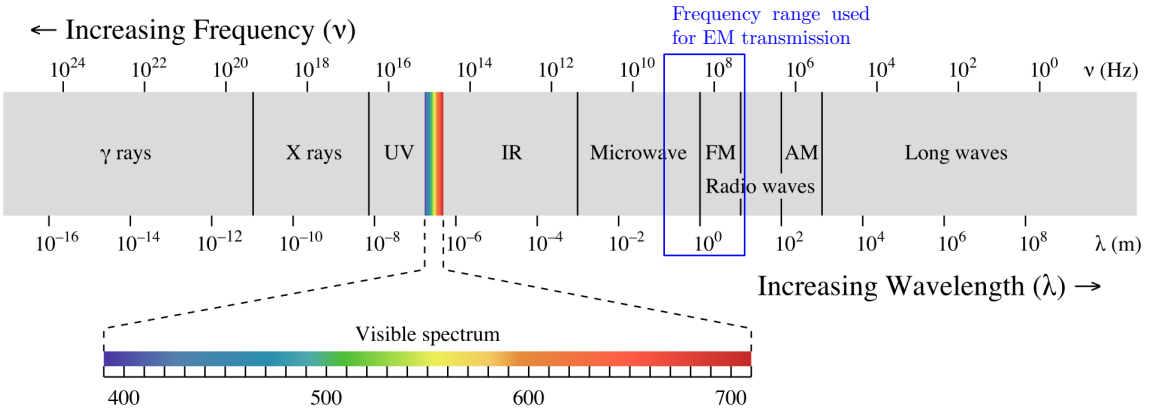

Figure 2.5: Spectrum of electromagnetic waves. *Adapated from Philip Ronan [87].*

2.5.2 Electromagnetic waves

Type and source of Electromagnetic (EM) waves are identified by their spectral band. Waves at different frequencies have extremely different characteristics of penetration into the body, bioeffects, wave energy, and dispersion. Figure 2.5 depicts the EM spectrum and identifies the different types of waves.
Some wave types can be immediately excluded as energy carrier candidates, because of their adverse bioeffects. Waves at frequencies higher than the visible range (about 10^{14} Hz and beyond) are ionizing radiations, that is to say they are able to create ions and free radicals in living tissue, thus damaging the body even at low energy intensity. All frequencies of UV radiation have been classed as Group 1 carcinogens by the World Health Organization [44]. Ultraviolet radiation from sun exposure is indeed the primary cause of skin cancer. It is therefore evident that Ultraviolet, X-rays, and Gamma rays cannot be used as energization carrier for IMDs.
Also non-ionizing radiations (infrared, microwave, and radiofrequency radiation) act on the tissues with an energy inversely proportional to their wavelength. Infrared and microwaves radiations induce heating in the body by acting on the water dipolar molecules. Frequencies in the radio range, which possess the lowest wave energy, are therefore the most suited for wireless energy transfer. Radiofrequency radiation is suspected to be carcinogen, but with weak evidence [44].

The International Telecommunication Union (ITU) dedicated several bands to EM transmission for IMDs [45]: 9-600 kHz, 30-37.5 MHz, 401-406 MHz (Medical Implant Communication Service (MICS) [33, 34]), 2.4835-2.5 GHz. Furthermore, the Wireless Medical Telemetry Service [4] is defined in the USA in the bands 608-614 MHz, 1.395-1.4 GHz, and 1.429-1.432 GHz.

To date, magnetic induction is the most widespread energization method for many devices, both in medical domain[5] [96] and in day-to-day life (e.g., wireless recharge of electric cars[6], rechargeable toothbrushes[7]).

Transcutaneous energy transfer by magnetic inductive coupling involves the placement of two coils positioned in close proximity to each other on opposite sides of the cutaneous boundary. The internal

[4] http://www.fcc.gov/encyclopedia/wireless-medical-telemetry-service-wmts
[5] http://www.sjmneuropro.com/Products/US/Eon-Rechargeable-IPG-System.aspx
[6] http://www.pluglesspower.com/
[7] http://www.oralb.com/products/vitality-floss-action/

coil, or secondary coil, is integrated in the IMD. The external coil, or primary coil, is associated with an external power source. A current is induced in the secondary coil through inductive coupling. This current can then be used to power the implanted medical device or to recharge the local battery, or a combination of the two.
Primary and secondary coils can be adjusted to the target transmission to be achieved by acting on their size, number of turns, and working frequency [42]. Several patents issued by Medtronic propose technologies and methods to manufacture an IMD powered or recharged by magnetic induction. Using a metallic casing as encapsulation for the IMD, a magnetic shield should be foreseen in the device design [47], in order to improve energy transfer, and reduce the electromagnetic flux lines coupling with the housing, thus reducing the eddy currents responsible for the heating around the device. Furthermore, particular titanium-alloys can be exploited as suitable housing materials for IMDs, in order to ease inductive coupling [58]. With respect to pure medical grade titanium, the alloys proposed exhibit greater power coupling efficiency, thus improving the achievable transmission distance.
As the efficiency of the magnetic link is a crucial point in the device, it is not unusual that magnetic emitters and receivers are custom-designed, in order to optimize the energy transfer in a particular IMD [50, 85]. The best coil and signal characteristics are assessed based on target application and device specifications.

In other cases, devices rely on RF transmission for wireless energy transfer: the implant is equipped with a RF receiver and usually an internal power storage, conceived as a backup [5]. The RF emission from an external control unit can power up the implanted device and/or recharge the local power storage. The internal supply is able to autonomously power the implant for 24 hours continuous activity. The carrier is an electromagnetic wave, like in previous method, but its frequency is higher, so that the electric field is dominant with respect to the magnetic field. The boundary between magnetic coupling and electromagnetic power harvesting is defined by $d = \lambda/2\pi$, where, d and λ are the distance and the wavelength of the signal, respectively [117]. For a chosen wavelength, if the distance between the coils is smaller than d, the magnetic coupling gives more efficient wireless power transmission than RF.

Using EM waves, the presence of external electric and magnetic fields encountered by the patient during daily activity, may expose the patient to the risk of false positives, i.e., accidental activation or deactivation of the transponder. RF telemetry systems can interfere with other RF wireless systems, such as mobile phones, home power tools, and aviation electronics.
Magnetic induction will in principle interfere with MRI, unless particular care is taken in the design. Moreover, magnetic coupling requires accurate positioning for efficient energy transmission.
Finally, at a given working frequency, the EM energy transfer is strongly dependent on the shape and size of the coil (antenna). Thus, the integration in small size IMDs can be cumbersome and results in a trade off with respect to efficiency and penetration depth. Indeed, electromagnetic energy may only penetrate into the body up to a distance equal to the size of the antenna, because of the dielectric nature of the body [40]. Therefore it may not be able to communicate effectively with a transponder that is located deep within the body and which has a small size.

For this reason all methods and devices presented in literature have a subcutaneous part, in which the antennas/coils are placed, and a sensing/actuating part, in the same housing or connected with wires to the energy harvesting part. The presence of wires between the implant and the receiver is of course unwanted, but may be necessary to ensure sufficient energy transfer to a deep implant.

2.5.3 Mechanical waves

Recent work shows how ultrasonic waves, that is mechanical waves at a frequency higher than the human audible range (> 20 kHz), are emerging as an alternative way to transmit energy to IMDs [86]. This technique exploits the ability of acoustic waves to penetrate deeper in the body tissue without being significantly attenuated. A system consisting of an external CU and an IMD can be conceived, which transfer energy and data by acoustic link [25]. An electrical signal is transformed into an acoustic wave by a piezoelectric transducer contained in a CU external to the body. Then, this acoustic wave propagates in the direction of the implanted device. Another piezoelectric transducer is integrated inside the implanted device. It receives the acoustic wave coming from the CU and converts it to electrical energy, to be stored in the internal battery. Special housing may ease intrabody ultrasonic communication among implants, acting as an acoustic diaphragm to the underlining transducer [26]. With respect to EM waves, ultrasound allows a lower working frequency keeping an efficient directionality [86]. Denisov *et al.* [22] compared acoustic and electromagnetic wireless energy transmission. Although maximum efficiency of ultrasonic energy transfer is only about 40%, while EM waves can achieve 80%, ultrasound scales much better with the size of the transducer and with the penetration depth to the implant. For coil/transducer sizes smaller than 10 mm and for implantation depth higher than 10 cm, ultrasound clearly outperformes magnetic induction and RF transmission.

Transducer efficiency can be considerably improved by exploiting piezocomposite technology [29, 37], in which an array of thin piezoelectric ceramic rods are embedded into a polymer material. E.g., piezocomposite materials manufactured by IMASONIC (Voray-sur-l'Ognon, France) have a structure called 1-3, depicted in Figure 2.6. Their physical properties depend on the ceramic and polymer properties and on the microstructure dimensions. Piezocomposites present interesting acoustic and mechanical properties. Most importantly, piezocomposite materials have a high coupling coefficient, i.e., a high capacity to convert acoustical energy into electrical energy, and vice-versa. The resulting transducer has higher sensitivity and signal to noise ratio (10 dB to 30 dB compared to conventional technology). The high coupling coefficient also contributes to enlarge the bandwidth while keeping a good sensitivity. The acoustic impedance of the piezocomposite is always lower than that of monolithic piezoceramic elements and can be adjusted by playing on the geometry of the rods. This allows better adaptation to the transmission medium, in particular to water and therefore to body tissues, which acoustic impedance is close to water (1.5 MRayl). The 1-3 structure of the composite attenuates lateral modes of vibration, thus improving the beam pattern and keeping the cross talk among elements as low as -40 dB. Due to the modular geometry and to the presence of polymer, piezocomposite materials can be mechanically shaped, thus producing focused beams without using acoustic lenses. This avoids lens attenuation and allows a more predictable beam pattern. Piezocomposite materials also have a higher mechanical resistance, which confers to the transducers a higher resistance to mechanical shocks, vibrations, temperature, and pressure constraints.

Acoustic telemetry methods and apparatus have already been reported and patented in the medical field for heart pressure monitoring, insulin pump assisting [75] and cerebrospinal fluid draining in the case of hydrocephalous disease [78]. From 1997 up to 2007, Remon Medical Technologies Inc. (Caesarea, Israel, now Boston Scientific) has been one of the main actors developing systems in this field. Reported systems include an external or implanted CU and one or several implanted Transponders (TRs) that can wirelessly communicate, using acoustic transducers. These transducers are used either to exchange data or for energy scavenging. These acoustic transducers are flexural mode transducers [79] working at a low ultrasonic frequency, e.g., 40 kHz. These transducers are said to be omni-directional due to the low

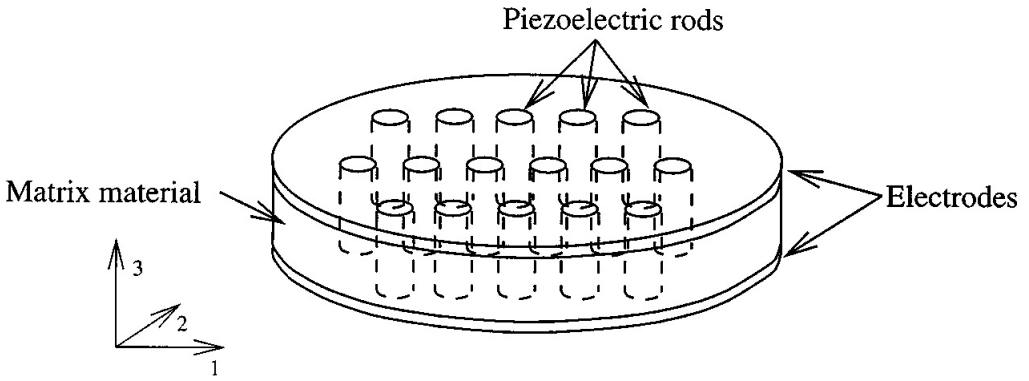

Figure 2.6: Piezocomposite structure 1-3. *Source: O. Sigmund et al.* [93].

operating frequency. Moreover, due to the use of low frequency acoustic signals, their system does not suffer from significant attenuation in the surrounding medium.

2.6 Data communication

Implanted Medical Devices, and especially long-term devices, need to communicate with the external world. Depending on the application, they need to inform a CU about a hardware problem [71]. Once in a while, an implanted sensor may need to download the physiological parameters sensed. An actuator may need to receive modified settings from the external world.

Telemetry capabilities allow conceiving a network of IMDs, each with an autonomous sensing or actuating role [75, 76]. Intra-body communication is proposed, where an implant carries the role of Control Implant, which activates the other implants. The link can also be used to switch on and off the implant from the exterior world, in order to reduce its power consumption [77].

The medical Implantable RF Transceiver ZL70102 (Zarlink Semiconductor, now Microsemi, Aliso Viejo, CA, USA) is used in most commercial IMDs. It operates in the frequency band 402-405 MHz, which is the dedicated band defined by the MICS specification for bi-directional radio communication with IMDs [33, 34].

In order to ensure miniaturization and autonomy, the communication strategy needs to consume little power, so that the local battery lasts longer. This work exploits a communication concept in which the data carrier is a wave coming from the external CU, which is reflected back by the implant according to the message to be sent. The power needed to create the wave is provided by the external CU, where power consumption is not an issue. The implant only spends energy to modulate that wave to transmit the message. This process is based on the backscattering principle, which is best known in RFID applications.

RFID is an automatic identification method, relying on storing data on devices called RFID tags, and remotely retrieving those data by interrogating the tags from a RFID reader. As an example, that is how badges control access to buildings.

A standard RFID tag is usually completely passive: it does not require a battery, as it is powered from the wave supplied by the RFID reader. The reader sends an electromagnetic wave to the tag and the tag answers, for example with its serial number. As illustrated in Figure 2.7, the working principle is based on the fact that an electrical wave is reflected or absorbed by a device according to the electrical impedance of the device itself. A device can be therefore recognized by how it reflects back an incoming

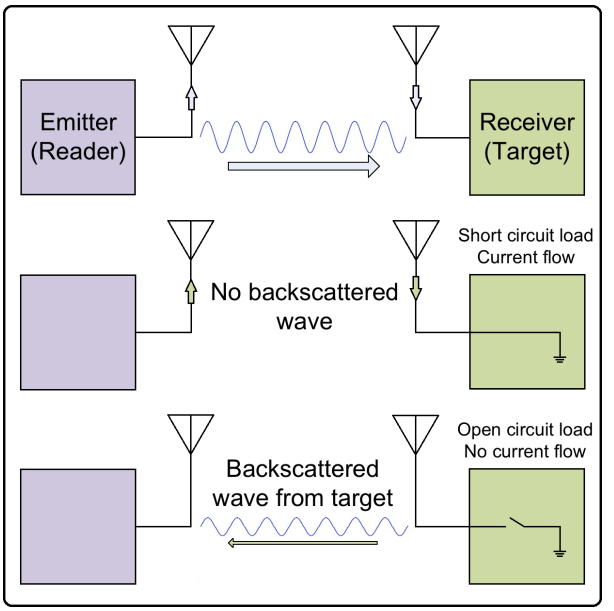

Figure 2.7: Concept of Backscattering with RF waves.

wave. If the tag device is able to dynamically change its own impedance, for example by electrically switching a component in and out, it can modulate the reflection of the wave received and, by this mean, transmit information.

This process is called Backscattering Modulation, and it is a promising technique for communication with IMDs. In principle, any kind of wave can be associated with backscattering technique. If a mechanical wave (e.g., ultrasound) is exploited as a carrier, instead of an electromagnetic wave, the modulation will occur by changing the mechanical (acoustical) impedance instead of the electrical one, exploited by RFID [79].

2.7 Applications of Ultrasound

Ultrasound is already widely used in the medical domain.

The ability of ultrasound to differentiate tissues based on their acoustic impedance is the basis for ultrasonic imaging (ultrasonography), which can be differentiated in many subtypes. Most important to mention is the Doppler imaging, which renders tissue in motion, for example blood flow.

The ultrasonic image is created by first transmitting sound waves into the body and then interpreting the intensity of the reflected echoes. The principle is very similar to the backscattering telemetry, described previously. The ultrasonography is achieved using a hand held scanner, which contacts the body. A water-based, acoustic adaptation gel is used to optimize the contact and to match the ultrasonic impedance between the probe and the body. The data collected is then processed within the body of the external scanner and displayed as a gray scale image. The frequency of the scanner beam directly influences the depth of analysis: low frequencies (5-12 MHz) are well-adapted to image large, deep elements, such as organs. Higher frequencies result in higher resolution images, closer to the transducer surface. As an example, epidermis is best imaged with beam of 50 to 100 MHz.

Dermatology exploits sonography in several ways, as overviewed by Kleinerman *et al.* [51]. Based on the fact that skin echoes ultrasound according to its content in creatin, collagen, and water (among others), the skin regions can be clearly recognized. Skin conditions can be diagnosed, for example inflammations, skin cancer, cellulites, foreign bodies in wounds, etc. Evaluation of skin thickness by ulltrasound is reported to provide better precision than using biopsy or palpation.

Ultrasound imaging has a strong relevance in regional anesthesia in infants and children [104], where target nerves to be blocked are very close to critical structures. Being able to precisely image tissues borders, the right injection point and quantity of anesthetic can be met.
Other than for imaging, ultrasound is widely used for their ability to manipulate matter at cellular scale. High Intensity Focused Ultrasound (HIFU) exploits the bioeffects of ultrasound on tissues (thermal effect and cavitation), which are normally avoided for other applications, in order to destroy tumoral masses within healthy tissues. This technique allows a precise and less invasive treatment, because no incision is required to reach the mass to be removed. Physiotherapy takes advantage of the heat produced by ultrasound to speed up the healing process in injured tissues [108]. In cell therapy, Low-Intensity Pulsed UltraSound (LIPUS) can improve cell properties prior to their injection as a therapy. As an example, LIPUS increases angiogenic activity of cultured cells, i.e., their ability to build blood vessels. Those "improved" cells can be later implanted in patients suffering from vascularization problems, such as Critical Limb Ischemia [70]. Drug delivery at specific targets can be achieved by trapping drugs inside microbubbles (e.g., liposomes, artificial vesicles made out of a double layer of lipides) and opening them at the target location by ultrasonic vibration [35, 72]. In the same way, lithotripsy (disintegration of kidney stones) and acolysis (disintegration of blood clots) are efficiently performed by ultrasound [95, 118].

Finally, cosmetics has its fair share in ultrasound applications: exploiting the heat produced by the acoustic beam in a well-confined region, cells composing the adipose tissue (*adipocytes*) can be destroyed, improving the natural fat resorption; skin tightening can be performed in a less invasive way with respect to standard surgical incision techniques, by destroying a cone of tissue under the epidermis; definitive body hair removal can be obtained damaging the hair root with an ultrasonic beam.

2.8 Conclusion

Implanted Medical Devices are very promising tools for further development of minimally invasive medicine. They allow new applications and better adaptation of therapies to the needs of the patient. Table 2.1 gives an overview of the main methods and technologies used for IMDs, underlining their main features and drawbacks. Minimally invasive surgery methods are ready or under development, which allow implantation of the devices with minimal adverse reactions. Titanium keeps its place as principle material for IMD housing, due to its excellent characteristics and biocompatibility.

Developments in IMDs tend towards autonomous devices to be implanted at long term. To achieve this goal, an internal power supply must be provided, which in turn does not dramatically influence the size of the device. A system composed of an external CU periodically sending energy to the implant is the strategy privileged over integration of big batteries inside the implant or exploiting physical and chemical energy of the human body. A method for communicating between implant and external world is also an important requirement for active IMDs.

To date, magnetic induction performs very well as energy carrier to recharge an internal battery in subcutaneous IMDs. It nevertheless shows limited propagation inside the body and interferes with electromagnetic sources in the external world.

Table 2.1: State of the art of technologies and materials for IMDs.

Technology	**Advantages**	**Drawbacks**	**State of Development**
Titanium	Biocompatible	Obstacle for ultrasound	Standard for IMDs
Polymers	Easy manufacture Hypoallergenic	Battery colonization	Commercial
Minimally Invasive Implantation	Minimizes damages Cheaper	Requires small IMD size	Commercial
Ultrasound	Deep penetration Many applications	Requires contact	Commercial for imaging Research for IMDs
Magnetic Induction	Efficient energy transfer	Depth ~ Receiver size Interference MRI	Commercial
RFID	Low power	Proximity	Commercial
Primary batteries	Reliable Assessed technology	Size Needs replacement	Commercial
Body Energy Harvesting	On-site Continuous	Not steady source	Research for IMDs Some commercial use

On the other side, ultrasonic waves are already extensively used in the medical domain, because of their good propagation inside aqueous media and their ability to precisely recognize different tissues based on their echo response. Ultrasonic energy transfer through small transducers and to deep implanted devices proved more efficient than magnetic induction and RF waves. Therefore, this wave type is investigated as a promising carrier for energization and communication in active Implanted Medical Devices.

3 Towards a new generation of IMDs

3.1 Introduction

As described in Chapter 2, IMDs are promising tools for continuous monitoring of physiological indicators. However, in many situations, a compromise has to be found between the desire of monitoring a given parameter as frequently as possible and the resulting risks and constraints for the patient, in terms of health, time, costs, and life quality. As an example, glucose monitoring in diabetic patients is normally performed three to four times a day by peripheral blood analysis. Already this benefits from portable devices, developed in the last few decades, which allow patients to perform the measurements themselves. Ideally, patients would like to know more precisely their glucose level, in order to adjust the medication accordingly. On the other hand, each sensing event costs time, money, and pain.

For this and others applications, an implanted system which would autonomously measure relevant parameters, and possibly alert in case of need, would be a great improvement for the patients. The long-term goal is a closed feedback loop, in which the same IMD contains a sensor, which monitors a specific physiological parameter, and an actuator, e.g., a micro pump releasing a drug, which adjusts its operation according to the sensor information.

This can be especially beneficial to elderly patients and in case of chronic diseases: the patient's condition could be monitored often and autonomously, without requiring frequent visits to the hospital, thus preserving privacy and autonomy, as well as saving money.

The technology evolution in the last decade has promoted the development of new sensing and monitoring devices for health care. The design issues for deeply implanted devices remain numerous, especially regarding miniaturization and power budget.

Because of the body dielectric properties, energizing and communicating with implants that are located deep within the body, using conventional techniques like Radio Frequency (RF) or magnetic induction, may not work effectively. Another important concern is the compatibility with MRI and the interference with other electromagnetic wave emitting devices, such as mobile phones, at home or in surgery rooms. Finally, such implanted system should imply a minimum invasiveness to reduce the implantation risk and the possible discomfort to the patient. Consequently, new roads need to be opened to overcome these limitations and develop deeply implantable medical devices.

Ming-Li *et al.* [67] review several challenges in the development of IMDs.

This chapter presents a generic, modular device platform containing an IMD and an external unit for power supply, control, and data communication. Such a medical system is intended to be the basis for many applications, which will differentiate by the sensor or actuator connected. The devices, and in particular the implant, are analyzed according to several requirements towards a new generation of IMDs able to be more deeply implanted and to act on a longer term. The technologies and tools necessary to achieve this goal are discussed and some potential applications of the resulting implant concept are listed.

3.2 Implant requirements

Several key points were identified in the design of the ideal IMD for chronic sensing / action:

- **Implantability:** the technology developed for the device should be highly flexible and modular, in order to be easily adaptable to any kind of application. Implantation should be possible everywhere, including in **deep** locations. The **size** plays therefore a major role: the implant must be small and light, allowing being placed either by using open surgical or minimally invasive implantation techniques.

- **Long term** implantation: the foreseen applications being monitoring of chronic illness and elderly patients, the implant needs to stay in place at least 5 to 10 years. As the device could be potentially deeply implanted, surgery to replace the implant or part of it could be not feasible. Furthermore, the IMD must exhibit an excellent **biocompatibility** to allow long-term implantation.

- **Autonomous** sensing and action: in order to achieve a continuous monitoring, the device has to work autonomously once implanted. A continuous drive and interrogation from the outside would not address the need of independence of the patient. **Connection periods** with an external control unit are necessary, but they will be kept as rare and short as possible. To this end, the local energy stored in a small battery must be carefully managed: the implanted device must have an **ultra-low power consumption**.

- **Cost**: finally, the whole device should ideally be cheap to produce, maintain, and operate.

3.2.1 Body Sensor Network

The implant proposed in this work is conceived as part of a bigger Body Sensor Network (BSN), as defined by Yang [116]. Figure 3.1 depicts a BSN: an external Control Unit (CU) is secured to the patient's skin and able to energize and to communicate with a network of implanted nodes (Transponders). A single TR may include one or more sensors for monitoring a variety of properties, such as temperature, pressure, strain, or fluid flow, as well as chemical, electrical, or magnetic properties. It may also perform therapeutic functions such as drug delivery, defibrillation, or electrical stimulation. The TR should perform some (simple) steps regularly during the day, e.g., to sense a parameter and to store it into the memory. To achieve the trade-off between long-term operation and size, i.e., acceptably small batteries, the device should be rechargeable: once in a while, the implant will have to be connected to the CU. During these sessions, both the battery will be recharged and the data sensed during the autonomous period will be downloaded to the external world. This operation could be performed by the patient himself, or by his physician. Obviously, wires coming out the skin are not acceptable for a long-term implant. Therefore, a wireless energy transmission and telemetry must be used.

3.2.2 Implantability

The conception effort towards an innovative device should benefit different applications. The IMD should be easily adaptable to different sensors or actuators, and be exploited at different locations and according to different use patterns.

As an example, the requirements in terms of power consumption vary according to the application: the device would ideally host a modular battery, in order to adjust its capacity (and size) to the optimum

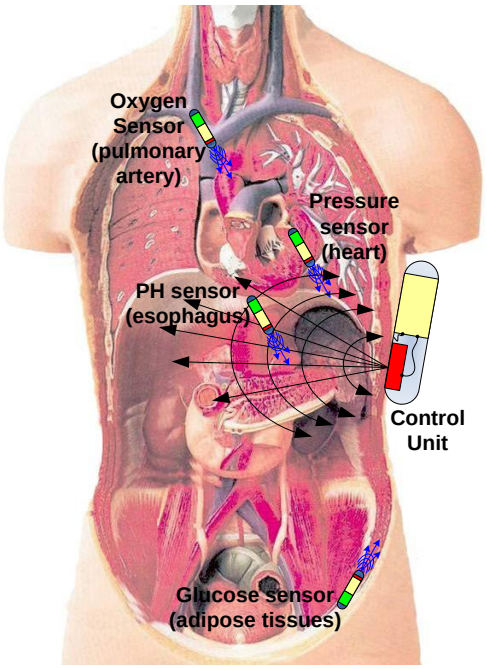

Figure 3.1: Concept of Body Sensor Network: several implants perform autonomous duties. An external Control Unit manages the network and recharge the devices.

interval between recharge sessions and to the size allowed for the device. As a consequence, the casing should as well be modular.

The fixation method, if any, also depends on the device application. For the most IMDs, the device will be kept in place by the surrounding tissues. The housing can be treated with a coating increasing *biofouling*, i.e., colonization of the casing surface by the surrounding tissue.

3.2.3 Deep Implantation

As the device should be exploited at different locations, it might be implanted in tissues far away from the skin. If the device needs to interact with the external world, the link used must take into account the implantation depth, overcome the distance between CU and TR, and deal with the characteristics of the tissues on the path. Those parameters can be foreseen based on the Visible Human Project [98]. That project was run by the United States National Library of Medicine between 1989 and 1995 and consisted in digitalizing the human body (female and male) for 3D visualization. Cadavers were frozen and high-resolution photographs were taken, grinding away up to 1 mm from the top surface of the specimen before each step. As a result, images of the body "slices" from head to toe are achieved. In the perpendicular plane, computed tomography visualized the body from arm to arm.

Implant depth can range from some millimeters (for a subcutaneous device) to tens of centimeters (e.g., for an implant in the abdomen).

3.2.4 Size

The target size of an ideal device is of course the smallest possible and the weight is as light as possible. Its dimensions and weight are strongly dependent on the implantation location: the IMD must be small

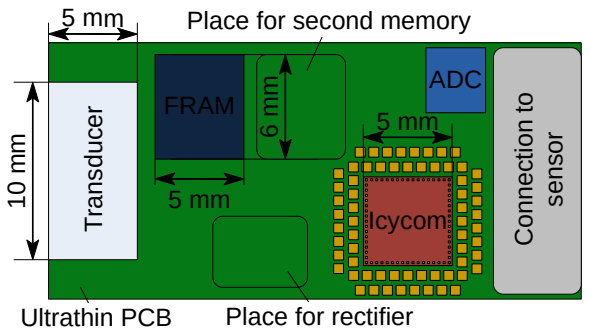

(a) Top view

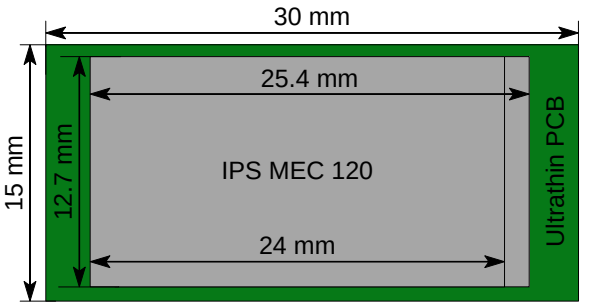

(b) Bottom view

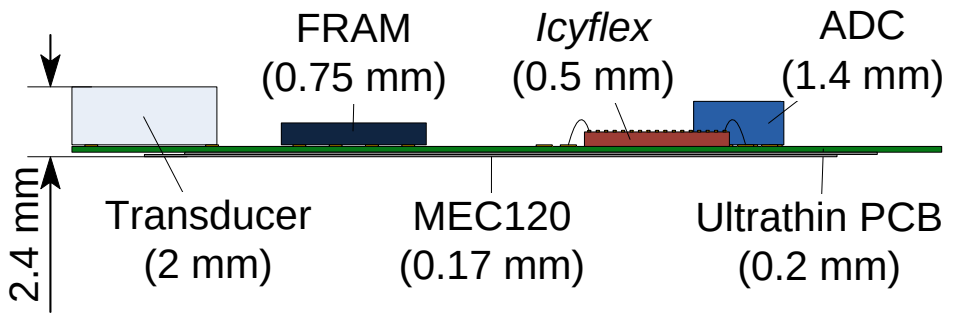

(c) Side view

Figure 3.2: Thin electronics concept for reducing the Implanted Medical Device size.

compared to the surrounding organs, in order to not impact their performance. The implantation method further affect the maximum allowable size of the device. The ideal implantation technique towards minimal invasiveness consists in inserting the implant into a blood vessel through a catheter. The position of the device can be monitored by X-rays, and the device is fixed at the intended site. According to the application, the maximum acceptable size is also influenced by the device shape. In some cases, an ultra-thin device could be an interesting option, as it could adhere to flat body structures.

Figure 3.2 visualizes this concept by an example of device. Keys of the thin-device strategy are the choice of an ultra-thin battery, an ultra-thin PCB, and the clever choice and disposition of further components. An appropriate casing, not shown in the figure, should be conceived.

Pushing the concept further, a flexible ultra-thin device could be imagined. This would impose that all the device components are flexible, including the sensor or actuator, or small enough to not disrupt the bending. Both solutions, on the other end, are not general approaches to IMDs. The best choice for a general implant is therefore a stiff housing with the smallest dimensions. As a reference, the target size of the IMD developed within the ULTRAsponder project was 2 cm^3 for a weight of about 10 g.

3.2.5 Long-Term Implantation

Another crucial requirement towards the ideal IMD is a long-term implantation. Reason for this is the potential implantation depth, which makes it unpractical to explant the device. In order to be competitive with commercial devices, future IMDs must ensure at least ten years of maintenance-free implant life.

To carry out device operations over a long period of time, internal batteries need to be sized accordingly. To keep an acceptable device size, the device conception must focus on rechargeable batteries.

An ideal implant, and in particular a long-term implanted device, should also not interfere with the external world, in order to avoid malfunctioning, and it should not prevent other medical treatments.

Finally, long-term implants require excellent biocompatibility over time, thus increasing the constraints on housing materials.

3.2.6 Biocompatibility

The IMD must possess some characteristics in order to be compatible with the surrounding tissue. Long-term implants are particularly concerned by these restrictions.

Biocompatibility is first of all conceived as the absence of adverse response from the body to the implanted device.

For the integrity of the device itself, the packaging material should be resistant to chemical attack by the surrounding tissues. In case of metallic materials, they should not be oxidized by the oxygen dissolved in the blood and in other body fluids. They must be compatible with the wet environment, containing acids (in gastric fluids for example) and salts.

Casing materials can be intrinsically resistant because of their chemistry, or they should undergo a surface treatment, for example by coating on them a passivation layer, which should last for the entire device life.

Intrinsically oxidation-resistant material are for example gold, platinum, magnesium, and zinc. Their oxidized form is either chemically less favorable than their pure form, or the oxidation process takes place at a very slow rate. Some other materials, such as titanium and stainless steel, do oxidize, but their corrosion products form an ultra-thin passivation layer, which prevents further degradation. Contrary to applied coating on corroding materials, this spontaneous passivation layer regenerates if damaged.

The chemical and physical reaction of the casing with the surrounding tissues also plays a very important role. The IMD must be in contact with the tissue, in order to sense and/or deliver drugs. For this reason, formation of a fibrotic, inert tissue around the implant must be avoided.

Also, for the protection of the living tissues, the casing should not release undesired chemicals into the surrounding medium. As a particular example, leakage from the internal battery should not occur, and it must be at least stopped by an hermetic casing.

The casing also protects the electronics from mechanical stress, which can be more or less important depending on the implantation site.

Biocompatibility is also a matter of size and shape of the device. IMDs need to target a shape having the smallest external surface and avoiding sharp edges, which could hurt the surrounding tissues. The shape should be adapted to the natural movement of the surrounding organs. Also, the casing should not offer attachment sites for bacterial colonies. The preferred shape is in many case a cylinder with rounded endings.

Another constraint on the housing material is given by the sterilization of the IMDs prior to use. Potentially infectious agents must be neutralized before the device is implanted, in order to avoid immune reaction from the body. Sterilization relies on high temperature and high pressure. Currently used methods are sterilization by autoclave, in which the device is held at 121-132 °C at 1-2 bars for 5-45 minutes, or sterilization in an ethylene oxide gas (EtO) environment, at a temperature of 25-75 °C under 2 bars for 1 to 12 hours. The device housing must be able to withstand the sterilization without degradation.

The casing will have an influence on the energy transmission, which has to be taken into account.

Finally, all the characteristics mentioned above should be maintained through the whole life of the implant.

3.2.7 Autonomy

The ideal IMD is an autonomous system carrying out both a sensing and an actuating role, in which the sensor part adjusts the actuator delivering drugs or electrical impulses, in a closed feedback loop.
The device will autonomously evolve through a series of states, in order to complete its tasks. The processing unit is therefore the core of the device: it drives the different components, treats the sensed data, controls the actuation signals, if any, and manages the communication with the external world or the rest of the BSN.

In order to be autonomous, the implant should possess a local energy source, for example a battery, which should reliably supply power. The long-term requirement imposes an intelligent management of the power consumption, in order to most effectively exploit that local energy storage. The internal processor should shut down the components not required for the current task.

Even if the device works autonomously, it will need to connect wirelessly with the external CU for data communication. The implant could for example alarm the CU when a physiological parameter reaches a critical level; when a series of sensing have been acquired, the TR should communicate them to the CU; the device could inform the CU about technical problems; the CU could reprogram the TR according to new therapy requirements.

In order to keep the device as small as possible, but achieving long-term, autonomous applications, the local battery could be recharged by the CU during the data transmission sessions.

Unfortunately, this approach may not be applied to lifesaving devices, such as cardiac implants as in this case the power supply of the device cannot fully rely on an external recharge. The patient may tend to forget to perform the recharge or perform it inefficiently.

A relevant choice in the device design is whether or not the implant will receive modulated instructions from the CU. If this is the case, the TR must have a demodulation circuitry. This would allow programming the device function from the external world, thus best targeting the therapy or sensing. On the other hand, avoiding the additional circuitry would make the implant simpler, cheaper, less power consuming, and increase the reliability of the system.

3.2.8 Connection to a Control Unit

As already stated, the autonomous device must interact with the external world, and more precisely with the external CU. The internal state machine is partly autonomous and partly driven by inputs coming from the CU. Connection to the CU is necessary to download the sensed data, and to monitor the working state of the device. Also, the link between CU and TR is necessary to recharge the local energy source of the implant. Figure 3.3 visualizes a general algorithm for an autonomous sensing device interacting with a CU. When no external stimulus is received, the implanted device is in sleep mode (*TR idle*) and wakes up at predetermined times (e.g., each 24 hours) to autonomously sense the required parameter (*TR senses*). Once in a while , the CU is put in contact with the implant, in order to download the data sensed and to recharge the TR. The CU sends energy wirelessly and the TR treats the incoming wave to recharge its internal battery (*TR under recharge*). While recharging, the TR sends back its internal battery level (*TR sends Vbat level*) at regular intervals (e.g., each 2 seconds). In this way, the CU has a feedback on the successful wave transmission. As soon as the battery in the TR reaches a sufficient

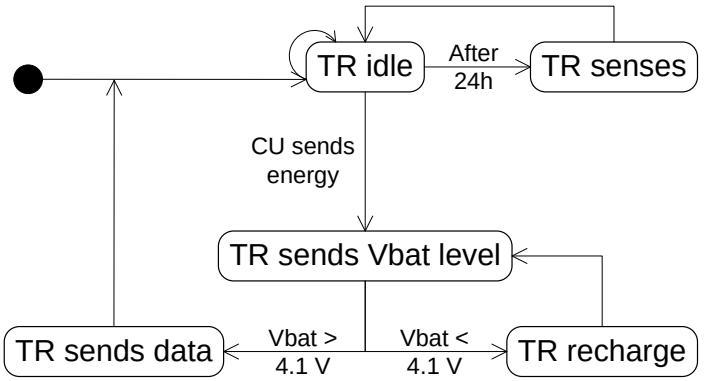

Figure 3.3: Example of an algorithm for an implanted sensor device.

level of charge (e.g., 4.1 V), the TR accesses its internal memory and sends to the CU the stored data (*TR sends data*).

Acceptable duration of the connexion phase varies according to the application, to the device characteristics and, if possible, to the patient's requirements. A small device carrying out a particularly power consuming task will need to be recharged more often than a device with less size constraints, and thus with larger batteries. Based on informal discussions with surgeons and usual practice, a recharge period of approximately 30 minutes each week seems acceptable for chronic measurement in human. For devices implanted in animals for research purpose, it can be imagined to sedate the animal during connection periods, or to take advantage of periods in which the animal is kept in a tight environment or in a particularly still position (e.g., eating time or periodical medical check). The appropriate data sensing frequency depends on the target application and on the available electric power.

The CU itself may need to be connected to the external world, for example in oder to raise an alarm to a medical doctor when the physiological parameters are indicating a disease. This connection can be performed by standard techniques relying on electromagnetic waves. It is therefore not a challenge addressed in this work.

3.2.9 Ultra-low power consumption

In order to best exploit the internal power supply, and to keep the recharge events as infrequent as possible, the implant should operate at very low power. The integrated microprocessor should be able to efficiently power up and shut down components when needed and according to their power consumption in normal, sleep mode, and during their wake-up time. During the idle state between two sensing events, only a timer will be active,while the other components will be in sleep mode. In order to reduce power consumption, each component must be chosen accordingly. The ability of placing each component in hibernation, and their wake-up time, are particularly important.

As an example, Figure 3.4 represents the power consumption expected from a device containing a microprocessor and a sensor. The microprocessor consumes about 2 mW when in full activity, and only 2 µW in sleep mode. The sensor consumes 1 mW when in activity and will be powered up only during sensing time. Its wake-up time is 0.4 s. The device is programmed to perform a measurement each day during 5 s.

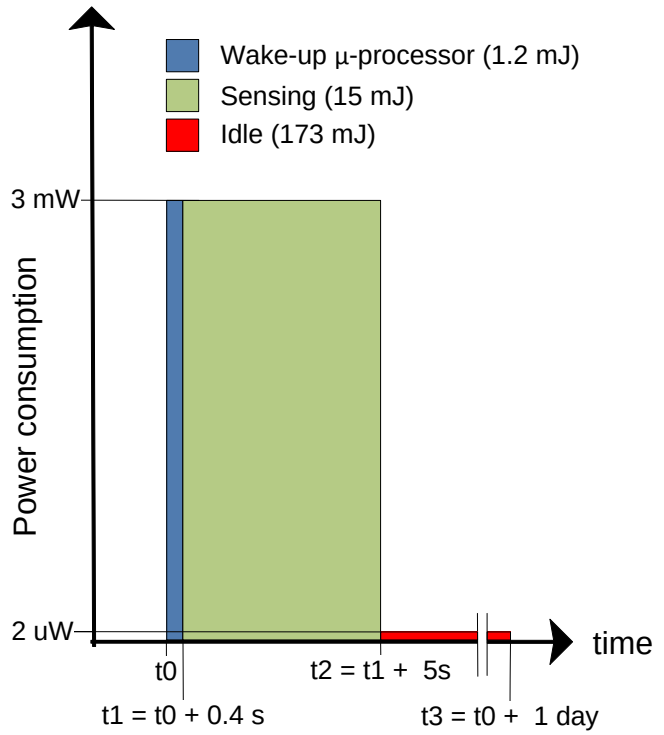

Figure 3.4: Chronograph of a possible device sensing 5 s per day.

It is important to notice that the power consumption during the idle state can account for almost the totality of the power budget, even if the device consumes thousand times less when in sleep mode. Indeed, the most relevant parameter in chronic sensor devices is the power consumption while waiting for the next sensing event.

3.2.10 Cost

Finally, the IMD should be produced at a cost appropriate to the target application. Ideal IMDs, as described in this chapter, are intrinsically cost efficient. Minimally invasive techniques ease the implantation process and shorten the patient's recovery, thus decreasing the hospitalization costs.

Long-term devices result in a lower quantity of implants for a single patient in a lifetime. Therefore, the single implant can be amortized over many years.

Wireless recharge methods release from the need of explanting the device in order to change the local batteries. This results again in less hospitalization and hardware costs.

A generic, modular device platform, such as developed within the ULTRAsponder project, can ideally be the basis for many applications, which will differentiate by the sensor or actuator. The design costs of a device would therefore be reduced.

Finally, the development of more performing, longer term, smaller, autonomous devices opens up new application possibilities. The market of IMDs is just emerging.

Table 3.1: Attenuation comparison of ultrasound, RF, and magnetic induction.

Attenuation @ 10-20 cm	
Ultrasound	8-16 dB (@ 1 MHz) [28]
RF	60-90 dB (@ 2.45 GHz) [115]
Magnetic Induction	50 dB (@ 1 MHz, @ 13.5 MHz) [115]

3.3 Gap between the state of the art and the ideal implant

Technologies answering to the single challenges of IMD design partly exist. Nevertheless, a global approach, integrating different technologies into an efficient device, still lacks. Following sections report on some aspects which would improve an IMD.

3.3.1 Energy and communication carrier

In order to fulfill the requirements of deep implantation and size, a carrier must be chosen, which is able to travel through the body.

3.3.1.1 Carrier type

Wireless transfer of energy is already exploited by many medical devices, both in medical domain and in day-to-day life. Most of them rely on electromagnetic waves [96]. According to the application, either the magnetic or the electric component of the wave is predominant.

Nevertheless, electromagnetic waves have some drawbacks, which jeopardize the achievement of the key characteristics of an ideal implant. Mechanical waves, specifically ultrasound, are hereafter proposed as an alternative wireless carrier, because of their very promising characteristics.

Energy transfer efficiency in deep implanted device: ultrasound propagates very well in body soft tissues, which have similar characteristics to water. Proof of this fact is the wide use of ultrasonic waves for prenatal imaging. The acoustic intensity varies on the distance according to a diffraction inverse-square law, and undergoes an attenuation of about 0.3 dB/cm due to the absorption on the tissues. Radiation at depth up to 20 cm can be achieved.

On the contrary, electromagnetic waves can only penetrate a few cm into the body, because of tissue dielectric nature. Deep implants can therefore not be achieved.

Both RF and magnetic induction proved to be less efficient than ultrasound for implant distances bigger than 10 cm and for antenna sizes smaller than 10 mm, as described by Denisov *et al* [22]. Table 3.1 summarizes the attenuation constants retrieved from the works of Duck [28] and Yamada *et al* [115].

Furthermore, the transmission efficiency in magnetic coupling strongly depends on the alignment of the primary and secondary coils. An accurate positioning and a sufficiently big coil dimension are required for efficient energy transmission. The penetration depth is linearly dependent on the coil size. This is a major obstacle to reduced implant size and deep implantation.

Ultrasonic transmission relies on piezoelectric materials, i.e., on materials having the ability to translate an electrical flow into a mechanical strain, and vice-versa to create an electrical potential when submitted to a mechanical stress. The efficiency of the process depends on the material piezoelectric coefficients, and on its thickness, which is in the order of magnitude of the wavelength.

Several small piezoelectric elements allow beam-forming, which compensates the diffraction effect for long distance transmissions. The dimension of the elements depends on the working frequency chosen.

As a result of its properties, ultrasound allows conceiving small transducers and radiation deep into the body, which fulfills the requirements of small size and deep implant.

Compatibility with MRI: the proposed implant is intended to be a long-term device, and it addresses chronic diseases. The compatibility of the device with MRI is very important, because a patient carrying the implant should not be automatically excluded from using this diagnosis tool.

Ultrasound is intrinsically compatible with MRI, because it exploits a different physical carrier (mechanical vibration) which is not affected by the magnetic field produced in the MRI facility.

Electromagnetic waves on the contrary are strongly affected by MRI equipment, possibly inducing high currents in the device. Especially magnetic induction may therefore not be compatible with MRI.

Compatibility with external radiators: the long-term IMD will be part of the patient's everyday life. It must therefore be as inconspicuous as possible. Given the wide distribution of mobile phones, electronics, and wireless devices, the interaction of an IMD with those radiators is a pertinent question.

Ultrasound is immune to external electromagnetic radiation, because it is a different type of wave. Ultrasound will not interfere with mobile phones or medical machinery. This is a big advantage with respect to recharge systems based on electromagnetic radiation or magnetic induction. EM waves surely can be exploited for energization and communication with an implant, but particular care must be taken and particular exposure must be avoided. Ultrasound on the contrary is natively compatible with external electromagnetic sources.

Hacking prevention: as for today, wireless driven medical devices have no particular protection protocol regarding the CU. The risk exists for IMDs to be maliciously controlled or deactivated, by communicating on the same frequency as the CU [43]. Even though no attack has been carried out until now, the risk is concrete and the potential effects of the attack are frightening, e.g., for implanted drugs pumps, on which the life of the patient depends. This is no blocking point on the use of wireless communication strategies, but may require in the future the development of a more complex implant electronics, providing wireless security for the communication [23].

An advantage of ultrasound compared to electromagnetic waves, which propagate in air, is that mechanical waves require a non-gaseous medium in order to be efficiently propagated. Therefore, no malicious intervention can occur without contact with the patient's skin.

Patient safety: any kind of energy transfer between an external CU to the IMD has an effect on the patient's body. In case of electromagnetic wave, this consists essentially in a current flow induced in the tissues. For ultrasound, it is a cyclic displacement of the tissue particles around their initial position. For both carriers, the main result is heat production inside the tissues, which should not exceed a certain limit. For both electromagnetic and mechanical waves, regulations set the maximum intensity that can be safely sent to the implant without adverse bioeffects [1, 94].

Given the low electrical impedance of tissues and the spherical wave front of EM, the beam will highly spread into the body, and the "useful" intensity reaching the implant will be a small part of the power originally sent. The most part of the electrical power will contribute to the heating of the surrounding tissues.

On the contrary, ultrasound in soft tissues essentially propagates in the longitudinal direction and undergo small attenuation on the propagation path, so that the implant receives a bigger share of the acoustical power sent by the CU, thus affecting less the surrounding tissues.

This is beneficial to the patient, as (almost) only the power required for the implant needs to be sent, and the adverse bioeffects are reduced.

For all these reasons, the exploitation of ultrasonic waves is preferred over magnetic induction for the application targeted in this work, i.e., small, deep implanted, long-term medical device.

3.3.1.2 Carrier frequency range

Given the choice of ultrasound as a carrier for energy transfer between the external CU and the implanted TR, the choice of the working frequency is very relevant.

The influence of the wave frequency on the characteristics of ultrasound is presented in more detail in Chapter 4, and it is shown that an appropriate frequency for the application can be chosen, which minimizes adverse bioeffects.

The system presented in this work exploits wireless transmission to two different aims: energy transfer from the CU to the implanted TR, and communication of the data from the TR to the CU by backscattering. In both cases, the carrier is generated by the CU. In principle, a lower frequency could be used during energization, in order to face less attenuation and more efficiently recharge the implant. Conversely, higher frequency is advantageous during data transmission, in order to increase the data rate of the backscattered signal and achieve shorter communication sessions.

3.3.2 Ultra-low power consumption

In order to optimize the power consumption during autonomous operation of the implanted device, low power components must be chosen.

Moreover, as the system will be in idle state most of the time, an intelligent strategy for switching the components on and off should be elaborated. Therefore, the microprocessor is a key element of the system. Its power consumption when inactive should ideally be in the order of magnitude of few μW. The power budget for the whole system, i.e., when all components are switched on, should remain below 10 mW.

Further action can be taken in order to reduce the energy spent during communication with the CU. The energy required to create the wave on which the information will travel accounts for most of the power consumption. This is reduced by the backscattering principle exploited in the ULTRAsponder project, as it lets the CU create the communication carrier (e.g., the ultrasonic wave) and the carrier on TR side is modulated by varying its input impedance. This requires little power, to basically switch on and off an additional circuit element. This mismatches the power transfer, thus reflecting the incoming wave to different extents.

3.3.3 Casing

Among the biocompatible materials, titanium is the most suited option for long-term devices.

Unfortunately, titanium has a non-negligible effect on ultrasonic waves, which will be exploited as energy and data carrier. Titanium acoustic impedance (22.5 MRayl) is about 20 times bigger compared to that of the human body (about 1.5 MRayl). It will therefore induce an acoustical mismatch and will act as a barrier: ultrasound will be partially reflected off it. The energy transfer will be inefficient. An appropriate impedance matching layer in the transducer can adapt the acoustic transmission and compensate the effect of titanium.

From another perspective, the influence of the titanium layer on the ultrasonic transmission depends on its thickness. Therefore, an ideal implant exploiting ultrasonic link would ideally have a casing as thin as possible.

On the other hand, the casing should protect the electronics inside the device, both from chemical and mechanical degradation agents. A housing-less device is not (yet) conceivable.

An important technological challenge to overcome for the next generation of IMDs will therefore be the development of a housing layer compatible with ultrasonic energy transfer while ensuring sufficient protection to the electronics of the implant. This basically means to have a housing which is as thin as possible, at least in the region of the transducer.

Thin layers of titanium can be either manufactured by deposition, maybe even directly on the piezoelectric transducer, or locally thinning a thicker titanium plate on the position of the transducer.

Thinning down appears most advantageous when transducers are small with respect to the housing size. This allows the preservation of the thickness, therefore the mechanical strength, in the rest of the casing.

3.3.4 Choice of electronic components

Each component of the implant electronics plays an important role towards meeting the characteristics of the whole device. All components should be MRI compatible: the metals contained in them must be non-ferromagnetic, i.e., not sensitive to the fixed magnetic field created in the MRI equipment. Also, all of the electronics must be able to stand the chosen sterilization procedure (e.g., high temperature), which depends on the target application. In addition to that, the different components have their own requirements. An overview is hereafter presented.

Battery: A very crucial component of the targeted device is the rechargeable battery. The size plays a major role, as well as the form fitting the casing geometry. In order to allow long-term implants, the battery should be able to be recharged as many times as possible. Ideally, the battery should not contain biohazardous materials. At least, liquids should not leak from the electronics into the body. For these reasons, ultra-thin solid state batteries are the ideal solution.

Memory: A non volatile memory is required inside the implanted device, in order to store both the instructions needed by the microprocessor to perform its actions, and the data coming from the sensor. For a given size, the more data that can be stored, the better the choice. The memory chip, like the other components of the implant, should be non-ferromagnetic, in order to preserve compatibility with MRI. This leads to the choice of Ferroelectric Random Access Memory (FRAM) devices, which store the data into a ferroelectric layer instead of a dielectric layer. The ferroelectric layer reacts to an electric field according to a hysteresis loop. Similar to ferromagnetic materials, which are constituted of semi-permanent magnetic dipoles, ferroelectric materials contains semi-permanent electric dipoles in their crystalline structure: when an external electric field is applied across the storage cell, the dipoles tend to align themselves with the field direction. After the charge is removed, the dipoles retain their polarization state. Binary "0" and "1" are stored as one of two possible electric polarizations in each data storage cell. Due to the ferroelectric layer, and contrary to other memory types based on a ferromagnetic layer, FRAM is insensitive to magnetic fields, thus compatible with MRI. Power consumption is reduced, because FRAM does not require DC-DC converters like other non-volatile memories. FRAM has an extremely high endurance, which is well suited for long-term implants. Its speed is much higher than other non-volatile memories.

Microprocessor: the microprocessor will be the core of the implanted device: it will manage the power management circuitry, enable the recharge of the internal battery or the use of the stored power for sensing/actuation operations. It will drive and set up the sensor/actuator and store the sensed data. During connection periods with the CU the microprocessor will retrieve the data stored in the memory, condition them into a modulated message, and drive the backscattering circuitry. The microprocessor

contributes to the power budget of the implant in several ways. It contributes directly with its own power consumption, which must therefore be as low as possible. As an indirect contribution, the microprocessor drives the implant components, wakes them up or shuts them down according to the chosen power saving strategy, thus reducing the power consumption to the minimal needed for the operation.

Sensor/Actuator: the sensor or actuator is the component differentiating the devices according to the application, while the rest of the implant is conceived to be as generic as possible and able to adapt to many sensors/actuators. In itself, the component should be as low power as possible. An appropriate connection between this active block and the TR electronics must be foreseen. A front-end circuit will care about the exchange of data and operation commands. A necessary part of this interface is an Analog-to-Digital Converter (ADC), which will convert the sensed parameter (analog) into a digital signal. The microprocessor can then interpret that signal into a data to be stored in the memory. Vice-versa, in the case of an actuator, it will drive the actuator in an efficient way.

3.4 Scientific and Technological impact

If the described challenges can be overcome, uncountable new possibilities for diagnostics, therapy, and research can be conceived. Better diagnosis could be achieved, wherever a continuous, long-term monitoring of physiological parameters in real life conditions is required. In this domain, future applications of next generation IMDs may include:

Congestive Heart Failure (CHF): Heart failure is a condition in which the heart is not able to efficiently deliver blood to the body. In many cases, fluids are accumulated inside tissues, and cause swellings in the lungs (pulmonary edema) or in the legs. This particular case is called CHF. The heart tries to compensate its inefficiency by beating more often and stronger. Therefore, the heart walls thicken. At the same time, the kidneys retain more salts, in order to increase the blood quantity at disposal. This causes even more fluid accumulation, thus leading to a chronic condition and a sure weakening of the kidneys. Ability to monitor the change in size of the heart would be a very precious tool to predict heart failure. Also, the size would indicate the level of heart congestion, so that the therapy can be tailored to the patient's need: the exact amount of drug could be delivered, and the moment of major need could be chosen. Ambulatory monitoring is costly and greatly impairs the patient's autonomy. Continuous monitoring [12] and home-monitoring [15] would be very beneficial.

Myocardial Ischemia: This disease is generally associated with increasing Left Atrial Pressure (LAP). At the moment, no efficient mean is available to monitor LAP. Ritzema-Carter *et al.* [83] presented a LAP monitoring device able to detect Myocardial Ischemia. Challenge for future IMDs is to be implanted directly inside the atrium for a long term, deliver the necessary information to diagnose ongoing Myocardial Ischemia, and possibly give an alarm before irreversible damages occur.

Hypertension: An IMD small enough to allow intra-vascular pressure monitoring would ease the diagnosis of hypertension and its therapy. As an example, the precise shape of the blood pressure variation could be obtained, instead of a minimum and maximum value. The peaks of blood pressure could be detected and treated, and links between blood pressure and external environment may be assessed. Schmitz-Rode *et al.* [90] developed an IMD for telemetric intra-vascular blood pressure monitoring. Refinements of the transmission technology are needed to extend the transmission distance between capsule and reader antenna.

Smaller and deeper implanted devices would also allow several IMDs in the body. This would be extremely beneficial in neural stimulation, for example for chronic pain treatment. Nerves in several locations could be stimulated, for a more efficient effect. Also, the diagnosis of back pain and its

evolution could be better understood. As an example, Brisby *et al.* [13] proposed a system to investigate the concentration of nitric oxide in the joints between the vertebrae in patients with chronic low back pain.

Finally, optimized IMDs would boost the medical research possibilities, by allowing closer observation, thus helping understanding physiological mechanisms. Some examples of mechanisms, which surgeons would like to explore are:

Arterial pressure variation over 24 hours: The human body behaves according to a circadian rhythm, that is to say its physiological parameters display oscillation of about 24 hours. It would be very interesting to study the variation of arterial pressure over the course of a day, and to understand which external or internal cues influence it. In order to do this, long-term, easily implanted, and self-expelled IMDs should be developed.
Another aspect to be improved concerns the type of measurement performed. Currently, blood pressure is measured at the circulation periphery (e.g., on the arm). There the pressure variations, corresponding to the heart beat phase, are dumped according to the blood vessel compliance, which is related to personal morphology, size of the vessels, and atherosclerosis. Therefore, only the maximum and minimum pressure value can be exploited. On the contrary, a sufficiently reactive sensor could retrieve information about the blood pressure dynamic as well (i.e., its instantaneous changes), which would give more insight into heart activity. To do this, the measurement must be performed right inside the heart. Therefore, the IMD must be very small and easily reach and stay in the heart chambers. Wang *et al.* conceived a soft catheter [111] inserted in the heart of laboratory mice, in order to test the effect of different drugs and external factors on heart activity during the day [110].

Diabetes evolution: The causes of diabetes mellitus type 2, which arises with age, are not yet understood. A genetic predisposition was observed, but external cues surely intervene, such as lack of physical activity and alimentary habits. Minimally invasive IMDs could be deployed in healthy subjects, both with familiar history of diabetes or with none. This could allow observation of the disease in its early stages and understand its evolution. Also, larger screening for diabetes in people at risk would be beneficial, because this disease has a prolonged asymptomatic phase [106]. Detection at an early stage would prevent complications.

Idiopathic Pulmonary Arterial Hypertension (IPAH): Pulmonary hypertension is a condition in which the blood vessels around the lung progressively thicken and eventually leak fluids inside the lungs. This pathology leads to irreversible damage in the lungs, heart failure [100], and early mortality. The disease can be an effect of pre-existent vascular diseases or be congenital. IPAH is a particular form of pulmonary hypertension, which arises spontaneously. Its underlying causes and risk factors could not yet be defined. IMDs offer a promising tool for better understanding the evolution of the disease and thus develop a better treatment. Ideally, a serial monitoring of hemodynamics should be performed in affected patients. Karamanoglu *et al.* [49] proved the link between right ventricular pressure and IPAH. For research purpose, clinicians may also want to monitor healthy cavies and try to induce the disease.

3.5 Conclusion

Implanted Medical Devices have played an increasing role in health care in the last decades and expectations have risen for less invasive therapies, more precise sensing, and continuous monitoring. Despite the remarkable technological advances, among others in device miniaturization, several technical challenges still need to be overcome towards a new generation of IMDs.

Table 3.2: Technical challenges towards a new generation of IMDs.

Challenge	**State of the art**	**Proposed solution**
Power supply	Permanent battery	Recharging
Energy transfer	Subcutaneous	Deep implant
Carrier type	RF, magnetic induction	Ultrasound
Battery	Li-Ion	Solid-state electrolyte
Memories	Flash, EEPROM	FRAM

In this chapter, a set of requirements for a new generation of implants were identified. The long-term aim is an autonomous device containing both sensing and actuating capabilities, to be chronically implanted. To achieve this, several aspects of the device must be taken into account, and a good trade-off must be found. Biocompatibility on the long term, small size, connection to the outside world, and very low power consumption are some key parameters.

A particular system was discussed, composed of an external CU and an implanted TR. Solutions for the communication carrier, the biocompatible casing, and the power consumption were proposed, which can be exploited together. Most important, the compatibility between the ultrasonic carrier and the titanium casing was questioned, and plans for the adaptation were conceived.

Chapters 5 and 6 describe in more detail the device concept and the demonstrators manufactured.

Table 3.2 overviews the main challenges that the new generation of IMD needs to overcome. The ULTRAsponder project, to which the author of this thesis contributed, addresses some of those challenges.

4 Physics of Ultrasound

4.1 Introduction

Ultrasonic waves are a promising carrier for communication to an IMD from the external world. They are especially advantageous with respect to magnetic induction for deep implanted and small devices [22]. For this and other reasons, the system presented in this thesis work exploits ultrasound as a carrier for both energy and data transfer. Another very important feature of the implant proposed is its biocompatible casing, made of medical grade titanium. This material has a strong effect on ultrasound. It is therefore to investigate if an ultrasonic link can be established through a titanium casing, and under which conditions.

The main goal in this chapter is to demonstrate that ultrasonic propagation through titanium can be achieved, given an adapted design of the casing. As a related topic, the characteristics of the wave are defined, which best suit the intended application in human body. The physics governing ultrasound is presented, both for application in fluids and in solids. Significant characteristics of the ultrasonic transmission are explicitly calculated, such as the wave intensity and the acoustical impedance of the material. The effects of ultrasound on tissues are presented and the wave characteristics are adjusted in order to minimize the adverse bioeffects. The theory presented follows the procedure and the demonstrations of the book *"Basics of biomedical ultrasound for engineers" by H. Azhari* [3].

A model of the proposed transmission chain between the Control Unit and the Transponder is developed, including two piezoelectric transducers and a medium representing the body soft tissues. The propagation of ultrasound through the receiving transducer is simulated using a MATLAB® function, based on the Krimholtz Leedom Matthaei (KLM) model [55]. Particular focus is set on the effect of the titanium casing in the ultrasonic path.

4.2 Definition

Ultrasounds are mechanical waves traveling at a frequency higher than the human auditive range ($f \geq 20\,kHz$). They exert a pressure on the medium, cyclically compressing and rarefying the particle network in the direction of propagation. The physical unit of measurement for mechanical waves is the Pascal (Pa), defined as a force (Newton, N) per unit surface (square meters, m^2): $Pa = N/m^2$.

Like any kind of wave, mechanical waves can be classified according to their propagation direction (*longitudinal* or *transversal* waves) and their wave front (*planar* or *circular* waves).

When an object is subject to an *ultrasonic wave*, several physical characteristics have a wave-like variation: the local particle displacement, the particle velocity, and the material density for example.

4.3 Mathematical description

An ultrasonic wave can be represented by the general wave function (in one dimension) $u(x \pm vt)$ where v is the wave velocity, x the propagation axis and t the time. The complete form in three dimensions

substitutes x with $\hat{n}$, the unit vector defining the direction of wave propagation, and $\vec{r}$, the spatial location vector.

$$u(\hat{n} \cdot \vec{r} \pm vt) \tag{4.1}$$

The function complies with the general wave equation

$$\nabla^2 u = \frac{1}{v^2} \frac{\partial^2 u}{\partial t^2} \tag{4.2}$$

The Fourier's theorem demonstrates that any periodic function of period T can be written as the sum of infinite sine and cosine terms, which angular frequencies are $\omega = \frac{2\pi}{T}$ and its multiples 2ω, 3ω and so on. The lowest frequency (ω) is referred to as the *fundamental frequency*, and its higher multiples are known as *harmonics*.

Therefore, the wave function (in one dimension) can be written as $u = A\cos(\omega t - kx + \phi)$, where A is a scaling factor accounting for the amplitude of the wave, ω is the wave frequency, and k the so called wave number. The parameters ω and k take the place of the previously mentioned wave velocity and are linked to it by the relation $v = \frac{\omega}{k}$. By definition, k is linked to the wavelength λ by the relation $k = \frac{2\pi}{\lambda}$, and the wavelength is the displacement of the wave at velocity v after a period ($T = \frac{1}{f}$): $\lambda = v \cdot T$.

Euler's formula $e^{jx} = \cos x + j \sin x$ allows exploiting either the exponential or the trigonometric formulation, as best suited for the calculations. In trigonometric form, the wave behavior is expressed by both the real and the imaginary part. Therefore, it is sufficient to keep either $\sin x$ or $\cos x$ in the calculations.

$$u = A \cdot e^{j(\omega t - kx)} \tag{4.3}$$

4.3.1 Ultrasonic wave in fluids

Mechanical waves, and thus ultrasound, in fluids can be described by the pressure variation inside the medium, due to the change in fluid density. The pressure variation is by definition

$$\Delta p = -\frac{1}{\beta} \cdot \frac{\Delta V}{V} \tag{4.4}$$

where V is the volume and β the compressibility of the fluid at a given temperature.

The displacement of a given point in the fluid under the effect of the ultrasonic pressure can be calculated by considering an infinitesimal volume $V = dx_1 \cdot dx_2 \cdot dx_3$, as depicted in Figure 4.1 and applying Newton's law linking force and acceleration

$$F = m \cdot \frac{\partial^2 \eta}{\partial t^2} \tag{4.5}$$

where m indicates the mass of the considered volume and η is the displacement along the propagation axis x_2.

The change in volume $\Delta V/V$, caused by the pressure applied, can be developed as

$$\frac{\Delta V}{V} = \frac{dx_1 \cdot dx_3 \cdot \frac{\partial \eta}{\partial x_2} \cdot dx_2}{dx_1 \cdot dx_2 \cdot dx_3} = \frac{\partial \eta}{\partial x_2} \tag{4.6}$$

The sum of the forces acting on the volume is

$$F = \left[p - \left(p + \frac{\partial p}{\partial x_2} dx_2 \right) \right] \cdot dx_1 \cdot dx_3 = -\frac{\partial p}{\partial x_2} \cdot V \tag{4.7}$$

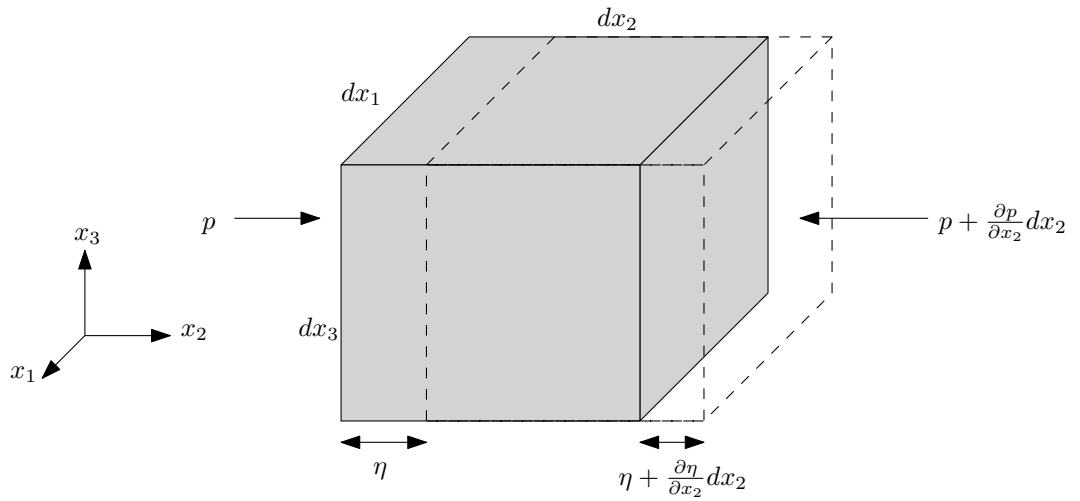

Figure 4.1: Effect of a mechanical wave on a fluid element of infinitesimal volume. *Adapted from Azhari [3].*

and the mass, given the fluid density ρ, is

$$m = \rho \cdot V \tag{4.8}$$

From this and by removing the volume from both sides, the Newton's law results in

$$-\frac{\partial p}{\partial x_2} = \rho \cdot \frac{\partial^2 \eta}{\partial t^2} \tag{4.9}$$

Introducing the notion of *velocity potential* φ, defined as

$$\frac{\partial \varphi}{\partial x_2} = \frac{\partial \eta}{\partial t} \tag{4.10}$$

the equation can be rewritten as

$$-p = \rho \cdot \frac{\partial \varphi}{\partial t} \tag{4.11}$$

Now, substituting eq. 4.6 in eq. 4.4, the expression of the pressure variation Δp as a function of displacement η is obtained

$$\Delta p = -\frac{1}{\beta} \cdot \frac{\partial \eta}{\partial x_2} \tag{4.12}$$

Noting that $p = \Delta p + p_0$ (with p_0 constant) and therefore

$$-\frac{\partial p}{\partial x_2} = -\frac{\partial (\Delta p + p_0)}{\partial x_2} = -\frac{\partial \Delta p}{\partial x_2} = \frac{\partial}{\partial x_2} \cdot \left(\frac{1}{\beta} \cdot \frac{\partial \eta}{\partial x_2} \right) = \frac{1}{\beta} \cdot \frac{\partial^2 \eta}{\partial x_2^2} \tag{4.13}$$

The wave equation can finally be developed as

$$\frac{\partial^2 \eta}{\partial x_2^2} = (\beta \cdot \rho) \frac{\partial^2 \eta}{\partial t^2} \tag{4.14}$$

from which can be derived the wave velocity of the ultrasonic radiation

$$v = \frac{1}{\sqrt{\beta \cdot \rho}} \tag{4.15}$$

To sum up, in an isotropic fluid medium, the behavior of the ultrasonic wave can be completely described by the velocity potential φ, and by the associated particle velocity $\dot{\eta}$, acoustic excessive pressure Δp, and density variation $\Delta\rho$

$$\dot{\eta} = -\nabla\varphi \tag{4.16}$$

$$\Delta p = -\rho_0 \frac{\partial\varphi}{\partial t} \tag{4.17}$$

$$\Delta\rho = -\frac{\rho_0}{\dot{\eta}^2} \frac{\partial\varphi}{\partial t} \tag{4.18}$$

It is important to keep in mind that soft tissues are very similar to fluids when exposed to ultrasound. Hence, the analysis of ulltrasound in fluids apply in first approximation also to the propagation inside the body.

An important characteristic of fluids and soft tissues is the strong attenuation of shear waves, because of the mobility of different fluid layers within the medium. Therefore, almost exclusively longitudinal waves are expected in fluids (and in soft tissues).

4.3.2 Ultrasonic wave in solids

Solid materials, contrary to fluids and gases, support the propagation of both longitudinal and transversal waves. The external forces acting on the volume are measured as a *stress*, defined as the ratio between the force applied and the surface on which the force is applied. In that sense, stress has the same physical dimension and meaning as the (e.g., ultrasonic) pressure. Stress values are defined by both the direction of the force, and the plane on which the force is applied. Stress coefficients σ_{ij} are therefore identified by two subscripts, the first indicating the surface on which they act, and the second the propagation direction. Figure 4.2 depicts the stress vectors acting on a volume element and Equation 4.19 develops the stress tensor σ into its different individual coefficients.

$$\sigma = \begin{pmatrix} \sigma_{11} & \sigma_{12} & \sigma_{13} \\ \sigma_{21} & \sigma_{22} & \sigma_{23} \\ \sigma_{31} & \sigma_{32} & \sigma_{33} \end{pmatrix} \tag{4.19}$$

Every stress coefficient generates a force trying to displace the material. It is therefore intuitive that for every stress σ_{ij} there must be a stress σ_{ji} in the opposite direction, and that those two stresses must be equal: $\sigma_{ij} = \sigma_{ji}$.

As a reaction to stress, the material deforms according to its elastic coefficients C. The *strain* ε measures this deformation and the strain coefficients are indicated as ε_{kl}. The effect of ultrasound in solid materials is a linear-elastic wave, complying therefore with Hooke's law stating that strain is directly proportional with stress. The strain-stress relation can be described by

$$\sigma_{ij} = C_{ijkl} \cdot \varepsilon_{kl} \tag{4.20}$$

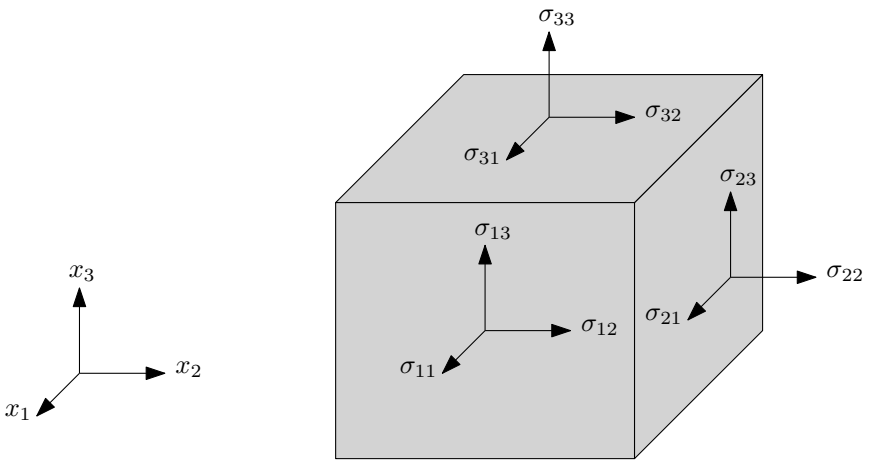

Figure 4.2: Effect of a mechanical wave on a solid element. *Adapted from Azhari [3].*

where σ is the stress, ε the resulting strain, and C is the matrix of elastic coefficients of the material. The accepted approximated definition of the strain coefficients for small displacements (which is the case for ultrasound) is

$$\varepsilon_{kl} = \frac{1}{2}\left[\frac{\partial \eta_k}{\partial x_l} + \frac{\partial \eta_l}{\partial x_k}\right] \tag{4.21}$$

where η indicates as usual the displacement. It is clear from this equation that $\varepsilon_{kl} = \varepsilon_{lk}$. Figure 4.3 depicts a two-dimensional deformation.

Both σ and ε have 9 elements (every combination of the three axis), so that their relation possesses 81 parameters in total. Fortunately, the independent parameters can be strongly reduced keeping in mind that $\varepsilon_{ij} = \varepsilon_{ji}$ and $\sigma_{ij} = \sigma_{ji}$, and in many cases they can be even further reduced. A particularly advantageous case are isotropic materials, for which the independent parameters are only two, so called Lamé parameters.

The elastic properties of a material can be expressed by a series of coefficients, which are linked to each other:

Young's modulus E is the ratio between tensile *stress* and *strain* in one direction, and under the conditions of validity of Hooke's law. Given that the strain is dimensionless, the Young's modulus has the units of the stress, a pressure (Pa). It can be expressed as

$$E = \frac{1D\ stress}{1D\ strain} = \frac{\sigma}{\varepsilon} = \frac{F \cdot L}{A \cdot \Delta L} \tag{4.22}$$

where A is the medium surface perpendicular to the wave propagation and L the length when no wave is applied.

Poisson's ratio ν indicates the cross-influence of strains in perpendicular directions. It is based on the observation that an extension of the material in one direction results in a contraction in a perpendicular direction. Poisson's ratio is defined as

$$\nu = -\frac{d\varepsilon_{trans}}{d\varepsilon_{axial}} \tag{4.23}$$

Bulk modulus B measures the material resistance to an uniform pressure in all directions of a certain volume V. It can be expressed both according to the density variation $\Delta\rho$, or the volume variation ΔV

$$B = -V\frac{dp}{dV} = \rho\frac{\partial p}{\partial \rho} \tag{4.24}$$

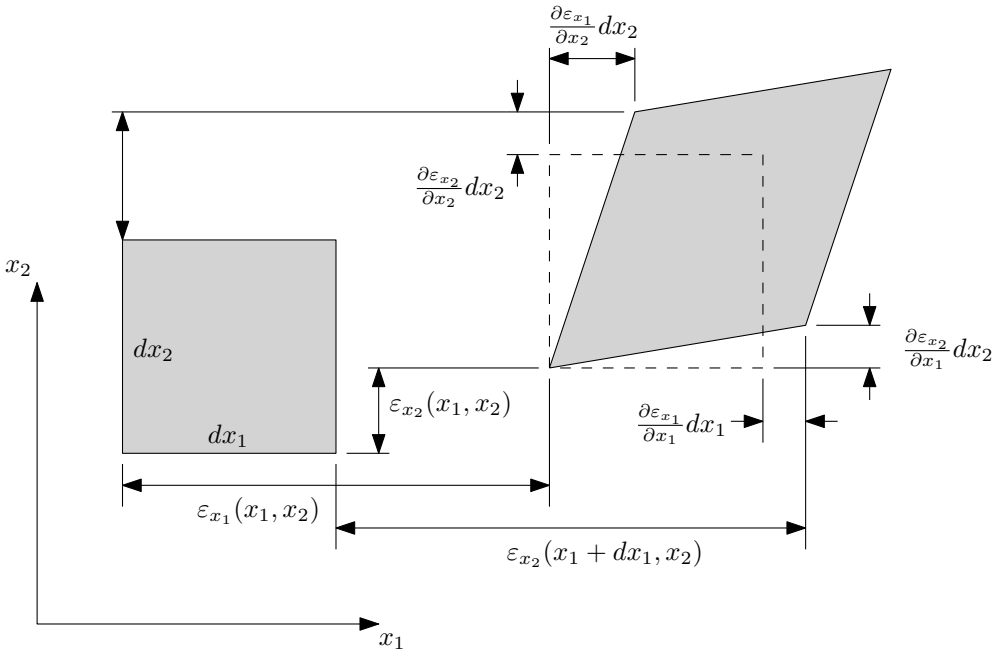

Figure 4.3: Deformation of a 2-dimension shape, evidence of the strain coefficients. *Adapted from Sanpaz [88]).*

Shear modulus G or modulus of rigidity indicates the ratio between a shear stress (i.e., a stress in a direction perpendicular to the wave propagation), and the resulting shear strain. Assuming a wave acting on a surface A on the xy plane of a volume element of length L, and a resulting strain Δx, the shear modulus is by definition

$$G = \frac{\sigma_{x_1 x_2}}{\varepsilon_{x_1 x_2}} = \frac{F \cdot L}{A \cdot \Delta x_1} \tag{4.25}$$

In case of homogeneous, isotropic materials, these coefficients are not mutually independent, but linked by conversion relations, so that two coefficients fully determine all others.

As previously done for the displacement in fluids, the wave equation for the displacement in one direction (e.g., along x_2) can be obtained applying Newton's second law on an element of infinitesimal volume, shown on Figure 4.4.

The Newton's law applied to this case states

$$\Sigma F_{x_2} = m \cdot \ddot{\eta}_2 = \rho \cdot dV \cdot \ddot{\eta}_2 \tag{4.26}$$

where each contribution to the force will be a function of σ_{i2}

$$F_{i2} = \frac{\partial \sigma_{i2}}{\partial x_i} \cdot dV \tag{4.27}$$

$$\Sigma F_{x_2} = \left(\frac{\partial \sigma_{12}}{\partial x_1} + \frac{\partial \sigma_{22}}{\partial x_2} + \frac{\partial \sigma_{32}}{\partial x_3} \right) \cdot dV \tag{4.28}$$

and expressing the stress σ by the elastic coefficient C and the strain ε (Equation 4.20), and expressing the strain ε by the displacement η (Equation 4.21), the resulting wave equation for the displacement is

$$C_{ijkl} \frac{\partial^2 \eta_k}{\partial x_i \partial x_l} = \rho_0 \frac{\partial^2 \eta_j}{\partial t^2} \tag{4.29}$$

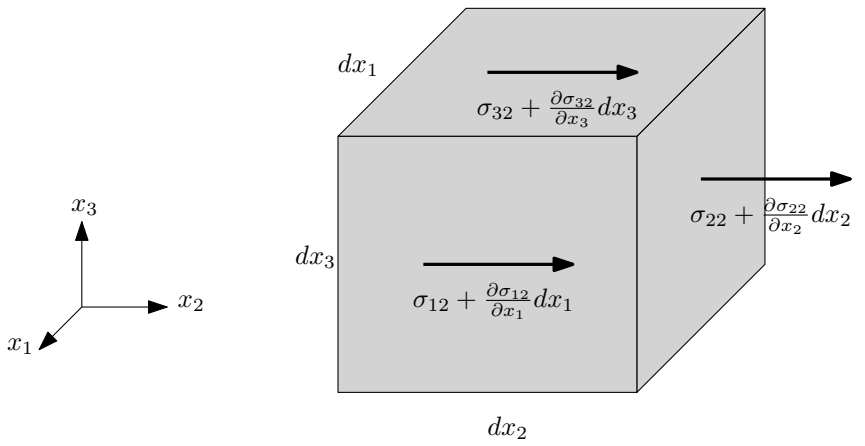

Figure 4.4: Set of stresses on an element of infinitesimal volume. *Adapted from Azhari [3].*

where the indexes *ijkl* indicate the plane and the direction of the stress and the strain. This equation is of course generally valid for each axis, not only for the example given x_2. Writing explicitly the indexes, a system of equations arises.

Now, keeping the assumption that the wave propagation direction lies on the x_i axis (which does not reduce the generality of the notation), the displacement can be described by the general wave function

$$\eta_i = \eta_{i0} \cdot e^{j(\omega t - \vec{k}\vec{r})} \tag{4.30}$$

and the wave equation simplifies to

$$-C_{ijkl} \cdot k_j \cdot k_l \cdot \eta_{k0} = -\rho_0 \cdot \omega^2 \cdot \eta_{i0} \tag{4.31}$$

Or, introducing the notation

$$\eta_{i0} = \delta_{ik} \cdot \eta_{k0} = \delta_{i1} \cdot \eta_{10} + \delta_{i2} \cdot \eta_{20} + \delta_{i3} \cdot \eta_{30} \tag{4.32}$$

where δ_{ik} (Kronecker's delta function) is equal to 1 if $i = j$ and equal to 0 otherwise,

$$(C_{ijkl} \cdot k_j \cdot k_l - \delta_{ik} \cdot \omega^2 \cdot \rho_0) \cdot \eta_{i0} = 0 \tag{4.33}$$

Exploiting the delta function, this equation develops into a system of only three independent equations according to the three axes.

The terms C_{ijkl} are the elastic coefficients of the material, they are therefore known. The unknown are the wave numbers k_1, k_2, and k_3 along the three axes. The solution of the previous system of equations determines the behavior of the displacement wave $\eta(x_i, t)$.

4.3.3 Wave energy and intensity

In order to analyze the energy of an acoustic wave, the medium material should be considered as a matrix of particles, with a certain mass, linked together by spring-like interparticle connections. The incoming wave displaces the particles, therefore "stretching" and "pulling" the interconnections. A purely longitudinal wave is considered, traveling along axis x_2. The kinetic energy associated with a mass m

traveling at a speed v is known by classic mechanics to be $E_{kin} = \frac{1}{2} \cdot mv^2$. In the case of an acoustic wave, following the usual notation for the particle velocity $\dot{\eta}$, it can be written as

$$E_{kin} = \frac{1}{2} m\dot{\eta}^2 = \frac{1}{2}\rho \cdot dV \left(\frac{\partial \eta}{\partial t}\right)^2 \tag{4.34}$$

The wave function for the displacement in its trigonometric form being $\eta = \eta_0 \cos(\omega t - kx_2)$, its velocity is therefore

$$\frac{\partial \eta}{\partial t} = -\eta_0 \omega \sin(\omega t - kx_2) \tag{4.35}$$

The kinetic energy per unit volume will be

$$E'_{kin} = \frac{E_{kin}}{dV} = \frac{1}{2}\rho \left(\frac{\partial \eta}{\partial t}\right)^2 = \frac{1}{2}\rho \eta_0^2 \omega^2 \sin^2(\omega t - kx_2) \tag{4.36}$$

The kinetic energy in a specific point $x_{2,0}$ is equal to the energy at the time t_0 in which the wave passes through that point. By definition, t and x_2 are such that $sin(\omega t - kx_2) = 1$. From that it can be concluded that the wave energy is

$$E' = \frac{\rho \eta_0^2 \omega^2}{2} \tag{4.37}$$

The wave intensity is by definition the amount of energy per unit time and unit volume

$$I = \frac{E}{dV \cdot dt} = \frac{E' \cdot dV \cdot dl}{dV \cdot dt} \tag{4.38}$$

where the length l traveled during dt can be expressed, knowing the wave velocity v, as $dl = v \cdot dt$. Therefore, the intensity of the wave will be

$$I = \frac{E' \cdot v \cdot dt}{dt} = E' \cdot v \tag{4.39}$$

and using Equation 4.37, it results that

$$I = \frac{\rho \cdot \eta_0^2 \cdot \omega^2 \cdot v}{2} \tag{4.40}$$

It is interesting to note that the intensity of the wave is proportional to the square of the angular frequency ω.

4.3.4 Acoustical Impedance

Now that the general behavior of ultrasonic waves in homogeneous media is defined, it is interesting to analyze the effect of a wave crossing different media. In order to do this, the concept of *ultrasonic impedance* Z_{ac} of a medium must be defined, and from that the *reflection coefficient* R and the *transmission coefficient* T can be calculated.

An ultrasonic wave is a pressure gradient acting on the volume element. This pressure gradient will induce strain and therefore displacement in the medium particles. In analogy with Ohm's law for electric circuits, the pressure gradient $\mathbf{p} = p - p_0$ can be considered as a potential differential, and the resulting particle velocity $\dot{\eta}$ as a current. The acoustic impedance Z_{ac} is therefore by definition

$$Z_{ac} = \frac{\mathbf{p}}{\dot{\eta}} \tag{4.41}$$

The ultrasonic pressure effect was previously analyzed in both a fluid (Equation 4.9) and a solid (Equation 4.26). The equations can be rearranged into

$$-\frac{\partial \mathbf{p}}{\partial x_2} = \rho_0 \cdot \ddot{\eta} \tag{4.42}$$

This equation should be expressed in a way that underlines the relation between $\mathbf{p}$ and $\dot{\eta}$. To that end, both sides are integrated along the wave propagation axis (e.g., x_2) and $\ddot{\eta}$ is further integrated along the time. The equation becomes

$$-\mathbf{p} = \int \rho_0 \ddot{\eta} \, \mathrm{d}x_2 \tag{4.43}$$

Given the general form of the displacement wave

$$\eta(x_2, t) = \eta_0 e^{j(\omega t - k x_2)} \tag{4.44}$$

each derivative in time is equal to the function multiplied by $j\omega$. Its second derivative is therefore

$$\ddot{\eta} = j\omega \cdot \dot{\eta} \tag{4.45}$$

and the integral of $\dot{\eta}$ along x_2 is

$$\int \dot{\eta} \, \mathrm{d}x_2 = \int \dot{\eta}_0 e^{j(\omega t - k x_2)} \, \mathrm{d}x_2 = \dot{\eta}_0 \cdot (-\frac{1}{jk}) e^{j(\omega t - k x_2)} = -\frac{1}{jk}\dot{\eta} \tag{4.46}$$

A more detailed and rigorous calculation can be found in Azhari [3].

Equation 4.43 can therefore be rewritten as

$$\mathbf{p} = -\int \rho_0 \ddot{\eta} \, \mathrm{d}x_2 = -\rho_0 \cdot j\omega \int \dot{\eta} \, \mathrm{d}x_2 = \rho_0 \frac{\omega}{k} \cdot \dot{\eta} \tag{4.47}$$

which finally results in

$$Z_{ac} = \frac{\mathbf{p}}{\dot{\eta}} = \rho_0 \frac{\omega}{k} = \rho_0 c \tag{4.48}$$

This relation is valid both for planar and circular ultrasonic waves, under certain conditions. The unit of measurement of acoustic impedance are mega Rayleigh (MRayl), corresponding in the Système International d'unités (SI) base units to

$$Rayl = \frac{kg}{s \cdot m^2} \tag{4.49}$$

Table 4.1 presents the main acoustical parameters for some common materials, for biological tissues, and for some materials used in the manufacture of transducers. Characteristics are retrieved from Zhu [119] and from manufacturer datasheets [41].

The definition of the acoustic impedance links the excessive pressure $\mathbf{p}$ to the wave intensity I. It is known by Equation 4.40 that $I = \frac{1}{2}\rho_0 c \dot{\eta}^2$, and that $Z_{ac} = \rho_0 c$. It is therefore valid that

$$I = \frac{1}{2} Z_{ac} \left(\frac{\mathbf{p}}{Z_{ac}} \right)^2 = \frac{\mathbf{p}^2}{2 Z_{ac}} \tag{4.50}$$

It is important to note a small break in the analogy between the electrical and the acoustical world: while the electric power is by definition the product of voltage and current ($P_{el} = V \cdot I$, expressed in $[W]$),

Table 4.1: Acoustic characteristics of various materials.

Material	ρ [kg/m^3]	B [GPa]	v [m/s]	Z_{ac} [MRayl]
Blood	1025		1570	1.61
Muscles	1070	~ 2.5	1542-1626	1.65-1.74
Bone	1380-1810	~ 10-30	2700-4100	3.75-7.4
Air (0°C)	1.2		330	0.0004
Water (25°C)	988		1497	1.48
Aluminum	2875	~ 100	6260	18
Gold	19290	~ 200	3240	62.5
PZT-5A	7750	~ 150	4350	33.71
Rubber	950	~ 2.5	1550	1.472
Titanium	4500	110	~ 5000	22.5

the product of the corresponding parameters in the acoustical world (applied pressure $\mathbf{p}$ and particle velocity $\dot{\eta}$) gives the acoustic intensity $I_{ac} = \mathbf{p} \cdot \dot{\eta}$ in $\left[\frac{W}{m^2}\right]$.

The factor $1/2$ appearing in Equation 4.50 comes from the trigonometric expression of both pressure and velocity. The same factor appears in the electrical power, when voltage and current are expressed by sinusoidal waves. Given a pure sinusoidal wave of amplitude A, its effective value is equal to $\frac{A}{\sqrt{2}}$. Therefore, the product of two effective values will carry a factor $1/2$.

The acoustical power is by definition the product of force (pressure · surface) and particle velocity, and of course the product of wave intensity and surface:

$$P_{ac} = \mathbf{p} \cdot \dot{\eta} \cdot A \tag{4.51}$$

4.3.5 Piezoelectric materials

Piezoelectric materials are various solids having the property of reacting to an exterior pressure with an electric potential, and which viceversa generate an internal mechanical strain in response to an external electric potential. Such materials include for example crystals (e.g., SiO_2, $LiNbO_3$, $LiTaO_3$) and particular ceramics such as $BaTiO_3$ and Lead Zirconate Titanate $Pb(Zr_{1-x}Ti_x)O_3$ (PZT). Plastic polymer PVDF (polyvinylidene difluoride) has a piezoelectric behavior beyond 100 MHz. Strictly speaking, even several biological materials exhibit a certain degree of piezoelectricity, for example DNA molecules, tendons, and bones.

The piezoelectric characteristics of the material can be described by linear relationships between stress σ and strain ε on mechanical domain, and electric induction (electric charge density displacement) D and electric field E on electrical domain.

Several piezoelectric coefficients can be defined. The most relevant are the *direct piezoelectric coefficient d*, measuring the variation in charge displacement due to the applied stress, and the *inverse piezoelectric coefficient h*, measuring the variation in mechanical stress in the material due to the electric induction:

$$d = \left.\frac{\partial D}{\partial \sigma}\right|_{E=const} \tag{4.52}$$

$$h = -\frac{\partial \sigma}{\partial D}\bigg|_{\varepsilon=const} \tag{4.53}$$

Both the charge displacement density D and the mechanical strain ε will be the combined effect of both a mechanical stress σ and an electric field E. Therefore, the "extended" Hooke's law becomes

$$\sigma = c \cdot \varepsilon - h \cdot D \tag{4.54}$$

The electric field E, which in absence of piezoelectric mechanism is simply proportional to the induction D by the material permittivity ϵ, takes now into account a term due to the mechanical strain:

$$E = \frac{1}{\epsilon} D - h \cdot \varepsilon \tag{4.55}$$

As a reminder, the electric current I is linked to the electric induction D by the relationship

$$I = \iint_A D \, \mathrm{d}x_1 \, \mathrm{d}x_3 \tag{4.56}$$

which for harmonic waves becomes $I = j\omega D \cdot A$, where A is the material surface in the $x_1 x_3$ plane, as opposed to the wave propagation direction x_2.

PZT ceramics are the most used piezoelectric materials for medical purposes, mainly because of their very high piezoelectric and electromechanical coefficients. Care has to be taken when handling ceramics, that the temperature does not overcome their Curie temperature, over which the polarization of the material is damaged. For PZT, Curie's temperature is approximately 150 to 400 °C. This property has an influence on the implants containing PZT material: device sterilization at higher temperature cannot be taken into consideration.

4.3.5.1 Composites and multiple elements

In order to better exploit the piezoelectric behavior of materials, and adapt their characteristics to the target application, particular geometrical structures have been developed.

Piezocomposites are matrix structures of thin rods of piezoelectric material in a polymer ground. A piezoelectric block is cut along its thickness (keeping a common ground) and a polymer is flown in the resulting lines between the rods.

Piezocomposites offers superior piezoelectric characteristics due to the piezoelectric material, but lower Z_{ac} and larger bandwidth, due to the influence of the surrounding polymer. The effective density, acoustic impedance, and wave speed in composite depends on the percentage of piezoelectric ceramic [29, 37].

Multielements transducers follow the same concept but at higher scale: instead of a single thin piezoelectric layer, the active part is constituted of several piezoelectric elements. This optimizes the angular acceptance in reception.

It is important that the pitch between adjacent elements is on the order of magnitude of the wavelength, in order to avoid crosstalk. The effective coupling factor is as high as the free ceramic, because the surrounding polymer is allowing vibration in lateral direction.

Multielement transducers further allow beam forming by commuting the elements used. Different electric signals can be sent on each element, in order to focus the beam. Spatial sweep in a region is possible by varying the input to the elements, according to a sequence. For penetration in very inhomogeneous media, which attenuate the wave by scattering in various directions, time reversal techniques can be exploited: the input on the single elements is adapted based on the backscattering [17, 36, 114].

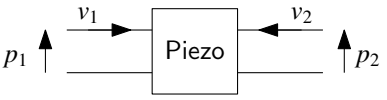

$$\begin{pmatrix} p_1 \\ v_1 \end{pmatrix} = T \cdot \begin{pmatrix} p_2 \\ v_2 \end{pmatrix} \tag{4.57}$$

$$\begin{pmatrix} p_1 \\ p_2 \end{pmatrix} = Z \cdot \begin{pmatrix} v_1 \\ v_2 \end{pmatrix} \tag{4.58}$$

Figure 4.5: Schematics and equation of an acoustic transmission line.

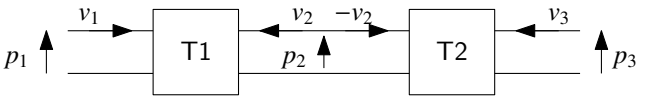

$$\begin{pmatrix} p_1 \\ v_1 \end{pmatrix} = \underbrace{T_1 \cdot \begin{pmatrix} 1 & 0 \\ 0 & -1 \end{pmatrix} \cdot T_2}_{T_{12}} \cdot \begin{pmatrix} p_3 \\ v_3 \end{pmatrix} \tag{4.59}$$

Figure 4.6: Schematics and equations for cascading of two quadrupoles.

4.3.5.2 Network notation

As already seen, the mechanical wave transmission can be described by an acoustic pressure (stress) producing a particle displacement (strain). The mechanism is analog to electrodynamics, where a potential difference (a voltage) displaces electrons and thus produces a current. Acoustic waves can therefore advantageously be described using the network notation.

A passive material in which an acoustic wave travels is a transmission line, which can be modeled as a two-port network element, depicted in Figure 4.5. Their behavior is associated with a 2x2 square *transfer matrix* T , which links the input parameters (p_1 and v_1) with the output (p_2 and v_2), and an *impedance matrix* Z, which links the pressures to the particle velocities.

This representation is particularly useful to describe the transmission through a stack of different materials. Using matrix calculation, the total effect can be expressed by the multiplication of each single matrix.

An acoustic line of transmission, that is to say materials without piezoelectric characteristics, possesses a transmission matrix T defined as

$$T_{passive} = \frac{1}{z_p} \begin{pmatrix} z_p + z_s & -(z_s^2 + 2z_p z_s) \\ 1 & -(z_p + z_s) \end{pmatrix} \tag{4.60}$$

where

$$z_p = -j \frac{Z_{ac}}{\sin k} \tag{4.61}$$

$$z_s = jZ_{ac} \tan \frac{k}{2} \tag{4.62}$$

being k the wave number, depending on the material thickness, and Z is the product of the acoustic impedance Z_{ac} of the material, described in section 4.3.4, times its surface S.

The piezoelectric material behavior in one direction can be described by a three-ports linear element, containing one electric port (injected current I, resulting voltage U), and two mechanical ports (characterized by pressures p_1 and p_2 and corresponding particle velocity v_1 and v_2). Figure 4.7 shows the hexapole schematic and Equation 4.63 resumes the relations between mechanical and electrical domain.

The KLM model [55] decomposes the piezoelectric hexapole in three quadrupoles, as depicted in Figure 4.8. The two acoustical output ports represent the backing and the radiation faces of the

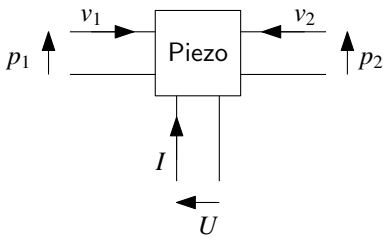

$$\begin{pmatrix} p_1 \\ p_2 \\ U \end{pmatrix} = -j \begin{pmatrix} Z_{ac}/\tan(kd) & Z/\sin(kd) & h/\omega \\ Z_{ac}/\sin(kd) & Z/\tan(kd) & h/\omega \\ h/\omega & h/\omega & 1/\omega C_0 \end{pmatrix} \begin{pmatrix} v_1 \\ v_2 \\ I \end{pmatrix} \quad (4.63)$$

Figure 4.7: Schematic and equation of a piezoelectric element.

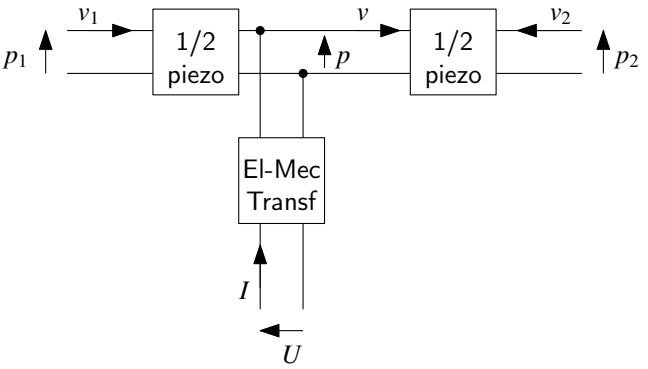

(a) Development of the hexapole.

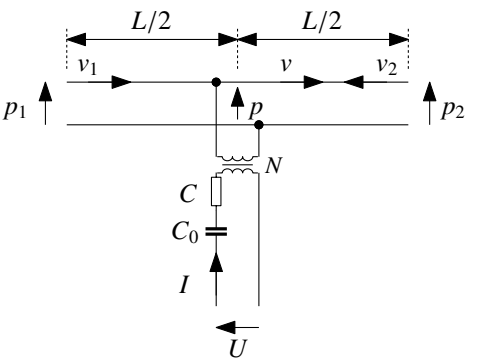

(b) Equivalent KLM circuit.

Figure 4.8: Equivalent KLM model of a piezoelectric element.

piezoelectric element. The two passive quadrupoles "1/2 piezo" account each for a half thickness of the material, and are described by the matrix $T_{passive}$ presented in Equation 4.60.

The active quadrupole accounts for the electric-mechanical transformation, and its transmission function, as modeled by Krimholtz *et al.*, is equivalent to the series of a capacitor C_0, a capacitor C and a transformer N. The capacitor C_0 accounts for the losses and for the permittivity in the piezo material, while C and N are the piezoelectric constant.

The material parameters are listed in Table 4.2.

From the mechanical parameters, the piezoelectric coefficient h, the wave speed v^* under the effect of losses Δ, and the acoustical impedance Z can be extracted [55]:

$$h = \frac{kt \cdot v}{(1 - j \cdot tde)} \sqrt{\frac{\rho}{\epsilon}} \quad (4.64)$$

$$\Delta = (1 - kt^2) \cdot tdm + kt^2 \cdot tde \quad (4.65)$$

$$v^* = v\sqrt{1 + j\Delta} \quad (4.66)$$

$$Z = Z_{ac} \cdot A = \rho v^* A \quad (4.67)$$

Finally, the circuit parameters are defined as follows:

$$C_0 = \epsilon \frac{A}{d}(1 - j \cdot tde) \quad (4.68)$$

Table 4.2: Parameters of a piezoelectric material.

Transducer surface	A
Thickness	d
Density	ρ
Permittivity ($\epsilon_r \cdot \epsilon_0$)	ϵ
Coupling coefficient	kt
Wave speed	d
Tangent of electrical losses	tde
Tangent of mechanical losses	tdm
Total losses coefficient	Δ
Wave speed (with losses)	d

$$C = -\frac{\omega \cdot Z}{h^2 \cdot \sin\left(\frac{\omega \cdot d}{v^*}\right)} \tag{4.69}$$

$$N = \frac{2h}{\omega \cdot Z} \sin\left(\frac{\omega d}{2v^*}\right) \tag{4.70}$$

The resulting transmission function is described by

$$\begin{pmatrix} U \\ I \end{pmatrix} = \begin{pmatrix} N & \frac{C+C_0}{jN\omega CC_0} \\ 0 & -\frac{1}{N} \end{pmatrix} \begin{pmatrix} p \\ v \end{pmatrix} \tag{4.71}$$

This model allows the description of the transducer block as a series of homogeneous layers with different acoustic characteristics. Passive layers, such as backing, impedance matching layers, electrodes, and casing, will contribute with a transmission matrix of type $T_{passive}$ as described in Equation 4.60. Piezoelectric material will contribute with a transmission matrix according to Equation 4.71. The model holds valid if the layer surface is much larger than the layer thickness, so that the vibration along the propagation direction (longitudinal wave) is predominant with respect to shear waves.

4.3.5.3 Reflection and transmission

Different materials have different acoustic impedances. Consider two elements of different material, put in contact along one edge, as shown in Figure 4.9, and a purely longitudinal wave propagating along the stack, perpendicularly to the boundary. The incoming wave experiences a medium discontinuity on the boundary between the two materials, it will therefore be partly transmitted and partly reflected, according to their acoustic impedances. In order to fulfill the continuity on the boundary, the resulting pressure on both medium must be equal on the boundary, that is to say

$$p_I + p_R = p_T \tag{4.72}$$

Also, the particle displacement on both sides of the boundary must be equal. Being the displacement equal, the particle velocities must also be equal, which is described by

$$\dot{\eta}_I - \dot{\eta}_R = \dot{\eta}_T \tag{4.73}$$

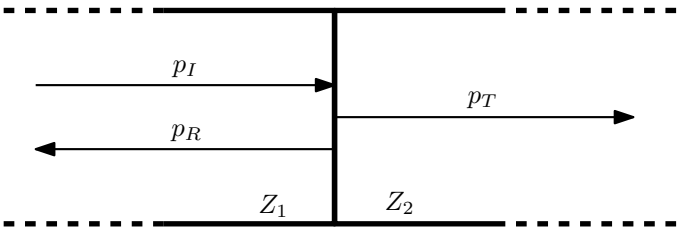

Figure 4.9: Wave propagation between two materials of different acoustic impedance.

If the wave is not perpendicular to the boundary, as assumed until here, the continuity relation becomes $\dot{\eta}_I \cos\theta_I - \dot{\eta}_R \cos\theta_R = \dot{\eta}_T \cos\theta_T$.

The particle velocity is linked to the pressure by the definition of the acoustic impedance, so that the equation can be rewritten by

$$\frac{p_I}{Z_I} - \frac{p_R}{Z_R} = \frac{p_T}{Z_T} \tag{4.74}$$

Now, remembering that the incident and reflected wave are in medium 1, and the transmitted wave is in medium 2, the acoustic impedances can be written as $Z_I = Z_R = Z_1$ and $Z_T = Z_2$.

By definition, the amplitude transmission coefficient T is defined as the ratio between the transmitted pressure p_T and the incident pressure p_I. In the same manner, the amplitude reflection coefficient R is the ratio between the reflected pressure p_R and p_I. Developing according to equations 4.73 and 4.74, it results that

$$T = \frac{p_T}{p_I} = \frac{2Z_2}{Z_1 + Z_2} \tag{4.75}$$

$$R = \frac{p_R}{p_I} = \frac{Z_2 - Z_1}{Z_1 + Z_2} \tag{4.76}$$

It is equally interesting to define the reflection and transmission coefficient of the wave intensities. This is achieved exploiting the link between pressure and intensity $I = p^2/2Z_{ac}$, and results in

$$\frac{I_T}{I_I} = \frac{Z_1}{Z_2} T^2 = T' \tag{4.77}$$

$$\frac{I_R}{I_I} = \frac{p_R^2}{p_I^2} = R^2 = R' \tag{4.78}$$

The expression of transmission and reflection coefficients as a function of the acoustic impedances gives very relevant information for the medical application of ultrasound. Soft tissues and water have an acoustic impedance of approximately 1.5 MRayl. On the contrary, gases have a very low acoustic impedance (approximately 400 Rayl for air), so that the reflection coefficient between soft tissues and gas-filled organs will tend to 1 and the transmission coefficient tends to 0. Therefore chest, lungs, bladder are not good for transmission.

When an ultrasonic probe is applied on the skin, the air layer trapped between the probe and the skin strongly reduces the efficiency of the transmission. For this reason, a so called acoustic gel is applied on the region to be imaged with the aim of matching the impedance of the probe to the skin. However, microbubbles of gas can successfully be used as a contrast agent, for better visualizing an organ or a tissue among similar soft tissues.

Bones possess an acoustic impedance of approximately 7.75 MRayl, that is 5 times the acoustic impedance of soft tissues. Therefore, a wave traveling from soft tissues to bones will be mostly reflected.

4.3.6 Attenuation

Waves in a medium undergo absorption (leading to local heat increase in the medium) and scattering. The two effects can be resumed in an attenuation coefficient α, which affects the wave propagation following an exponential term.

Considering an ultrasonic beam in an homogeneous medium, the pressure wave is described by

$$p(\vec{r}) = p_0 e^{-\alpha \vec{r}} e^{j(\omega t - \vec{k}\vec{r})} \tag{4.79}$$

and the acoustic intensity, being $I = p^2/2Z$, is

$$I(\vec{r}) = I_0 e^{-2\alpha \vec{r}} e^{j(\omega t - \vec{k}\vec{r})} \tag{4.80}$$

For ultrasonic waves at frequencies around 1 MHz, the attenuation is described by

$$\alpha = \alpha_0 \cdot f^b \tag{4.81}$$

where b is equal to 1 for soft tissues. The amplitude attenuation coefficient α_0, solely dependent on the material, is measured in [dB/cm/MHz].

The previous expression of the attenuation underlines an important characteristics of ultrasonic waves, usually referred to as *beam softening*: ultrasound at high frequency will be attenuated faster in the body than low frequency waves.

4.4 Biological effects

4.4.1 Thermal effects

The main effect of ultrasound on tissues is heat generation due to absorption of the wave energy by the tissue. The rate of absorption contributes to the attenuation coefficient of the medium together with the scattering effect. It therefore varies according to the tissue type. As a general rule, soft tissues have an attenuation coefficient on the order of 0.5 dB/cm/MHz while bones can reach 20 dB/cm/MHz. Of course, the ability of tissues to evacuate heat is equally important.

For the same tissue, the thermal effect depends on the ultrasonic beam intensity and on the duration of the radiation. From literature, it is accepted that a local increase of 1.5 °C does not damage the tissue independently on the exposure duration. However, an increase of 6 °C causes immediate tissue damage and an increase of 20 °C leads in most tissues to immediate necrosis. Within those boundaries, damages accumulate proportionally to temperature and exposure time.

The temperature elevation can be more precisely estimated by calculating the amount of heat generated by the ultrasonic radiation Q_{in} and the heat Q_{out} removed by blood perfusion. The relation between temperature increase over time and heat amount is given by the BioHeat Transfer Equation (BHTE)

$$\rho C \frac{\partial T}{\partial t} = k \cdot \nabla^2 T + Q_{in} - Q_{out} \tag{4.82}$$

where ρ is the tissue density, C the the tissue specific heat, and k the the thermal conductivity of the tissue.

The heat removed from the irradiated spot due to blood flow is

$$Q_{out} = C_B \cdot \rho_B \cdot W_B \cdot (T - T_A) \tag{4.83}$$

where C_B is the specific heat constant of blood, ρ_B the blood density, W_B a coefficient of perfusion in the tissue, and T_A is the temperature of the arterial blood.

Following the calculations done by Azhari [3] , and supposing that the whole attenuation is due to absorption, the heat absorbed by the tissue from the incoming acoustic wave is

$$Q_{in} = 2\alpha I(x) \tag{4.84}$$

Given the direct dependency of the attenuation coefficient from the wave frequency, it is worth noting that the thermal effect will be bigger for higher frequency as well.

The temperature increase over time is

$$\rho C \frac{\partial T}{\partial t} = k\nabla^2 T + 2\alpha \cdot I - C_B \cdot \rho_B \cdot W_B \cdot (T - T_A) \tag{4.85}$$

Two safety indexes are widely exploited, which take into account the variations in the beam intensity both in spatial and temporal domain. They are the *spatial peak temporal average intensity* (I_{SPTA}) and the *spatial peak pulse average intensity* (I_{SPPA}). The FDA defined the limit values $I_{SPPA} = 150\,\mathrm{W/cm^2}$ and $I_{SPTA} = 720\,\mathrm{mW/cm^2}$ for non-opthalmologic applications.

4.4.2 Cavitation

Ultrasonic waves propagate compressing and stretching the medium, e.g., the body tissues. The distance among molecules varies with the wave, oscillating around its mean value. An excessive negative pressure can pull the molecules apart by a distance which is bigger than the maximum distance required to keep the medium intact. In that case, *cavitation* occurs. Microbubbles are created, which size evolves with the amplitude of the pressure wave. In case of inertial cavitation, associated with high ultrasonic amplitude, the size can reach a critical value, usually more than ten times the equilibrium size of the microbubble. Shortly after reaching the critical size, the cavity implodes. This can result in extremely high temperature and a local pressure as high as a thousand times the atmospheric pressure [21], thus damaging the surrounding tissue. The implosion can be the result of a single, high intensity pressure cycle. On the contrary, *non-inertial* cavitation results in oscillation of the bubbles below their critical size, therefore without risk of collapsing.

The risk of cavitation is associated with the maximum negative pressure and also depends on the inverse of the square root of the wave frequency. The Mechanical Index (MI) expresses this ratio. It is defined by

$$MI = \frac{\max(p_{negative})}{\sqrt{f_0}} \tag{4.86}$$

where $\max(p_{negative})$ is the peak of negative pressure (expressed in MPa) and f_0 is the center frequency (expressed in MHz).

An ultrasonic wave with a MI lower than 0.7 is accepted by all regulatory entities as having negligible effect on cavitation. The FDA fixed its maximum value at $MI = 1.9$ for biomedical applications.

Equation 4.86 shows that the risk of cavitation is higher at lower frequencies.

4.4.3 Radiation force

Apart from cavitation, other non-thermal effects can be caused by ultrasound, due to the transfer of momentum from the ultrasonic field to the tissue. The force exerted on the tissue is equal to the total acoustic power emitted divided by the speed of the beam:

$$F_{rad} = \frac{P_{ac}}{c} \tag{4.87}$$

Dalecki [21] overviews several effects based on radiation forces, such as radiation torque, acoustic streaming, acoustic levitation, and fountain effect.

4.5 System Modeling

The models presented until now allow the description of the ultrasonic generation, transmission, and reception between two devices. The system proposed in the ULTRAsponder project consists of an implanted device (TR) and a external CU, conceived for being placed on the patient's skin.

Figure 4.10 depicts the main parts of the acoustic generation and transmission. A TR is depicted on the right side, which will be implanted in the body. An external CU is depicted on the left. Both the external CU and the TR are composed of a piezoelectric transducer (shown in red) and some electronics (in green). The transducers can be composed of a single element, or of an array of elements. In principle, both TR and CU can send and receive the carrier. Depending on the carrier and on the modulation algorithm, the same transducer may be used for emission and reception, or portions of it.

On the CU side, a power generator produces the energy that will be sent to the transducers in order to recharge and communicate with the TR. A wave generator block gives the suitable form to the signal to be emitted and drives the transducers accordingly. On reception mode, the dedicated transducer (or transducer section) translates the incoming message, which is then demodulated and converted to a digital signal.

The generation and propagation of the ultrasonic wave in the transducers can be described by the theory on ultrasound through solids and by the KLM model for the piezoelectric materials. The wave travel in the medium can be well described by the model for ultrasonic propagation in fluids.

The whole system can be modeled in several steps. On CU side, the electric power generator feeds the emitting transducer. The KLM model allows the calculation of the resulting acoustic power generated P_{ac_s}. The variation of the ultrasonic wave in the medium will be calculated according to the Rayleigh propagation model. It will link the acoustic pressure generated on the CU to the acoustic pressure P_{ac_i} impinging on the TR. This pressure is then propagated through the transducer. The KLM model again allows calculating the behavior of the different layers and the resulting electrical power $P_{el_{out}}$ translated, which then feeds the implant electronics and recharges the internal battery. The other way around, the TR circuit board actively changes its electric impedance, causing a variation of acoustic impedance of the transducer. An acoustic backscatter wave arises on the surface of the TR. The acoustic power P_{ac_r} can be calculated by the KLM model and its propagation back to the CU follows again the Rayleigh model. Finally, the backscattered acoustic power received on the CU is translated into electric power and the resulting signal is demodulated.

4.5.1 Acoustic propagation

The medium between the CU and TR transducers will be composed of soft tissues and of an ultrasonic gel for impedance matching and avoidance of air bubbles at the interface. For simplicity, it is assumed

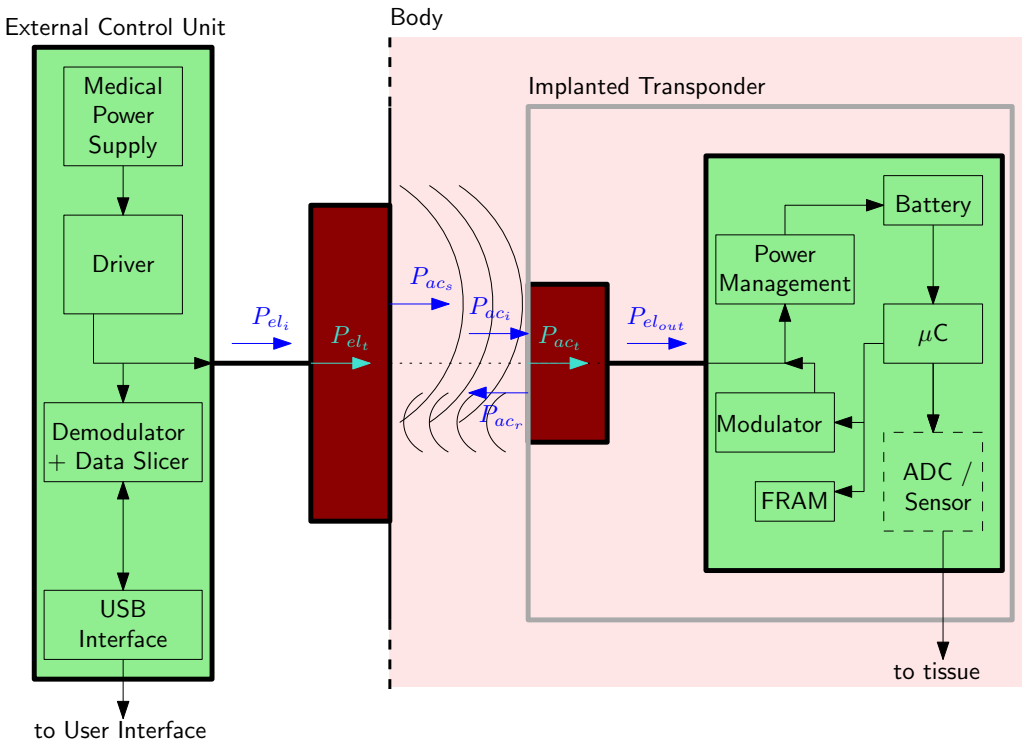

Figure 4.10: Schematics of the system to be modeled.

that the medium is quite homogeneous and that no hard tissues (e.g., bones) are present on the acoustic path. Indeed, bones have such a high acoustical impedance, that it is safe to assume them as blocking elements. The propagation therefore occurs either through soft tissues, or not at all.

The emitting transducer, having an active surface A, can be considered as a series of spherical sources. If the beam is not focused, the propagation follows therefore an inverse-square law. For each source, given the acoustic power P_{ac}, the resulting intensity in the radial direction at a distance r from the center of the source is:

$$I(r) = \frac{P_{ac}}{A} = \frac{P_{ac}}{4\pi r^2} \tag{4.88}$$

Taking into account the attenuation of the wave, which appears in the power as an exponential term $e^{-2\alpha r}$, the intensity becomes

$$I(r) = P_{ac} \cdot \frac{e^{-2\alpha r}}{4\pi r^2} \tag{4.89}$$

From there, knowing the implantation depth L and knowing the surface of both the CU and TR transducers (A_{CU} and A_{TR}), it is possible to relate the acoustic power P_{ac_s} emitted by the CU with the acoustic power P_{ac_i} received on the TR.

$$P_{ac_i} = I(L) \cdot A_{TR} = P_{ac_s} \cdot \frac{e^{-2\alpha L}}{4\pi L^2} \cdot A_{TR} \tag{4.90}$$

Vice-versa, once the backscattered wave sent by the TR is determined, the model predicts the backscattered wave reaching the CU.

More precisely, the Rayleigh propagation model addresses the wave transmission through the skin and into the body, between the CU and the TR.

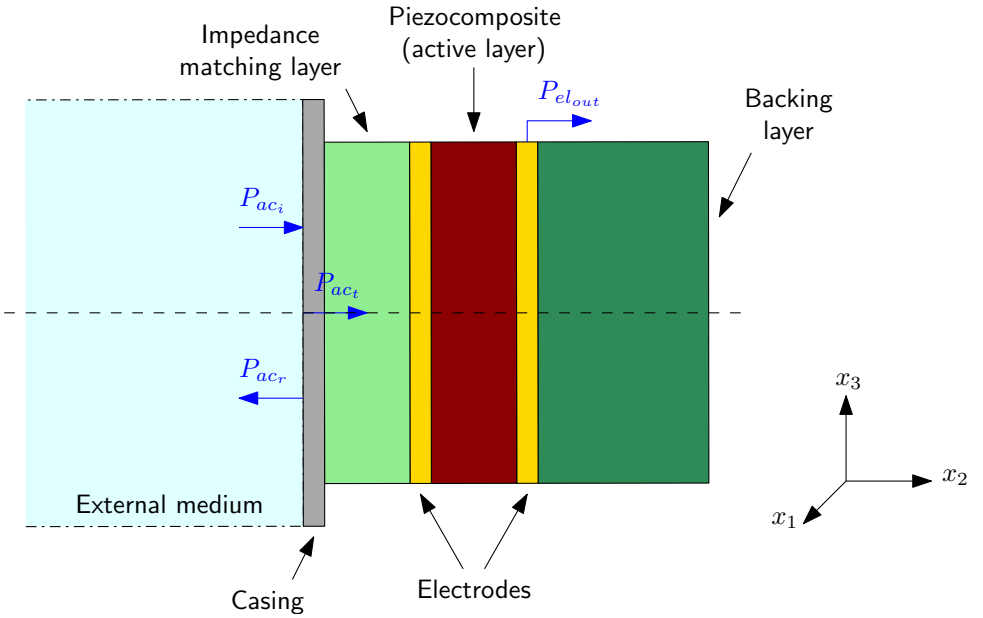

Figure 4.11: Generic transducer layers and acoustic power at different locations.

The aim is to receive on the TR surface the maximum possible intensity within the FDA range ($I_{SPTA} = 0.7\,\mathrm{W/cm^2}$), and to define which acoustic wave is required to be generated on CU side.

4.5.2 Transducers

Both on CU and TR side, transducers make the link between the ultrasonic wave and the electrical signals.

The typical structure of a medical piezoelectric transducer contains at minimum the active piezoelectric material and the electrodes relying the piezoelectric to the electronics. The electrodes are very thin metallic layers, which do not disrupt the acoustic transmission. Usually, passive impedance adaptation layers are present on the sides of the piezoelectric layer. On the exposed side of the transducer, the adaptation layer matches the active layer with the propagation medium, lowering the impedance difference at the interface. On the internal side of the transducer, a backing layer ensures mechanical strength to the otherwise fragile piezoelectric material, and acts as an acoustic damping layer. This also increases the bandwidth of the transducer and allows a better spatial resolution. On the contrary, the backing absorbs a part of the incoming energy. The presence of backing and its characteristics are therefore very much dependent on the target application. Typical materials for a backing layer are based on epoxy resin.

Figure 4.11 depicts the structure of a generic receiver transducer. The power on the interface between medium and casing are indicated: incoming power P_{ac_i}, reflected power P_{ac_r}, and transmitted power P_{ac_t}. The electric power $P_{el_{out}}$, produced by the piezoelectric layer under the effect of the acoustic power, is also indicated.

The device circuitry (not shown) is connected to the electrodes and the whole implant is encapsulated in a housing, which represents a further acoustic layer. A requirement of the proposed system is the encapsulation of the transducer into a titanium casing. Indeed, titanium is the golden standard for biocompatibility in long-term IMDs. The demonstrator proposed in this work is conceived as a prototype

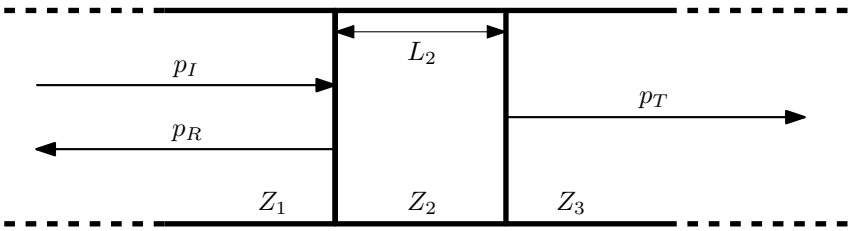

Figure 4.12: Wave propagation between three materials of different acoustic impedance.

for a future industrial device. Therefore, it must have a comparable casing in order to prove its concept. The presence of titanium on the acoustic path can greatly affect the acoustic transmission, because of its high acoustic impedance (22.5 MRayl) with respect to that of body tissues.

For the proposed system, the transducer active surface was arbitrarily chosen to be 5 mm × 10 mm, divided into six elements of 5 mm^2 each with a pitch of 1.5 mm, equal to the wavelength in water.

4.5.2.1 Impedance matching layers

The several materials required in the sandwich have different acoustic characteristics. Impedance matching layers are therefore essential towards an efficient transmission. Ideally, the whole energy emitted by the external CU should arrive to the electronics of the TR, without being absorbed by the transducer layers. This also prevents heating in the transducers, which would cause damages to the piezoelectric polarized material.

In particular, the acoustic impedance of piezoelectric materials very much differs from the one of soft tissues. A matching layer is particularly useful when the piezoelectric layer is in direct contact to the the propagation medium. This is less true for transducers embedded in a housing, as the one proposed in this work. In that case, the active layer and the casing are expected to have a similar acoustic impedance.

Usual matching layers exploited in transducer design are polymers, sometimes impregnated with metal particles to adjust their acoustic properties. Their acoustic impedance is in the order of magnitude of 1 to 10 MRayl.

Consider the three-layers structure depicted in Figure 4.12. Azhari [3] reports the solution of the energy transfer among three layers of different acoustic impedance

$$\Upsilon = \frac{I_3}{I_1} = \frac{4Z_1Z_3}{(Z_1+Z_3)^2 \cdot \cos^2(k_2L_2) + (Z_2 + \frac{Z_1Z_3}{Z_2})^2 \cdot \sin^2(k_2L_2)} \tag{4.91}$$

This drives the design of a matching layer for the transducer sandwich. Provided that the acoustic impedances do *not* fulfill the condition $Z_2 \ll Z_1Z_3$, the transmission relation is independent on the matching layer acoustic impedance in two particular cases:

- if the thickness of the matching layer L_2 is very small with respect to the wavelength in the layer: $L_2 \ll \frac{\lambda_2}{4}$
- if the thickness is a multiple of the half wavelength $L_2 = n\frac{\lambda}{2}$

$$\Upsilon = \frac{4Z_1Z_3}{(Z_1+Z_3)^2} \tag{4.92}$$

The perfect impedance layer has a length equal to $L_2 = (2n-1)\lambda_2/4$ and an acoustic impedance $Z_2 = \sqrt{Z_1Z_3}$. In that case, the energy transmission coefficient is equal to 1, that is to say all energy

incoming into the first medium is transferred to the third medium, which was the aim of the impedance matching layer.

4.6 Simulations and parameters chosen

The aim of the ULTRAsponder project was to assess the feasibility of a system, in which an IMD receives energy from an external CU by ultrasonic link and in which the two parts communicate by the same carrier. The most suited propagation conditions have to be defined, in order to efficiently send energy while complying with the FDA regulation. This includes the choice of the working frequency, such that the adverse bioeffects are minimized, and the choice of a suitable ultrasonic path, which does not attenuate too drastically the beam from the CU to the TR. Nevertheless, the main focus of the author is on the reception of the beam by the TR and its propagation through the transducer to the electronics. In particular, the effect of the titanium barrier on the wave propagation is assessed.

In the transducer model, only vibrations in the wave propagation direction will be considered, because the layers are thin compared to the surface of the transducer.

4.6.1 Working frequency

The appropriate working frequency for the system results from a trade-off among different characteristics of the wave. The beam attenuation linearly increases with the frequency, and the wave energy increases with the square of the frequency. On the contrary, the cavitation risk is inversely dependent from the square root of the frequency.

$$\alpha = \alpha_0 \cdot f^b \tag{4.93}$$

$$E' = \frac{\rho \eta_0^2 \omega^2}{2} = 4\pi^2 \rho \eta_0^2 f^2 \tag{4.94}$$

$$MI = \frac{max(p_{negative})}{\sqrt{f}} \tag{4.95}$$

Working at low frequency allows a very reduced attenuation. However, low frequency encounters other limitations and induces safety issues due to cavitation. The lower the frequency, the more the transmitted energy spreads in the body, so that only a small part can be recovered by the implanted TR. Also, the beam intensity is less homogeneously distributed: regions on hot spots can experience tissue damages, while energy transfer and communication is inefficient on cold spots.

Higher frequency contributes in decreasing the cavitation risk. The use of ultrasonic frequencies in the MHz range is particularly attractive because the wavelength will be in the *mm* range, i.e., smaller than the transducer elements. It is therefore possible to steer and focus the beam, thus increasing the intensity at target. This compensates the increased attenuation, thus providing a higher energy transfer, a better signal-to-noise ratio, and higher data flow during communication.

A review on ultrasonic propagation was recently performed by Roes *et al.* at Eindhoven University [86]: the successful use of ultrasound was shown, both to remotely power deeply IMD and to transmit power through a metal wall. The frequency used ranges from 0.5 to 2.25 MHz.

Ultrasonic Imaging usually exploits 2 MHz waves and reaches tissues down to 10-15 cm. Also, applications in which cavitation is aimed, may exploit 1 MHz waves, but at a much higher intensity.

Within the ULTRAsponder project, it was decided to work at 1 MHz. For the same reasons, *a center frequency of 1 MHz will be considered for the simulation presented in this chapter.*

4.6.2 Location

The medium between the CU and the TR is considered to be a soft tissue and its thickness is assumed to be 15 cm. This mimics the conditions of a deep implant accessible through an acoustic path [20].

The ultrasonic propagation in the medium is not simulated in this thesis work.

4.6.3 Titanium thickness

A key point in the ultrasonic transmission is the ability of overcoming the titanium barrier. As the titanium casing is a mandatory element of an IMD, the proposed system could not claim to be feasible for industrialization if the transmission through titanium would not be achievable. A strong attenuation of the wave due to mismatch in the acoustic impedance is expected, given the high acoustic impedance of titanium ($Z_2 = 22.5$ MRayl) compared to the acoustic impedance of soft tissues (close to that of water, $Z_1 = 1.5$ MRayl).

A rough estimation of the transmission coefficient for the acoustic power is given by Equation 4.77, assuming semi-infinite media:

$$T'_{Ti} = \frac{Z_1}{Z_2}\left(\frac{2 \cdot Z_2}{Z_1 + Z_2}\right)^2 = 0.23 \tag{4.96}$$

Less than a quarter of the incoming energy should enter the transducer due to the titanium barrier.

In reality, the titanium barrier is thin with respect to the wavelength, therefore its effect will be less important. Given this loss of energy at the surface of the device, it is important that the transmission inside the transducer (through the titanium, the adaptation layer and the piezoelectric material) would not generate further losses.

Simulations must be performed to assess the optimum thickness at which the acoustic wave can be transmitted through the enclosure and under which conditions. According to the results of the simulations, it may be necessary to thin down a small region of the casing. The amount of thinning required will be determined according to the results of the simulations.

A MATLAB® routine was developed, based on the work of Martinez [61]. A sandwich is considered, containing a piezocomposite structure and a titanium layer. Figure 4.13 visualizes the structure taken into account. Compared to the transducer depicted in Figure 4.11, the electrodes were neglected (because they are very thin) and the backing layer was not considered. The backing layer plays the role of a buffer for the piezoelectric vibration, thus enlarging the transducer bandwidth. However, this attenuates a part of the incoming wave and reduce the performance. In order to preserve the incoming wave as much as possible, the transducers manufactured within the ULTRAsponder project avoided backing layers. An impedance adaptation layer is at first considered, but the calculations will show that it is useless.

The incoming acoustic power P_{ac_i}, resulting from the CU emission, is considered to fulfill the FDA rating on the intensity $I_{ac_i} = 0.7\,\mathrm{W/cm^2}$.

The electrical power effectively transmitted to the device largely depends on the electrical impedance matching of the transducer with the electrical load of the PCB. The electric load seen by the transducer will correspond mainly to the internal battery of the device. This impedance is difficult to measure, as it varies in time according to the level of charge in the battery. A rough estimation gives 500 and 1000 ohms for the real part and the same for the negative imaginary part (capacitive circuit). Therefore, the electronics contribution to the power transfer was taken into account by a fixed charge $Z_{PCB} = (750 - 750\,j)\ \Omega$.

Objective is to determine the transducer behavior at the original casing thickness and, if ultrasound cannot be transmitted through that thickness, to estimate the amount of thinning required. The simulations

Table 4.3: Characteristics of the piezoelectric layer.

Piezoelectric element	
Bulk Modulus [GPa]	77.9
Density [kg/m^3]	6050
Longitudinal speed [m/s]	3590
Coupling coefficient	0.58
Relative permittivity	2170
Electrical losses	0.04
Mechanical losses	0.04

were performed for the original thickness of the titanium casing (0.3 mm), for a thickness of 0.2 mm and 0.1 mm, and for a transducer without casing.

The following parameters were calculated:

- Electric impedance of the transducer.
- Acoustic impedance of the transducer.
- Power budget: Acoustic power available, acoustic power consumed, electric power consumed.

4.6.3.1 Characteristics of the Transponder materials

Piezoelectric layer: several piezoelectric materials can be used. For our simulation, it was assumed to use a piezocomposite structure based on PZT material [66]. A high permittivity piezoceramic with a high electromechanical coupling coefficient and a ceramic volume fraction sufficiently high was chosen, in order to decrease the electrical impedance. The resulting acoustic characteristics were given by the transducer manufacturer and are listed in Table 4.3.

The material properties define the thickness of the piezoelectric element. The most efficient thickness is indeed equal to the half of the wavelength, so that the impinging and reflected power have the same phase, i.e., their interference is not destructive.

Given the frequency f, and remembering that the wave speed c depends on the material Bulk modulus B and density ρ, the thickness is defined by the relation

$$d_{piezo} = \frac{c}{2f} = \frac{1}{2f}\sqrt{\frac{B}{\rho}} \tag{4.97}$$

Choosing the material with the characteristics listed in Table 4.3, and given the working frequency $f = 1\,\text{MHz}$, the layer thickness must be 1.795 mm.

The acoustic impedance of the piezoelectric layer can be calculated from its density and wave speed:

$$Z_{piezo} = \rho \cdot c = 24.2\ MRayl \tag{4.98}$$

Titanium layer: The housing of the implant will be made of medical grade titanium, that is to say very pure titanium. Therefore, the characteristics of the pure material were taken into account [41]: material density $\rho_{Ti} = 4500\,\text{kg/m}^3$ and Bulk modulus $B_{Ti} = 110\,\text{GPa}$. This results in a wave speed

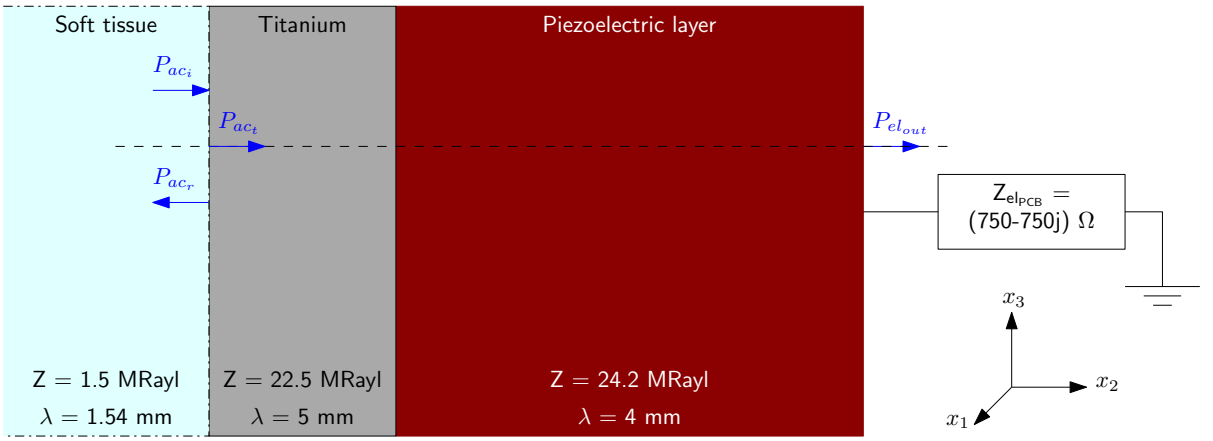

Figure 4.13: Transducer structure taken into account in the simulation.

$v_{Ti} = 4.95$ km/s and an acoustic impedance $Z_{ac_{Ti}} = 22.5$ MRayl. The thickness of this layer can vary from 0.3 mm, which is the original thickness of the casing walls, down to 0.1 mm, which was defined by experts as a safe limit to ensure the mechanical stability of the housing. Different thicknesses are simulated, in order to assess the influence.

Adaptation layer: Placed between the titanium casing and the embedded piezoelectric material, an adaptation layer matches their impedances, so that the incoming acoustic power on the titanium propagates into the piezoelectric layer. According to the transmission coefficient calculation in the three-layers structure, assessed in section 4.5.2.1, the best acoustic impedance matching layer has a thickness equal to a multiple of $\frac{\lambda_{match}}{4}$ and an acoustic impedance linked to those of its two neighbor materials.

$$Z_{match} = \sqrt{Z_{piezo} \cdot Z_{Ti}} \tag{4.99}$$

$$d_{match} = (2n-1)\frac{\lambda_{match}}{4} \tag{4.100}$$

Given the previously specified acoustic impedance of pure titanium and piezoelectric material, the adaptation layer should possess an acoustical impedance $Z_{ac_{match}} = 23.3$ MRayl.

Several materials can have similar acoustical impedance, from a combination of material density and wave speed. Once the required material is identified, its elastic and physical characteristics can be exploited to determine the wavelength in the material, and therefore the series of possible thicknesses of the matching layer, according to Equation 4.100.

From the small difference between the three acoustical impedances, it is evident that the matching layer would not improve in a significant way the ultrasonic transmission. Therefore, it was decided to avoid the adaptation layer in the simulation, and the system reduces as depicted in Figure 4.13.

4.6.3.2 Results

Aim of the performed simulation is to assess the influence of a titanium layer on the ultrasonic transmission, and to find an appropriate design for the transducer, which allow efficient ultrasonic propagation for the medical application.

The resulting acoustic impedance of the whole sandwich is ideally equal to the impedance of the medium in which the wave should propagate. In the present case, approximating the acoustic impedance

of soft tissues to that of water, the target equivalent acoustic impedance Z_{ac} is about 1.5 MRayl, without an imaginary part at the working frequency. This will be the first index of a good propagation.

On electrical domain, the best energy transfer is given for a transducer electrical impedance having the same active part as the PCB impedance, and an opposite reactive part. That is, the ideal transducer electrical impedance is (750 + 750j) Ω.

Figure 4.14 shows the simulated behavior of the transducer for different thicknesses of the titanium layer. The effect of titanium thickness, at a given thickness of the piezo layer, is that the peak of both electrical impedance Z_{el} and acoustical impedance Z_{ac} slightly increases and shifts towards a lower frequency. The thicker is the titanium, the bigger will be the shift and the increase in peak.

The higher peak is due to the slightly lower acoustical impedance of titanium (22.5 MRayl) with respect to the chosen piezocomposite (24 MRayl). The lower resonance frequency is due to the increased thickness of the sandwich.

It is evident that the value of the electrical impedance at 1 MHz is not even close to the ideal one, Consequently, the power budget at 1 MHz is poor (7.5 mW over the 35 mW available). The peak of transmission is around 850 kHz.

That required frequency shift can be obtained by using a thinner piezo layer, i.e., adapting the material resonation to a higher central frequency. Figure 4.15 shows the variation of thickness in the piezo layer, for a fixed titanium layer of 0.1 mm.

On the contrary, an increased thickness of the piezoelectric material has a slightly beneficial effect on the power budget.

4.7 Conclusion

In this chapter, the theory underlying the generation and the propagation of mechanical waves is presented, both for solid and fluid propagation media. The theory is in particular applied to the system under development. The acoustic transmission from an external CU to a TR is modeled. The ultrasonic link between the two transducers, i.e., in the body, is associated with a Rayleigh propagation.
The reception of an acoustic power on the receiving transducer, its propagation through the different layers of the transducer sandwich and its translation into electrical power is modeled based on the KLM model, assuming planar, longitudinal waves. Particular focus is reserved to the effect of the titanium barrier on the power transmission in the transducer. A thickness of 100 µm and an appropriate piezocomposite material proved to allow acoustic propagation at 1 MHz: this configuration is therefore acceptable for the proposed system.

Within the project ULTRAsponder, the design of the transducer sandwich was performed by an industrial partner, which performed more precise simulations and tests than the ones presented within this thesis work. Both transducers for use in direct contact with water and to be integrated in a titanium casing were produced. Different materials and geometrical characteristics were taken into account for the piezocomposite and the impedance matching layers, in order to compensate the titanium effect and achieve the best transmission at the chosen frequency. The glue joint between titanium and piezoelectric material was taken into account, which has a very low acoustic impedance, but also a very reduced thickness, thus not disrupting the acoustic link.

Nevertheless, an important result could already emerge from those simplified simulation: titanium encapsulation can coexist with ultrasonic propagation, given an appropriate matching layer, an appropriate piezocomposite design, and a locally thinned layer of titanium. This opens the way to a new generation of long-term biocompatible IMD, based on ultrasonic power transfer and communication.

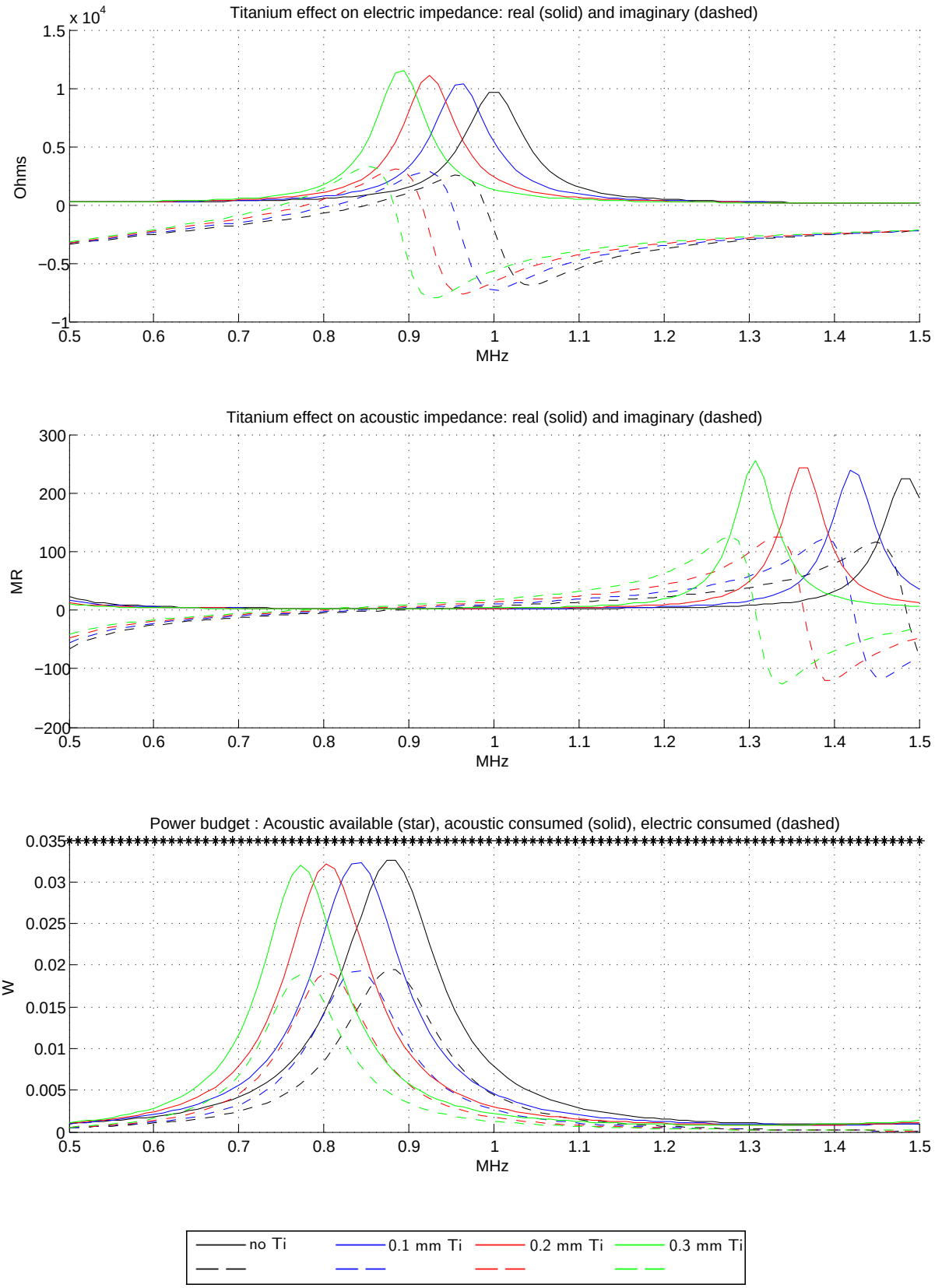

Figure 4.14: Simulated effect of a titanium layer at different thicknesses.

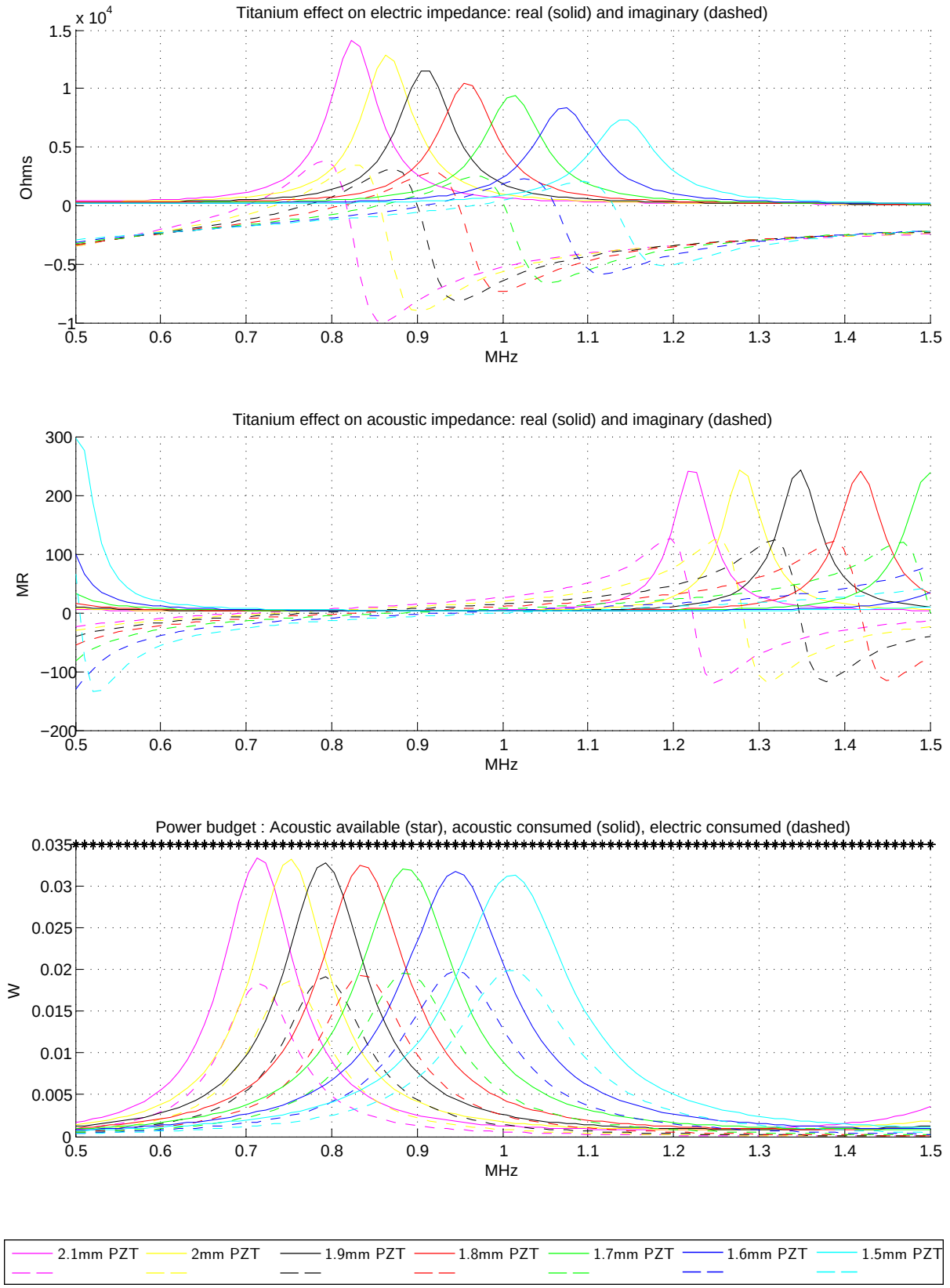

Figure 4.15: Simulated effect of different thicknesses of piezoelectric material.

5 ULTRAsponder project

5.1 Introduction

The European FP7 project ULTRAsponder, to which the author of this thesis contributed, aims to develop a generic Body Sensor Node structure that would adapt to different applications. The demonstrator manufactured is conceived to serve a cardiac application aiming to measure impedance at long-term.

Due to inefficient use of electromagnetic waves and their crippling limitations to recharge the implant, ULTRAsponder proposes to exploit acoustic waves (ultrasound) for communicating with, and efficiently energizing a network of transponders that could be deeply implanted in a human body (i.e., 5 cm to 10 cm).

An intelligent data communication strategy is proposed, based on backscattering technique.

A commercial titanium housing is taken into consideration, mostly because of its biocompatibility. Strategies for adapting the casing to the application are discussed.

The components of the system are carefully chosen to meet the requirements of the whole system. Custom, low-power microprocessor, ADC, energy harvesting, and backscattering circuitry are designed and manufactured within the project, as well as the electro-mechanical transducers. A FRAM device is chosen for data storage, because of its high operation speed, low power consumption, long life, and MRI compatibility. Ultra thin-film, solid-state batteries are exploited, which carry an integrated power management unit.

5.2 Functional Demonstrator

In the vision of the project, the IMD should act within a Body Sensor Network. The complete system could consist of several TRs implanted in the body, dedicated to the measurement of various physiological parameters, such as temperature, pressure, strain or fluid flow and chemical or electrical properties. They may also perform therapeutic functions such as drug delivery, defibrillation or electrical stimulation. A CU secured to the patient's skin is able to energize and to communicate with them, and can relay the recorded data from the transponders network outside the patient's environment via Global System for Mobile communications (GSM™), Universal Mobile Telecommunications System (UMTS), Plain Old Telephone Service (POTS), or Internet Protocol (IP) based networks.

The TR must be small and light, allowing its placement either by open surgery or minimally invasive techniques. Furthermore, it must exhibit an excellent biocompatibility to allow long-term implantation.

Figure 5.1 shows the general schematics of the proposed system. A TR is depicted on the right side, implanted in the body. An external CU is depicted on the left. Both the TR and the CU contain piezoelectric transducers, which convert ultrasound into exploitable electric power and vice-versa. Both TR and CU can send and receive the carrier. Depending on the application, the same transducer or portions of it can be used for emission and reception.

The transducers of the CU are in contact with the body skin through an acoustic gel for impedance adaptation, while those of the TR are at an undefined position inside the body. To be general, it should be assumed that the device is deep implanted. On the TR side, a power management unit receives and treats

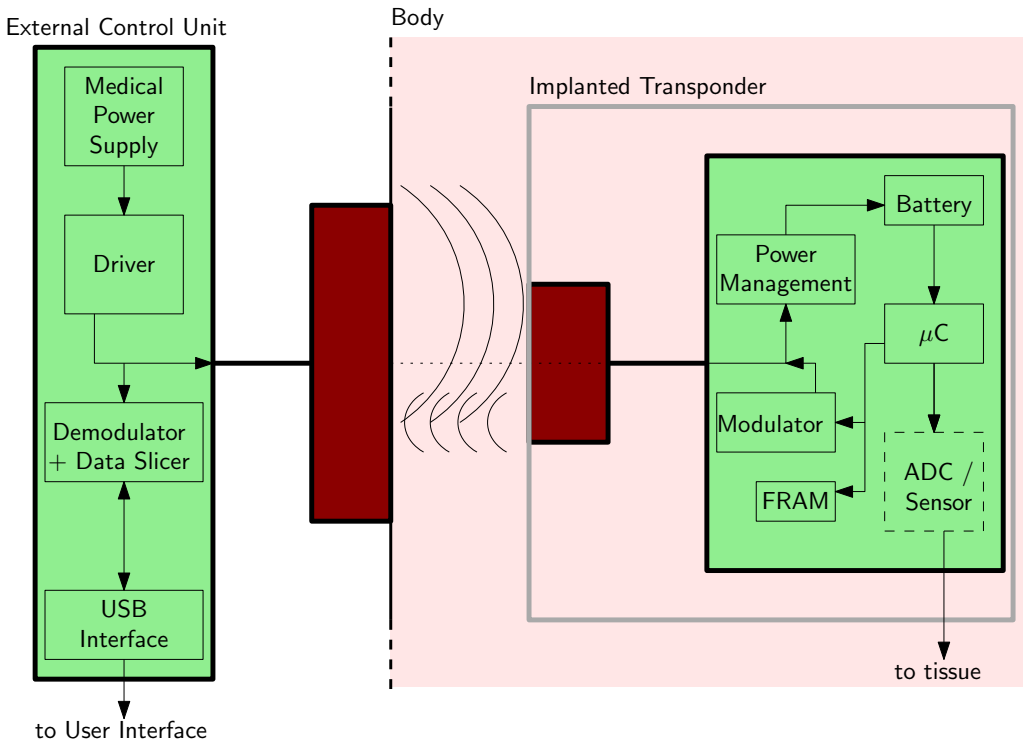

Figure 5.1: Overview of the proposed system.

the acoustic power coming from the CU, provides the necessary power supply to the microcontroller, and recharges an internal battery. A sensor unit is driven by the microcontroller through an ADC and is able to collect and store the sensed data or to perform some action. Communication from the TR to the CU is coordinated by the microcontroller through a modulation stage, which prepares the digital message that will be translated by the transducers and will be sent on the acoustic carrier backscattered to the CU.

On the CU side, a power generator produces the energy that will be sent to the transducers in order to recharge and communicate with the TR. A wave generator block gives the suitable form to the signal to be emitted, and drives the CU transducers accordingly. On reception mode, the dedicated transducer (or transducer section) translates the incoming backscattered message, which is then demodulated and converted to a digital signal. To complete the system, the CU should also be equipped with a user interface to the implant, in order to use manipulation by surgeons and medical staff. This aims to ease the seeking of a good position to recharge the TR, and to allow the interpretation of the message received. A USB link serves as bridge between the electronics and the user interface.

5.2.1 Application

Even if the development of the device wants to be generally valid and independent from a particular IMD, a specific application was chosen as a concrete case, and the demonstrator was designed based on that. The selected application is monitoring changes in cardiac function in patients at risk of heart failure. Those patients would greatly benefit from autonomous, long-term monitoring: their condition can stay stable for many years, thus not calling for daily visits at hospital, but changes are life-threatening and must be therefore rapidly detected.

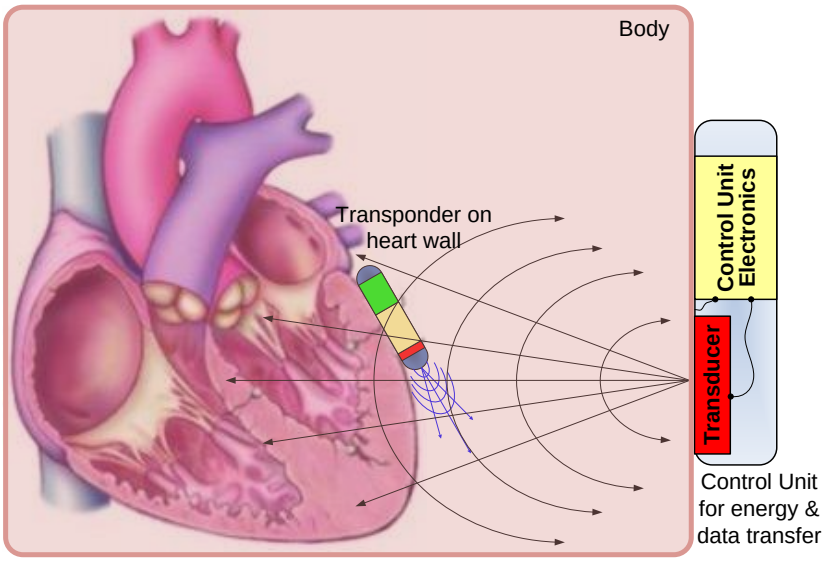

Figure 5.2: Proposed application: heart impedance measurement. The electrodes are not shown.

In order to assess cardiac function, three parameters are of interest: Electrocardiography (ECG), heart impedance (and particularly the impedance of the left ventricle), and the heart pressures.

Focus is put on left ventricle measurement, because it cannot be easily measured without invasive techniques. At the very best, a rough estimate could be made based on indirect blood pressure measurement performed by an external device. A regular monitoring of small differences may help in adjusting medical therapy. Information from the ECG complement the impedance measurement in order to establish the cardiac output [101]. Previous examples of cardiac monitoring through IMDs are reported by Ohlsson *et al.* [69], by Wong *et al.* [52], and by the COMPASS-HF Study Group [11].

Within ULTRAsponder it is proposed to deploy the developed IMD to measure the cardiac impedance. Being able to compare readings at different moments, the system can detect variations in the heart and reacts, e.g., warning the patient, the caregiver, or the medical staff during the next connection to the CU.

A TR will be implanted on the external heart wall, and from there four electrodes will be placed on different locations on the heart. The target method of implantation is a percutaneous procedure, e.g through the femoral vein into the left ventricle, the subclavian vein, or the femoral artery into the right ventricle. Flexibility of catheters for percutaneous procedure and size of sensor are most important.

Two electrodes send a current and the other two measure the resulting voltage in the same location. The CU is occasionally manually held on the patient's skin, it energizes the TR and communicates with it. It contains a power generator, the circuitry to drive the transducer, and a demodulator to interpret the message coming from the TR. Everything is directed by a user interface on a laptop: the user can turn on or off the input wave to the CU transducers, switch between a continuous emission and a transmission of groups of peaks (burst mode), and monitor on screen the received backscattered message.

The proposed application for chronic heart impedance measurement is depicted in Figure 5.2. The rough locations of TR and CU devices are shown, but the sensor electrodes are not depicted.

5.2.2 Carrier choice and implantation location

As discussed in Chapter 4, EM waves have several disadvantages in long-term, deep IMD, and therefore cannot be used as a carrier in the target application for this work.

Instead, it was decided to exploit ultrasound as energy and communication carrier.

A key factor of the system is the relative position of the CU with respect to the implanted TR. An appropriate acoustic path must be chosen, in order to have minimum attenuation between the transducers.

Cotté *et al.* [20] simulated several acoustic paths between the CU and the TR, based on the inner organs segmented data of the Visible Human Male Project [98]. This dataset enables to identify the tissue layers along the paths. Simulations of ultrasonic propagation and temperature rise were performed, and verified by *in vitro* experiments. Two suitable paths for the applications were identified, along which a safe and efficient acoustic transfer of energy can be obtained, while limiting the acoustic power radiated in order to minimize adverse bioeffects. The results validated the choice of an ultrasonic working frequency around 1 MHz, which offers a good trade-off between cavitation risk and efficiency.

5.3 Algorithm

The objective of the implanted system is to allow autonomous sensing of some physiological parameter during few seconds every day, and to store them in the internal memory for later download during recharge sessions. Measurement will be performed every 24 hours during 5 seconds.

The microprocessor is the core of the implant, as it coordinates its operations. A code must be developed and stored into the microprocessor memory, to be executed autonomously. The main operations performed by the TR are:

- Once a day, configure the sensor, perform a measurement, and store the result into the memory on board.
- Recognize when a wave is coming from the CU.
- During the recharge session, send the battery level at regular intervals as a feedback to the CU.
- When the internal battery is recharged, start the backscattering communication of the sensed data.

According to the data rate chosen for the sensing and the interval between two recharges, it may be necessary to reduce the power consumption of the implant through signal compression before storing the data sensed into the memory. Since signals resulting from the measurements of relevant physical parameters in the human body are highly correlated in time, compression prior to transmission can significantly reduce the bit-rate and thus the power consumption.

A potential strategy for removal of temporal correlation was suggested by Oslo University Hospital within the project [38]. It is based on Differential Pulse-Code Modulation (DPCM), which is known to provide significant compression at low complexity for correlated data . In their paper, Floor *et al.* show that a simple 2^{nd} order predictor (a 2^{nd} order Finite Impulse Response filter) gives significant compression of ECG signals. Moreover, the cost in terms of computational complexity is relatively low. The key result from the paper is shown in Figure 5.3: when measuring typical physical parameters of the human body, DPCM reduces the amount of bits required to achieve a certain fidelity compared to direct quantization. As an example, DPCM requires half so many bits per source sample to compress an ECG signals sampled at 250 Hz, compared to conventional quantization technique.

However, this compression method was not implemented in the system demonstrator.

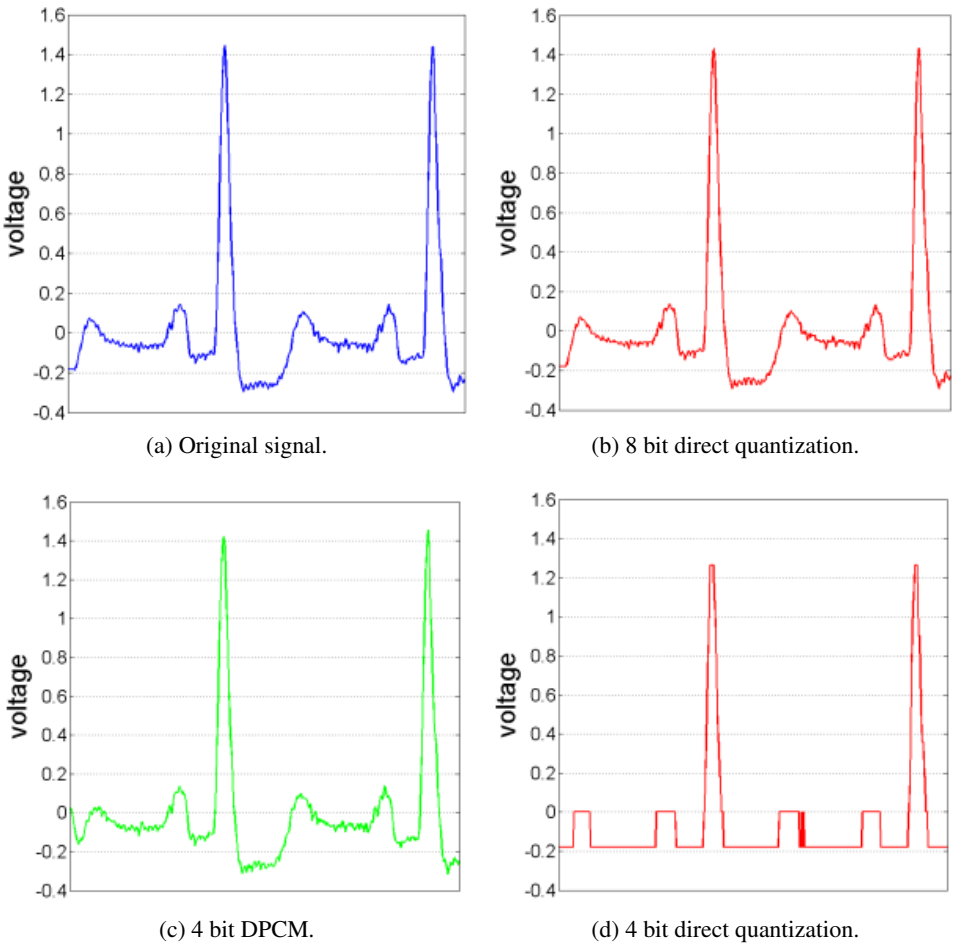

(a) Original signal.

(b) 8 bit direct quantization.

(c) 4 bit DPCM.

(d) 4 bit direct quantization.

Figure 5.3: Compression of a Electrocardiography signal: DPCM technique requires half so many bits as direct quantization.

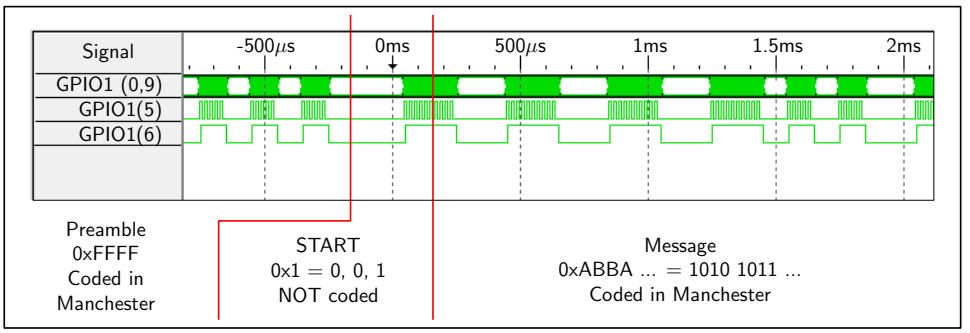

Figure 5.4: Message produced by the microprocessor

5.3.1 Backscattering

The transponder must work at low power to keep an acceptably long time between two recharge periods. In particular, a low power transmission strategy is necessary. Ultrasonic backscattering is a promising technique for this, as the power required to create the carrier is provided by the CU.

The reader is the CU and the tag is the TR. The communication is unidirectional: the CU provides the energy for the carrier wave, which illuminates the TR. The TR modulates this carrier by impedance modulation and scatters it back to the CU. Finally, the CU receives the backscattered wave and demodulates the message. Demodulation occurs only at CU level and modulation only at TR level. This helps reducing power consumption on TR, as the implant won't have to demodulate instructions coming from the CU. Ultrasonic backscattering relies on ultrasound instead of electrical waves, and on acoustic impedance instead of electrical impedance: the implanted tag modulates the signal by changing its acoustic impedance, which is related to the stiffness of the transducer. The TR modulates the acoustic impedance of the transducer element(s) used for transmission, in one of two possible states:

ON: closing the piezoelectric element over a short circuit; this makes it mechanically stiff and therefore reflective to an incident ultrasonic wave. The reflected amplitude will be high (logical "1").

OFF: open-circuit; this makes it mechanically soft, it can freely vibrate and is therefore absorbent to ultrasound. The reflected amplitude will be low (logical "0").

In the demonstrator developed within the ULTRAsponder project, the message generated by the microprocessor is fixed. A firmware was written for this task and stored into the FRAM memory on the TR. In an infinite loop, the message is prepared, coded and sent to the backscattering switch on the TR electronics. During the communication of the sensed data to the CU, synchronization tokens have to be added to the message, so that the CU recognizes the beginning and the end of the message sequence. Also, if the channel is noisy, the message should be coded and some error detection strategy has to be implemented. It was decided to exploit a Manchester code [99], a very simple technique in which a level is coded as a transition (e.g., "0" becomes "01" and "1" becomes "10"). This allows synchronizing the message between reader (CU) and tag (TR), and detecting some errors. A message packet is composed of a preamble, a Start sequence (i.e., a violation of the Manchester code, e.g., "000"), the actual message word, and a Stop sequence (again, a violation of Manchester code).

The resulting signal is shown in Figure 5.4.

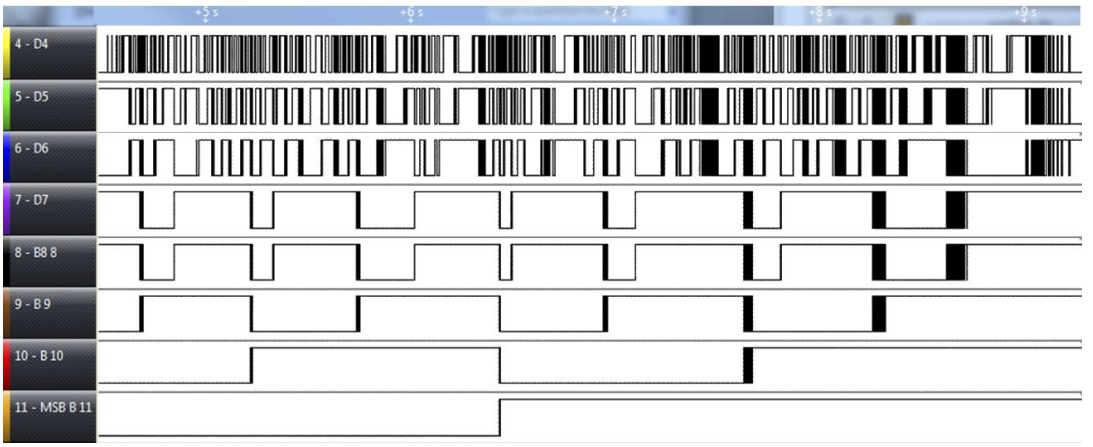

Figure 5.5: Conversion by the custom ADC of a DC voltage between 0 and 1.5 V.

5.3.2 Connection to the Analog-to-Digital Converter

A custom ADC was manufactured within the project by IMST GmbH (Kamp-Lintfort, DE), providing a test-platform for the assessment of the chip and the development of the interface to the microcontroller. A Serial Peripheral Interface (SPI) protocol was chosen. Figure 5.5 shows the successful digital conversion of a constant analog voltage sweeping between 0 and 1.5 V.

5.3.3 Graphical User Interface

A Graphical User Interface (GUI) for the CU has been developed within the project, in order to better manage the signal sent by the driver and to decode the backscattered signal.

The interface is based on a MSP430F22x4 microprocessor, manufactured by Texas Instruments (Dallas, TX, USA). It allows:

- the access to the CU electronics through Inter-Integrated Circuit (I^2C) protocol and the control of the channels and the power supply relay setting.
- the visualization of Received Signal Strength Indication (RSSI) and other internal voltage.
- the decoding of the message at the output of the CU. Incorrect messages are not displayed.
- the display of the decoded message.

The GUI is connected to the PC through a USB serial COM port. A commercial terminal software (free Docklight version) is used to send commands and to read messages produced by the micro-controller. The summary of the commands is given in Table 5.1. The command format is <0x02><ASCII_CMD><PARAM><0x03>.

5.4 Materials and components

Figure 5.6 shows the general schematics of the implanted device.

One of the biggest challenges of the proposed device concerns the physical size and on-board computational resources in terms of power and processing capabilities.

Table 5.1: Command summary for the GUI.

<ASCII_CMD >	<PARAM >	Description
RST	-	Reset the microprocessor
EPR	-	Enable power relay
DPR	-	Disable power relay
E1C	-	Enable 1 kHz carrier
D1C	-	Disable 1 kHz carrier
E1M	-	Enable continuous 1 MHz carrier
D1M	-	Disable continuous 1 MHz carrier
ERS	-	Enable RSSI monitoring
DRS	-	Disable RSSI monitoring
SIV	[0x00...0xFF]	Set I^2C value

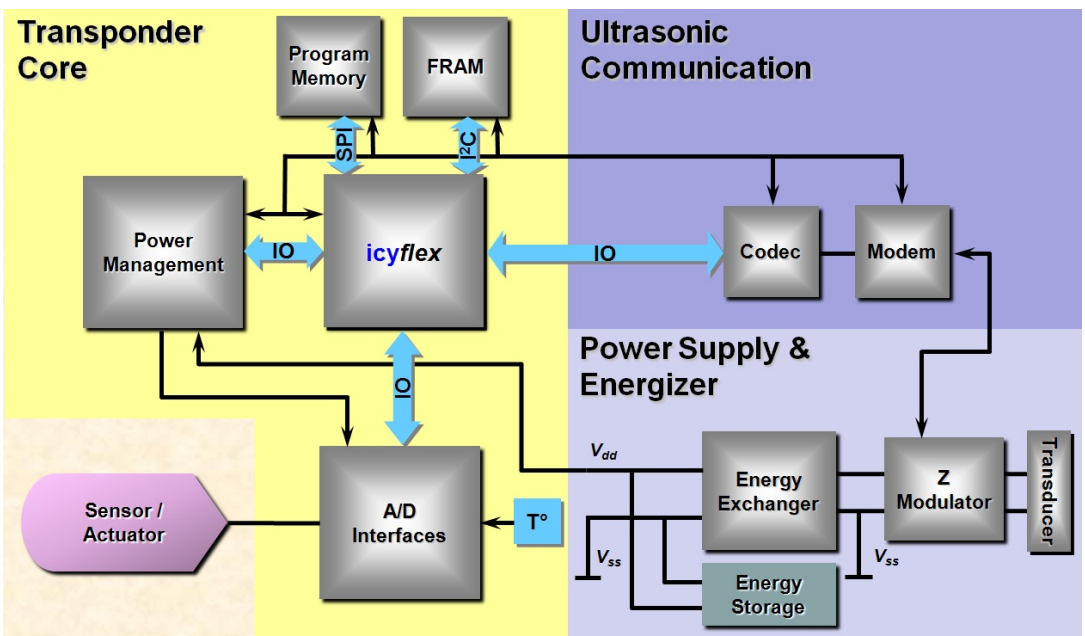

Figure 5.6: Concept of the transponder electronics. © *Eric Meurville.*

Figure 5.7: Kinetra® casing before adaptation to the project requirements. *Adapted from Medtronic Inc.* [65]

5.4.1 Casing

The demonstrator proposed in this work requires long-term biocompatibility; it was therefore a natural choice to use titanium, which is by far the most exploited material for IMD casing.

In order to prove the industrial viability of the implant, it was decided to integrate the electronics into an existing casing of a commercial device. This should assess the feasibility of the integration of the proposed system in standard manufacturing facilities. Furthermore, the surgeons being familiar with such casing, this will help for the *in vivo* assessments. Given the achieved size of the electronics, the neurostimulator Kinetra® produced by Medtronic was chosen (Figure 5.7). It is composed of two halves of Grade 1 titanium, which underwent homologation for biocompatibility. Each half is 300 μm thick.

Figure 5.8 shows the assembly of the device. In particular, it shows the bottom half of the titanium casing, thinned down in a small region, where the transducer will be later placed. The casing has eight pins (*feedthrough*) connecting the interior of the housing with the external world. They ensure waterproof connection to the leads, i.e., the cables going to the stimulation location. In the demonstrators presented in this work, which do not include a sensor, a modified version of the commercial leads is used to monitor some key parameters of the implant electronics.

The influence of a titanium casing on the ultrasonic transmission is of course not negligible. Because of its high acoustic impedance (22.5 MRayl) compared to the human body (~1.5 MRayl), titanium will induce an acoustical mismatching and will act as a barrier: the ultrasound will be partially reflected on it. As discussed in Chapter 4, a titanium layer of 100 µm allows ultrasonic transmission for the target application. A small region on the casing wall is thinned down and the transducer is glued inside.

The electronics are placed inside the casing, connected to the transducer and to the feedthroughs of the casing, for monitoring of the electronics behavior from the outside. The casing is then closed in a reversible way, in order to operate the TR device in water.

The thinning of the casing must lead to a clean end result, avoiding particles which could damage the electronics, or disturb the hermetic closing of the housing. The surface should be appropriate to glue the transducer to it, in order to transfer the ultrasonic vibration.

Wet etching consists in chemically attacking the material. The object to be etched is immersed in an etching solution, whose composition depends on the material chemical properties. Titanium is usually etched by chlorine- or fluorine-based chemistries (e.g., Hydrofluoric acid (HF)).

A disadvantage of this method is the immersion of the whole casing into the etching bath. This can be problematic when the casing already contains components (e.g., connectors) which would be more attacked by the etchant than the casing material.

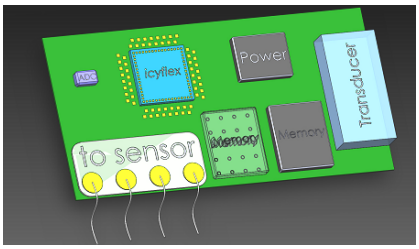

(a) Implant electronics.

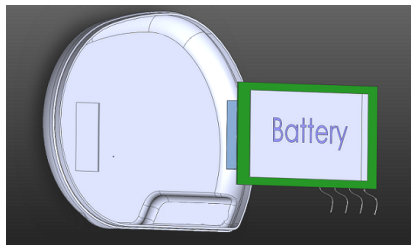

(b) Casing region thinned down. Transducer not shown.

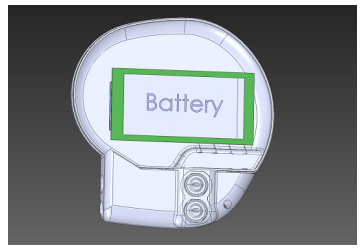

(c) Connection of the electronics to the casing feedthrough.

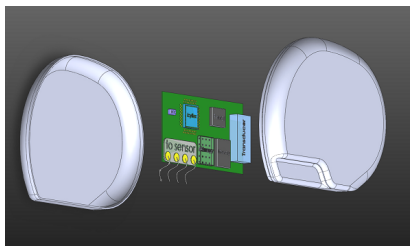

(d) Exploded view of the parts.

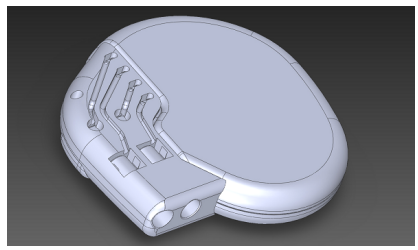

(e) Closed casing, with connector placed. Ready for implantation.

Figure 5.8: Assembly of the transponder device.

A localized etching furthermore requires masking of the remaining surface, thus introduces manufacturing steps. Finally, the chemicals used are highly polluting and toxic. Therefore, their use in IMDs imposes particular care and a strict protocol of post-etching cleaning.

Plasma etching relies on mechanical attack of high-energy ionized gas particles. For etching on titanium, Boron trichloride (BCl_3) is normally used.

The definition of the area to be etched can occur by coating the surface with a photo-resist, and exposing it to UV light through a mask having the target geometry. The exposed regions will softens and can be washed away. The remaining parts will protect the underlying casing regions from the etchant. The process is called in that case **photochemical etching**.

Both techniques require clean room facilities, which complicates the manufacturing process.

A far less clean technique consists in **electric discharge machining**: there, the metal is attacked by sparks (electrical discharges) between the tool-electrode and the metallic workpiece. This technique requires a dielectric material, normally oil-based. Disadvantages of this technique are the low speed and the contamination of the casing by oil, which needs then to be removed.

Another technique is **abrasive blasting**, in which the material to be thinned is bombarded by particles propelled at high pressure, such as coal slag, bauxite beads, or zirconia alumina crystals. This method is disadvantageous as it induces mechanical stress on the casing. Especially for thin material layers, the etching particles would deform the surface.

Finally, in **laser ablation** technique, material removal is achieved by hitting the surface by a laser beam. Normally, the beam reaches the surface by pulses rather than as a continuous beam. This allows a lower beam intensity. The etching characteristics, linked to the material properties, can be precisely adjusted by modifying the beam wavelength and pulse length.

A very high resolution can be achieved exploiting the fact that material to be etched quickly sublimates due to the high laser intensity, and therefore the surrounding material does not heat up. Further advantages

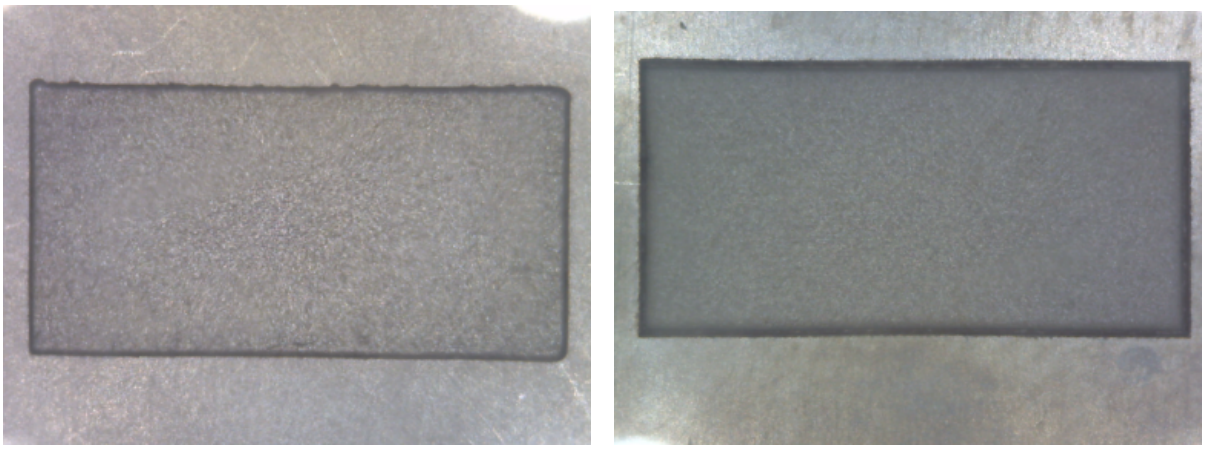

(a) Electric discharge machining. (b) Laser ablation.

Figure 5.9: Thinning result on a titanium sheet.

of laser ablation include absence of chemicals, ease in automation of the process, and precise control of the etching.

Preliminary tests are performed on titanium sheets of 300 µm thickness, manufactured by Good-Fellow Sàrl (Lille, France). Figure 5.9 visualizes the difference in surface condition between electric discharge machining and laser ablation. Laser ablation is the technique of choice for the manufactured demonstrators.

5.4.2 Transducers

The piezoelectric transducers for both the TR and the CU were designed and manufactured by IMASONIC. Both transducers are made of piezocomposite material realized using a *dice-and-fill* process, in which a bulk PZT material is shaped in rods and the resulting empty spaces among rods are filled with a polymer material. As seen in Chapter 4, the transducer material and the geometrical design of the piezocomposite were custom designed according to the project specifications. The piezocomposite thickness was chosen with regard to the 1 MHz working frequency. Copper electrodes were placed on both sides of the transducers.

5.4.2.1 Transponder transducer

The main role of the transducer in the TR is to receive the incoming acoustic waves. The TR is likely to move in the final application (because of the heart motion) and this will change the incidence angle of the ultrasonic waves on its surface. In order to optimize the angular acceptance in reception, the receiving area of a single element should be decreased. Therefore, the total transducer surface of 5 mm × 10 mm was divided into 6 elements of 1.2 mm × 5 mm each, for a total active surface of equivalent to 36 mm^2. The pitch of the array was set to 1.5 mm, corresponding to the wavelength at 1 MHz. The single element of the transducer array are separated by a soft polymer, in order to minimize the coupling between neighboring elements.

The TR transducer is either integrated on the thinned region of the Kinetra® casing or plugged in an aluminium prototype box. The most reliable method to connect the transducer to the Kinetra® casing

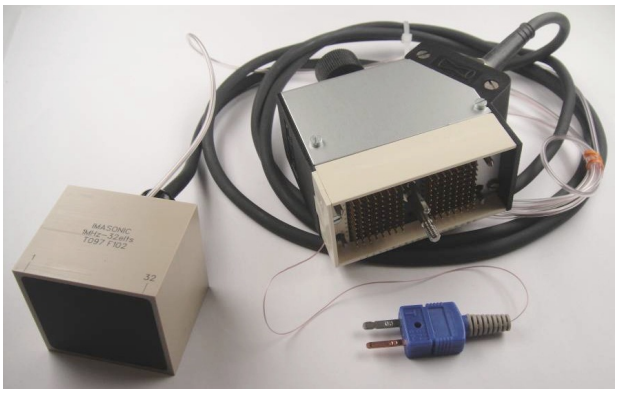

(a) Control Unit: 32-elements array.

(b) Transponder: 6-elements array.

Figure 5.10: Transducers exploited in the final demonstrator (not to scale).

is gluing: epoxy-based glues provide a flexible joint, which allows vibration of the transducer without creating fatigue in the glue. Appropriate glues can withstand the transducer operating temperature. Figure 5.10 shows the 32-elements transducer of the CU and the 6-elements TR transducer, covered by titanium and inserted in a plastic housing for integration in the aluminum casing. The same transducer, without the housing, was glued on the titanium casing.

5.4.2.2 Control Unit transducer

Two version of transducers were developed for the CU: in a first design, a shaped transducer was manufactured, consisting of 64 independent channels. The round shape intrinsically focuses the acoustic beam at around 15 cm. Each element of the CU transducer has an area of 30 mm $\times$ 1.55 mm, the pitch between each element is 2.05 mm and the whole transducer bandwidth at -6 dB is 65%.

In a further development, a flat transducer was preferred, in order to obtain a broader focus point. A smaller array was manufactured, which contains 32 elements.

Both CU transducers are equipped with a temperature sensor, in order to monitor the heat produced during emission and avoid excessive temperature, which could depolarize the transducer.

5.4.3 Power storage

For the system proposed, ultra-thin batteries were used (Thinergy® series by Infinite Power Solutions, Littleton, Colorado, USA). They possess a thin form factor (170 μm thickness) and are available in several surface dimensions and capacities, up to 1 mAh for 6.5 mm^2. Their very low thickness makes them particularly suitable for small size devices, as the battery can be fit under the printed circuit board and contributes very little to the device size. If needed, several cells can be stacked to reach higher capacity.

IPS batteries are all-solid-state batteries, containing non-combustible and non-reactive electrolytes (e.g., LiPON). This is advantageous for implantation to avoid leakage. They have a very high discharge rate capability and an ultra-low self-discharge rate, which makes them suitable for long-term operation. Their recharge occurs at constant voltage with no current limitation, thus allowing a rapid and easy recharge. Finally, they are RoHS compliant.

The battery needs a stable DC level to be recharged, between 4.1 V and 4.5 V. Moreover, the battery must not be discharged lower than 2.2 V; otherwise it will not be able to be recharged again. For this reason, IPS batteries come with an integrated interface between the battery, the recharging signal and the load: the MAX17710 power management chip (by Maxim Integrated, San Jose, CA, USA).

5.4.4 Digital Signal Processor

To coordinate the operations of all components of the device, a microprocessor is required. Within the ULTRAsponder project, a custom, very low-power Digital Signal Processing (DSP) processor called *icyflex* has been designed by the Centre Suisse d'Électronique et de Microtechnique SA (CSEM) (Neuchâtel, Switzerland).

The processor shows low power consumption with respect to competitor products [18]. As an example, Texas Instruments MSP430 (by Texas Instruments, Dallas, Texas, USA) draws at least 1 µA when in low power mode and 150 to 290 µA/MHz when in standard operation [102], in both cases under a 3 V supply voltage. Icyflex operates on an internal voltage as low as 1.8 V, but is able to generate on its pins regulated voltages ranging from 1 to 3.6 V. Average power is in the range of 150 µW/MHz when in operation and only 1 µA quiescent current in hibernation. A set of voltage regulators allow advanced power management features and different power modes [92]. The input/output pads are grouped into 4 supply banks. Each bank is powered with a separately selectable voltage, from 1 to 3.6 V, in order to supply external components from 0.9 to 2.7 V and 1 to 5000 µA. This allow switching off external components and parts of the chip, e.g., using General Purpose Input/Outputs (GPIOs) as power switches. The main voltage of the chip has to remain between 1 and 1.8 V because of the 0.18 µm Complementary MOS (CMOS) technology used for the Digital Processing chip. The microprocessor offers 4 possible clock sources: an internal RC oscillator at 16 MHz, a 32 KiHz quartz, a 48 MHz quartz, and an external pad. Frequency dividers allow adjustment of the clock period. The switch between clocks occurs without glitches.

The microprocessor offers three modes of operation:
A **normal mode**, where the complete circuit is powered up and running. In this state, the microprocessor has a maximum power consumption of 150 µA/MHz.
A **sleep mode**, in which all digital blocks are powered up, but the processor core is in sleep mode. Clocks are generated and distributed to peripherals. The microprocessor core can be waken-up on an interrupt request (e.g., from the Real-Time Clock (RTC) or from an external event). The microprocessor has a power consumption in the order of 10 µA.
An **hibernation mode**, in which all the digital blocks, except the RTC, are powered off and the system can be woken up at a predetermined date by the running RTC or by an external signal through a GPIO. At wakeup time, the Random Access Memory (RAM) will have to be re-loaded from the external Electrically Erasable Programmable Read-Only Memory (EEPROM) during a standard boot sequence. The power consumption in this state is on the µA range.
Table 5.2 summarizes the power consumption of the different blocks and the main characteristics of the icyflex device.

5.4.5 Memory

The data storage chosen is a FRAM device, developed by Ramtron International (Colorado Springs, CO, USA) [81]. A large spectrum of possible sizes and power consumption levels are available, thus allowing an optimum trade-off according to the application needs. Power consumption can be as low

Table 5.2: Main characteristics of the icyflex microprocessor.

Parameter	Comments	Value	Unit
Voltage supply	Alkaline cell supply	1-1.8	V
	Using step-ups	2.7-3.6	V
Hibernation mode	Only RTC active, for wake-up	5	μA
Normal mode	32-bit processor, max 3.4 MHz, 1.0 V	120	μA/MHz
High-current Step-up	95% current efficiency	4-13	mA
Low-current Step-up	50% current efficiency	10	μA

as 20 μA @ 1 MHz. Ramtron devices can withstand up to 10^{16} write/erase cycles while operating at 3.3 V. Finally, FRAM devices by Ramtron are gamma-ray tolerant, thus compatible with this specific sterilization method.

5.4.6 Sensor

To complete the device, a sensor and its interface to the Transponder electronics would need to be integrated in the implant.

For the targeted application, the impedance of the heart is measured. The sensor consists of four electrodes placed on the heart. Two electrodes inject a current, and the two others collect the resulting voltage, thus measuring the tissue impedance. The electrodes are a modified form of the Model 3889 leads, connected to the Extension Kit for Deep Brain Stimulation (Model 7482A), both manufactured by Medtronic (Figure 6.5).

The analog signal sensed by the leads needs to be converted into a digital data and stored into the memory. An ADC, custom made by IMST GmbH (Kamp-Lintfort, Germany), was connected in between the leads and the icycom unit. The microprocessor drives and controls the ADC actions through a Serial Peripheral Interface. The sensor and its ADC interface have been assessed within the ULTRAsponder project by IMST and Medtronic research groups. However, the sensor was not integrated in the demonstrator manufactured, and therefore no data are presented in this work.

5.4.7 Backscattering modulation switch

A very important point of the project is the data communication by backscattering modulation. This technique allows the data transfer with minimal energy consumption. In analogy with RF backscattering, the "0" and "1" logic levels are communicated by varying the acoustic impedance of the piezoelectric element. A switch is used to alternatively connect the transducer to a capacitor of high value, which increases the acoustical impedance and makes the transducer stiff (i.e., reflective, backscattering a "1" level), or to an inductor, which lowers the acoustic impedance, allowing energy absorption and thus backscattering a "0" level.

5.4.7.1 Subcarrier generator

The electronics show a strong crosstalk, i.e., the 1 MHz excitation carrier, which is much stronger than the backscattered signal, causes saturation problems in the receiver and reduces the modulation depth of the resulting AM signal, thus making the demodulation more difficult. In order to increase the

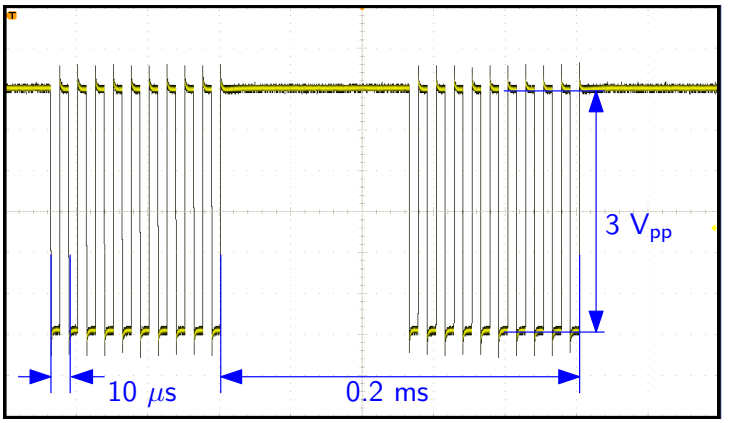

Figure 5.11: Resulting signal of a subcarrier at 100 kHz and a modulating signal at 5 kHz.

modulation depth and allow an efficient demodulation, the system takes advantage of the subcarrier modulation technique. Instead of directly modulating the data, the transponder modulates the data bits over a subcarrier. The new modulating signal, which drives the backscattering switch, is composed of the actual modulating signal (the data coming from the microprocessor) multiplied with the subcarrier, e.g., a 100 kHz square wave of amplitude 3 V_{pp} and 1.5 V DC offset. The resulting modulated signal is shown in Figure 5.11.

Exploiting the subcarrier, the modulated signal is shifted in frequency away from the carrier, which results in lower ratio between amplitude of the modulated signal and amplitude of the subcarrier (higher modulation depth) and therefore easier demodulation.

It was chosen to exploit a 90% AM subcarrier instead of a 100% AM, in order to avoid that no energy at all would be backscattered when in "0" state. Otherwise, the receiver would see only noise during that period, and this would disturb the modulation.

In a first moment, the subcarrier and the modulating signal have been implemented by an external waveform generator (HP33120A). In the final demonstrator, the generator of subcarrier was integrated on the CU electronics.

5.4.8 Phantom material

To facilitate the assessment of the ultrasonic transmission in conditions close to *in vivo*, a phantom material was manufactured by the Institut National de la Santé Et de la Recherche Médicale (INSERM) (Lyon, France), which mimics the properties of soft body tissues. It is composed of an Oil-Styrene polymer and has the form of a 16 cm diameter cylinder. Its acoustic attenuation is 0.3 dB/cm/MHz, close to that of soft tissues. Small plastic tubes were inserted in the mold, in order to mimic a blocking structure, for example ribs. Figure 5.12 shows the ready phantom.

5.5 Means of verification

In order to assess the functionality of the proposed device, and to validate the choices of technology, materials and methods, it is necessary to define the parameters according to which the system should be evaluated, and the tests and simulations to be performed for that purpose.

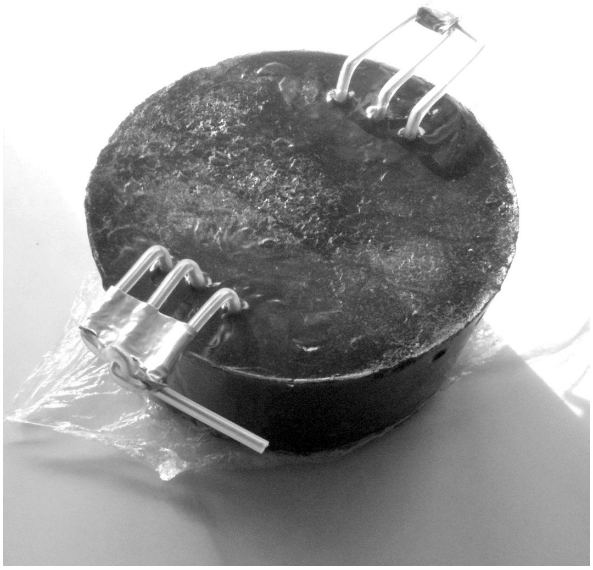

Figure 5.12: Phantom material mimicking a soft tissue and ribs.

Simulation of Ti influence: as a first test on the system, the effect of titanium casing on the acoustic link must be assessed. It is expected that titanium will attenuate and disturb the ultrasonic transmission. As described in Chapter 4, the TR sandwich is modeled and the transmission of the maximum acoustic intensity level allowed by the FDA for this application (0.7 W/cm^2) is simulated. The material properties are described based on the KLM model [55].

The goal is to define the maximum thickness of titanium through which the acoustic transmission can be established, in order to plan the thinning needed to improve the transmission. It is not possible to progressively test the acoustic transmission and thin down the titanium material. The optimum thickness needs to be determined in simulation, the casing thickness must be adjusted if required, and finally the *in vitro* assessment can be performed.

Energization possible within FDA limits: once the optimal casing thickness has been established, the casing is adjusted to that thickness. A second key factor of the system is the compliance with the regulation. This depends on the carrier parameters used (frequency, duty cycle, intensity), and on the efficiency of the electronics on both CU and TR side. Given a set of parameters of the CU electronics, the emitted signal along the path can be calculated, and it can be verified whether or not it complies with the regulation. Once the best trade-off is found, which gives the more powerful signal at the TR within the limits set by the regulation, those parameters should be verified *in vitro* and the recharge of the battery on the TR must be assessed.

Energization and Communication *in vivo*: finally, the system should be evaluated in conditions close to the target application. An *in vivo* measurement set is required, in which both energization of the TR and communication from the TR to the CU is successfully shown.

5.6 Conclusion

This chapter presented the ULTRAsponder project, to which the author of this thesis contributed. An IMD was conceived, which addresses several technological challenges in state-of-the-art devices.

It is proposed to exploit ultrasound as a carrier for both energy and data transfer between a CU and one or more implanted TRs.
Data transfer can be performed using very low power, due to the backscattering technology.
The electronics of the system are carefully chosen among commercial off-the-shelf components, or custom designed within the project. A FRAM device is chosen for data storage, in order to achieve long device life and MRI compatibility. Thin-film, solid-state batteries are exploited, which carry an integrated power management unit. Custom ADC and microprocessor modules are designed.
A commercial titanium housing is taken into consideration, mostly because of its biocompatibility. A region of the casing is thinned down by laser ablation.
A phantom material is manufactured, which mimics real test conditions.
A test procedure is established, in order to verify the good behavior of the demonstrator.

6 Demonstrators produced

6.1 Introduction

Within the ULTRAsponder project, several demonstrators were designed, in order to validate the components and strategies chosen at different stages of the concept development.

The first demonstrator presented in this chapter aimed to prove the concept of an energy transfer through acoustic waves between an external CU and a TR. The two transducer devices were held at about 15 cm distance in a testbed filled with water, in order to mimic a deep implantation, but avoiding at first the attenuation of soft tissues.

In a second step, the phantom material described in Chapter 5 was inserted in the ultrasonic chain.

The transducers and the electronics on both CU and TR side were refined based on the different tests and on the evolving specifications.

As a support for the improving implant two casings were provided, each of them adapted to the tests intended and the geometry of the electronics manufactured.

The final demonstrator of the complete system could be used for real-conditions assessment of both energization and data communication, performed by *in vitro* and *in vivo* tests.

A real sensor for the intended application, i.e., monitoring of the heart impedance, and its ADC were successfully manufactured and tested within the project, but could not be integrated in the final demonstrator due to time constraints.

6.2 Testbed

A platform was built to study ultrasound propagation and test the demonstrators produced [63] all along the development of the device. A cubic plexiglas tank of edge 50 cm is used as a container for a pair of electro-acoustic transducers, where a CU is fixed to one wall of the tank and a TR can be manually moved in three axes and rotated using a mechanical system. The tank is filled with water to allow acoustic energy and data transfer, and the system is optimized to avoid parasitic effects due to cables, reflection paths and cross talk problems. Fig. 6.1 shows the *in vitro* platform. In order to reduce standing waves and echoes, an absorber material made of silicone is placed all around the two transducers (Aptflex F28 by Precision Acoustics, Dorchester, Dorset, UK). In the CAD rendering, the absorber material is only present behind the CU transducer in order to clearly show the Transponder transducer. The mechanical system is used to move the piston transducer inside the tank along the x, y and z axes with a resolution of 50 µm, also having the possibility to be rotated $\pm 25^\circ$ along the x axis.

6.3 Housing

6.3.1 Aluminium casing for electronics development

In the development of the project, a prototype casing has been manufactured, which hosts the TR electronics under development. The casing was designed and fabricated by the transducer manufacturer,

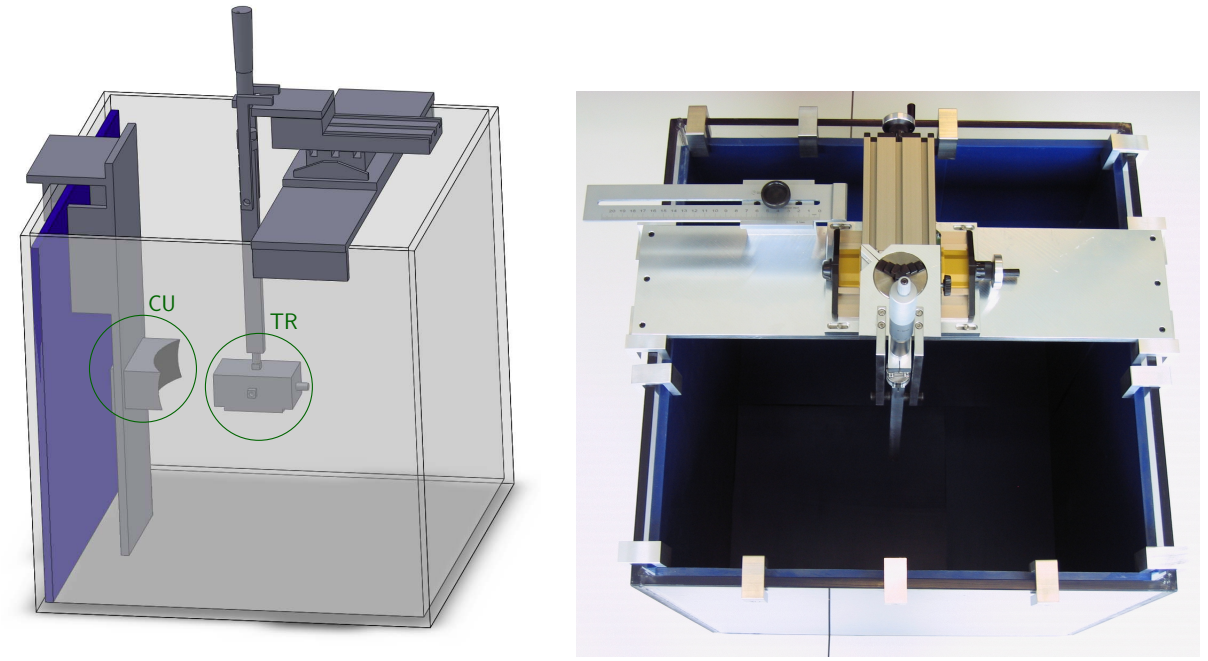

(a) CAD rendering of the testbed.

(b) Mechanical table to move the transponder.

Figure 6.1: Testbed developed for the demonstrator assessment.

for optimal integration of the transducer itself. It is made of aluminium and composed of a bulk part, holding the transducer and a cable bunch, and two lids to hermetically close the housing. Connector CLP-105-02 manufactured by Samtec (New Albany, IN, USA) is soldered on the transducer, and its complementary connector FTSH-105-01-X-DH is mounted on the demonstrator electronics. Signals from the electronics or from the transducer can be transferred to the external world by a bunch of coaxial cables (PC 64 Y manufactured by Axon' Cables SAS, Montmirail, France), which is hermetically clamped into the prototype housing.

The design of the housing and the connection between transducer and electronics are shown in Figure 6.2.

6.3.2 Titanium casing for *in vivo* measurements

Within the ULTRAsponder project, a commercial casing is chosen, in order to prove the acoustic link through an homologated housing. The casing of the Kinetra® neurostimulator is chosen. Its dimensions offer enough space for the expected size of the final electronics, while still allowing good implantability in pigs for *in vivo* tests.

6.3.2.1 Casing thinning

The Kinetra® casing chosen has a thickness of 300 µm. According to the simulations performed on the transducer (Chapter 4), it is decided to thin a region of the casing down to 100 µm, in order to allow a good transmission of the ultrasonic wave while keeping a good structural integrity. Among different options to machine titanium, laser ablation is chosen, performed by LaserJura (Rossemaison, Switzerland).

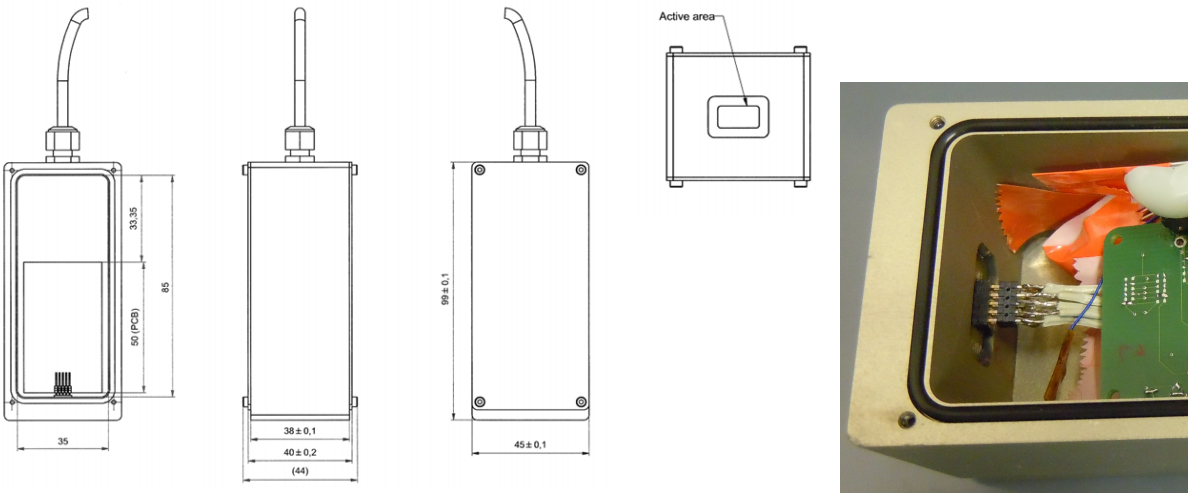

(a) Geometry of demonstrator casing.

(b) Connection to the electronics.

Figure 6.2: Aluminium demonstrator casing.

Figure 6.3 shows the geometrical plans for the thinning of the half casing. The shape of the thinned region is specified by the manufacturer of the transducer based on the transducer geometry and of the gluing method.

6.3.2.2 Connection to electronics

During the first steps of the electronics development, the electric signal from each transducer element are connected to the eight feedthroughs available on the casing, and from there to the external electronics.

In the final version of the TR electronics, the PCB is placed inside the casing, which provides better connection and more reliable signal transmission. In order to achieve an efficient acoustic coupling between the transducer and the titanium layer, the glue joint must be as thin as possible. A 10 μm thick epoxy joint is used. In order to avoid harmful strain on the piezoelectric elements, a connector (Micro-MaTch, by TE Connectivity Ltd., Schaffhausen, Switzerland) is glued next to the transducer and the TR's PCB connects to it, as shown by Figure 6.4.

6.3.2.3 Sealing method

In a first step, the new demonstrator has to be tested *in vitro*, to assess energy and data transfer through the titanium barrier. After the tests with the aluminium casing, the TR boards are assembled into the Kinetra® casing and the same energization and communication tests are performed. Proper casing sealing should be avoided at this moment, as it may be necessary to adjust the electronics inside the casing.Therefore, a sealing method must be developed, which ensures waterproofness during roughly a day, is reversible with as few as possible residual glue on the casing, and is possibly easy and quick to apply. Several sealants have been tested to this end on an empty casing, without connectors. Both the feedthrough locations and the joint between the two halves of the casing must be covered and sealed. Silicone-based sealant Dow Corning 734 has been applied on the joint. It proved to effectively adhere to the titanium surface, which has been previously cleaned with acetone.The glue layer could be removed by manual pulling off the layer, then with acetone solvent. Where needed, a cutter was used to remove glue

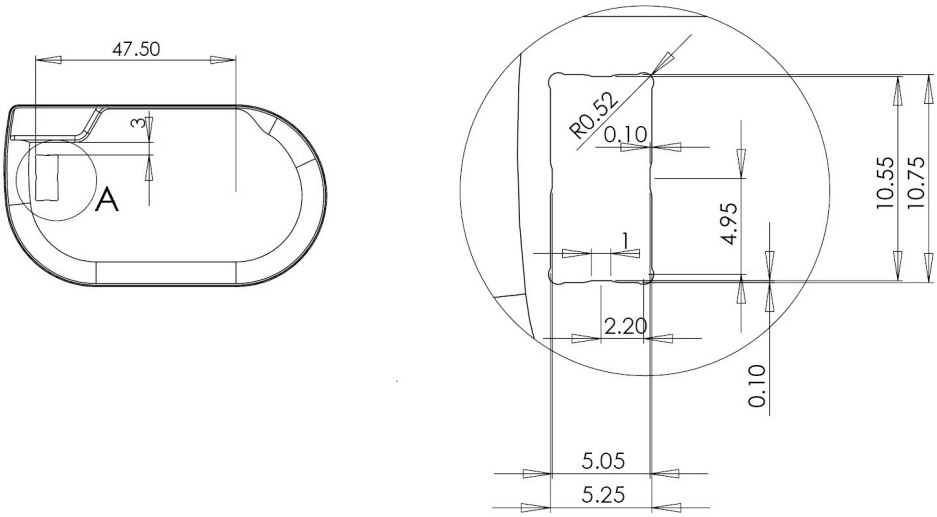

Figure 6.3: Geometrical plans for the thinning of a region on the Kinetra® housing.

from the joints. Cleaning with acetone was performed prior to further gluing tests. Dow Corning 734 is a solvent-less silicone elastomer in the form of a flowable liquid. It has been chosen because of the easy application method and ability to cure at room temperature. It is chemically not dissimilar to medical silicone glue, routinely used in implants. As the feedthrough connector was not used for this sealing test, a generous amount of silicone sealant is applied on the feedthrough pins on the casing, in order to protect them and ensure waterproof protection at that level. The glue was cured 24 hours at room temperature. The casing was then put into water for 3 hours to check waterproofness.

This sealing method was sufficient to perform the tests over several days *in vitro*, as well as *in vivo* conditions for few hours.

Figure 6.5 shows the sealed Kinetra® casing. Custom modified leads are attached to the feedthroughs.

6.4 Characterization of the TR transducer array

Prior to integration in the casing, the transducer for the TR was characterized according to its electrical impedance, sensitivity, directivity, and angular acceptance.

6.4.1 Method

The electrical impedance of each element of the transducer array was measured by a network analyzer. The array was coupled to water and connected to the analyzer through a 1 meter multicoaxial cable, which impedance was compensated for a precise result.

For each element, the sensitivity (peak-to-peak voltage) to a mechanical input, the fractional bandwidth, and the central frequency at −6 dB were deduced from pulse-echo measurements on a brass target in water.

The directivity in emission was measured in water with an hydrophone turning around the transducer in the far field region (14 mm from the transducer). The measurement was performed for each element using a sinusoidal excitation of period 1 MHz.

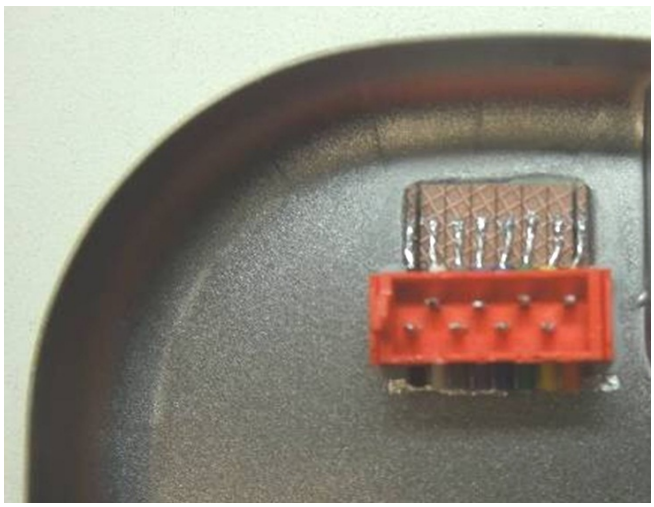

(a) Kinetra® casing hosting the transducer array (brown) and the Micro-MaTch connector (red).

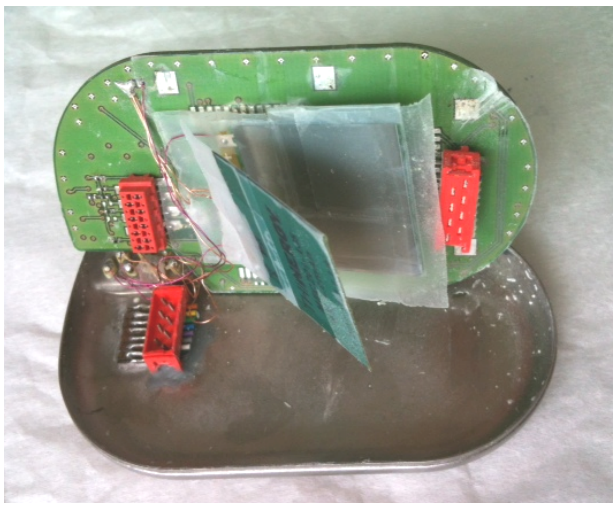

(b) Connection to the electronics.

Figure 6.4: Connection strategy in the Kinetra® housing: the transducer array is glued on the casing and soldered to the Micro-MaTch connector, on which the PCB is then connected.

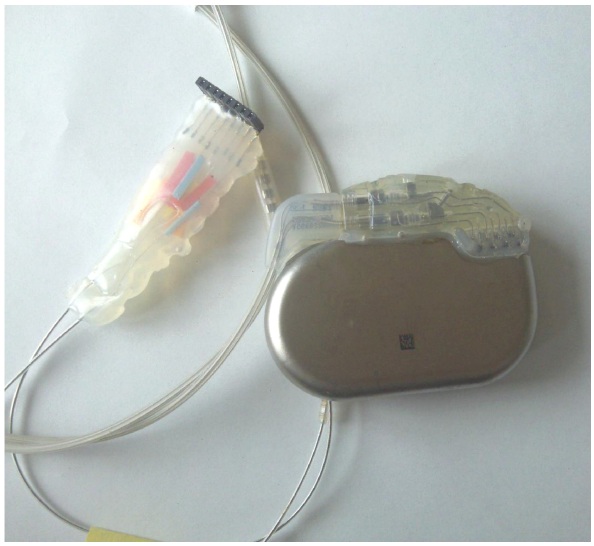

Figure 6.5: Kinetra® casing with modified leads.

Table 6.1: Electrical impedance, sensitivity, and central frequency of TR transducer.

	Element number						**Average**	**Simulated**
	1	**2**	**3**	**4**	**5**	**6**		
Z_r @1MHz [Ω]	937	806	778	825	825	855	838	732
Z_i @1MHz [Ω]	346	310	342	297	294	673	310	349
Voltage [mV_{pp}]	162	159	180	167	170	165	167	-
F_c [kHz]	943	956	969	957	964	950	957	947
BW/F_c @ -3dB [%]	17	13	15	14	16	18	16	15

The angular acceptance of the TR in reception was measured in water with one element on the CU emitting and one element on the TR receiving.

The CU was excited with a burst of 25 periods of sine 1 MHz and the generated voltage on the transponder was measured on an oscilloscope on 50 Ω. The TR was placed at 16 cm from the CU on the wave propagation axis. It was aligned with the CU array along both the elevation and the lateral axis, in order to maximize the reception. Afterwards the CU was turned around the lateral axis.

6.4.2 Results

Table 6.1 gives the characterization results for the electrical impedance, the sensitivity, central frequency and bandwidth. Simulation results are also given for comparison.

The electrical impedances is close to the ideal value (750 + 750j)Ω for each of the 6 elements in the array. It is interesting to note that the imaginary part is positive. This is due to the ringing behavior linked to the titanium presence. For a well damped transducer, the imaginary part is usually negative. For the present case, the positive imaginary part should be helpful for the power transmission efficiency, because it compensates the transponder PCB, which has a capacitive behavior due to the battery.

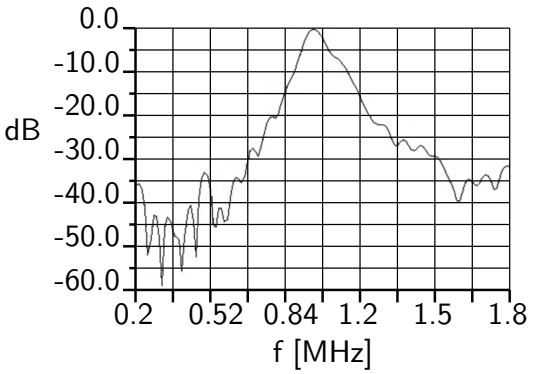

Characteristics at -6 dB:
Central Frequency: 969 kHz
Ratio Bw/F_c: 15%
Bandwidth: 144 kHz
Lower Cutoff Freq.: 897 kHz
Upper Cutoff Freq.: 1.04 MHz

Figure 6.6: Frequency spectrum of a single flat array element in emission-reception.

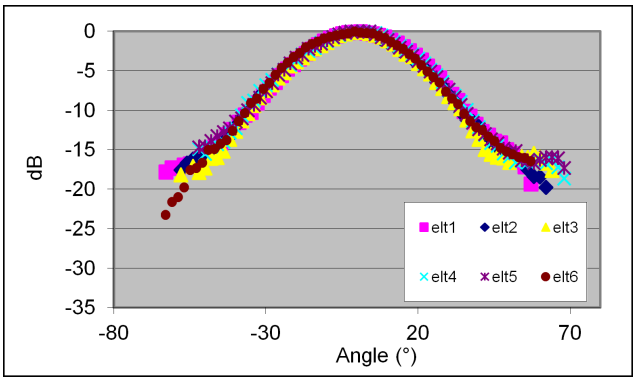

	Directivity [°]	
Element #	**@ -3 dB**	**@ -6 dB**
1	37	53
2	34	52
3	34	52
4	36	54
5	35	54
6	38	54

Figure 6.7: Characterization of the effect of tilting on the TR transducer in emission.

The 6-elements arrays exhibits a good homogeneity (between 150 and 180 mV). The central frequency is close to 1 MHz and the sensitivity homogeneity is about 1.1 dB. The bandwidth is approximately 16%. The relatively narrow bandwidth is due to the big mismatch in acoustic impedance between the titanium and the transmission medium. The presence of an adaptation layer, which is not feasible in the device proposed, would extend the transmission peak over a larger bandwidth. Figure 6.6 gives a typical spectrum obtained for one element.

There is a good matching between experimental results and simulations. The differences are due to the variability of properties of the transducer materials among samples, mainly resulting from layer effects in the sandwich and from fabrication-induced stress and heat.

Figure 6.7 shows the directivity of the transducer elements in emission. The directivity in emission exhibits a good homogeneity for all the elements: it was about 35 ° at −3 dB and 55 ° at −6 dB.

The angular acceptance (Figure 6.8) is about 40 ° at −3 dB and 60 ° at −6 dB along the lateral axis, and about 15 ° at −3 dB and 25 ° at −6 dB in the elevation direction. This gives a good flexibility for the system with regard to the TR motion.

The relative voltage is plotted in dB versus the angle θ between the transducer and the hydrophone as $20 \log \frac{V(\theta)}{V_{max}}$, V_{max} being the maximum voltage obtained for $\theta = 0$.

In order to further enlarge its angular acceptance, the transponder could be divided into elements in the elevation direction, similar to the division into six elements along the lateral axis.

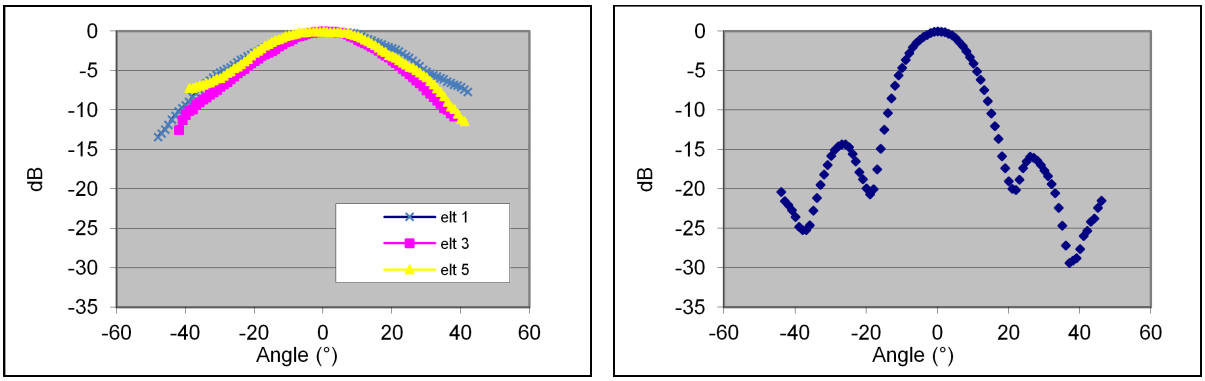

(a) Directivity along lateral axis.

(b) Directivity along elevation axis.

Figure 6.8: Characterization of the effect of tilting on the TR transducer in reception.

6.5 First proof of concept

In a first step of the ULTRAsponder project, preliminary demonstrators of the CU and of the TR have been designed and produced. Commercially available components have been used, while custom components were under development by the partners of the consortium. The functionality of the demonstrator has been tested, to prove the concept and to estimate the link budget between the CU and the TR. Key numbers on that stage are the efficiency of the power link and the power levels to be transmitted. Similarly, the data transmission from CU to TR and vice-versa were assessed. Key numbers are data rates and reliability of link. The test bench allows investigating the influence of the movement of transducer (translation and rotation) and the influence of CU and TR location on the above parameters.

The transducers used with this first demonstrator are the 64-channel array on the CU side, and the 6-element transducer, mounted in the aluminium prototype box, on TR side.

6.5.1 Electronics description

The system demonstrator manufactured is composed of three PCBs (namely TRANS, CU_base and CU_RX), which connect to the transducers. This prototype is intended to be extensively assessed and characterized *in vitro*. An external filter and a subcarrier generator have been added during the test evolution, to improve the performances of the signal received. No sensor is included in this demonstrator, the data message to be transferred is predefined and do not depend on the external environment. The block diagram of the demonstrator including the different elements is depicted on Figure 6.9, while Figure 6.10 depicts the manufactured circuits.

The components used in the demonstrator are commercially available but not necessarily optimized for the target application. This in order to prove the concept with a simple architecture and well established components.

6.5.1.1 CU baseboard

The interface between the transducer of the CU and the power generator is provided by the CU_base PCB. Eight elements of the transducer are reserved for reception, evenly distributed among the 64 available (elements 8, 16, 24, 32, 40, 48, 56 and 64); all the other elements are dedicated to ultrasonic emission.

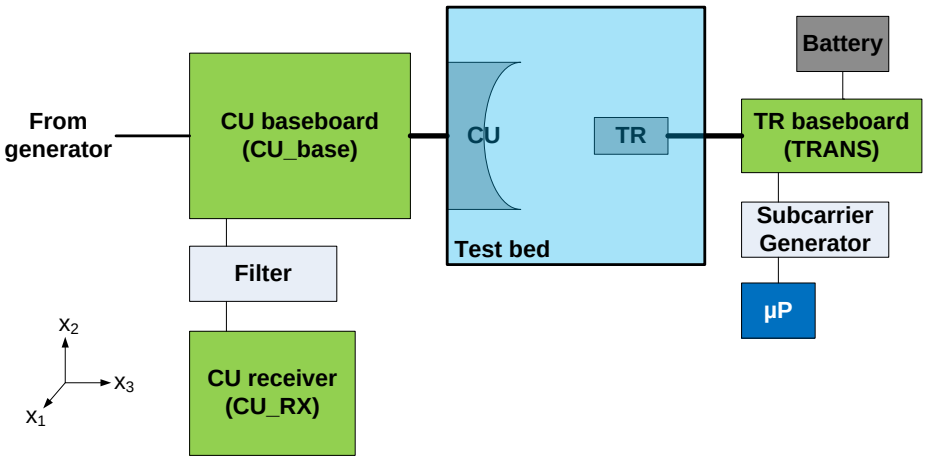

Figure 6.9: Block diagram of the first demonstrator.

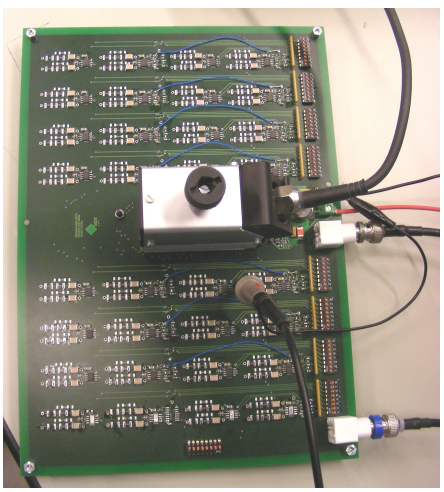

(a) Control Unit. Baseboard *CU_base*.

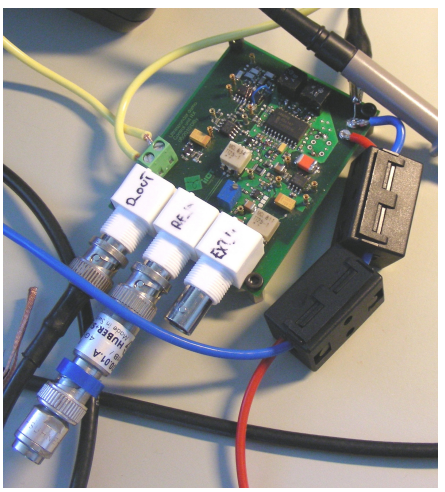

(b) Control Unit. Receiver circuit *CU_RX*.

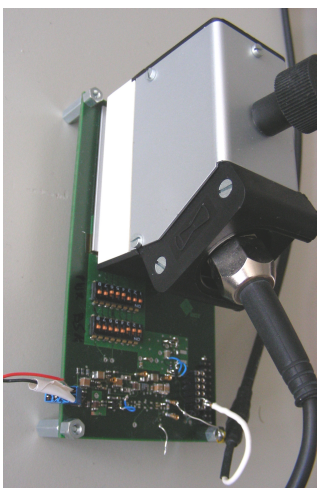

(c) Transponder.

Figure 6.10: First system demonstrator.

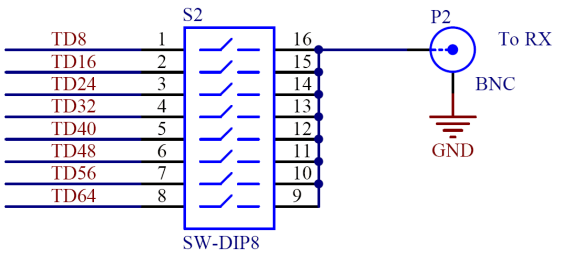

Figure 6.11: Detail of CU_base. Choice of reception elements.

The circuit responsible for the emission is divided in seven identical parts, each of them driving eight elements of the transducer. A manual switch allows connecting or disconnecting each element to the power generator. That is useful to shape the acoustic beam transmitted by the CU. The eight reception elements are connected to another switch (S2 in Figure 6.11), so that it can be decided whether or not to add the contribution of each single element to the total reception signal.

An input Transistor-Transistor Logic (TTL) signal is fed into the PCB and gives the form to the final wave transmitted. The amplitude of the wave is given by an external voltage generator V_{driver}, regulated into V_{DR}. A filtering stage has been foreseen but proved not necessary.

6.5.1.2 CU receiver and filter

The signal backscattered by the TR device is collected from elements of the CU reserved to this aim and redirected to CU_RX. This PCB is responsible for demodulating the received signal. Between CU_base and CU_RX there are a filter stage and an attenuator, which improve the signal transfer. The filter should remove the main carrier at 900 kHz on which the energy is transferred from CU to TR. The remaining signal will present the modulated message and the subcarrier. The attenuator may be placed on the coaxial connector of CU_RX, in order to reduce the power injected which could saturate the PCB.

6.5.1.3 TR baseboard

This PCB is a first prototype of the implanted transponder. It contains the circuitry for the energy harvesting from the transducer, and the electronics needed for the communication of the data. It does not contain yet the interface to the sensor, nor the sensor itself. Similarly to the choice of receiving elements implemented on CU_base, two switches on TRANS allow choosing which of the six elements are devoted to collect the energy received from the CU, and which elements will be used for communication.

The energization circuitry is essentially composed of three integrated circuits, manufactured by Linear Technologies (Milpitas, CA, USA) and Texas Instrument (Dallas, TX, USA): the LTC3588-1 rectifier combines the electrical wave of all contributing elements and outputs a 3.3 V DC voltage. The boost converter TPS61220 steps up that voltage to the 4.2 V level needed to recharge the thin film battery. Finally, a regulator (TPS78001) converts the battery voltage to power the microprocessor, which requires a 1.8 V voltage level.

The backscattering circuitry relies on an electronic switch performing the change in impedance. It is driven by the microprocessor signal. A series of diodes limits the voltage of the transducer elements dedicated to backscattering between −0.7 V and 3.6 V, in order to protect the switch from the incoming energization wave.

6.5.2 Test performed

The aim of the preliminary tests is to prove the concept of the system, i.e., to use an ultrasonic wave to recharge a thin film battery that will power an electronic circuit containing a microprocessor, and to establish a communication between the CU and the TR. All along the process of mounting the components, the different PCBs were checked against short circuits. The functionality of the system was assessed, starting from the single, separate functions of each bloc and evolving towards the behavior of the complete system.

In the energization tests, the transfer of energy from the generator, through the CU, through the acoustic link to the TR is assessed. In the backscattering tests, the aim is to evaluate the transfer of the wave carrying the information stored in the implant. The wave travels from CU to TR and back, so its transfer is affected twice by the medium and by the reflection on the TR interface.

6.5.2.1 Functional test of the CU baseboard

The circuit CU_base, connected to the two external power supplies V_{driver} and V_{logic}, creates the signal to be delivered to the transducer elements chosen. The switches drive the signal to the correct elements. The input to CU_base is a TTL signal, that is a 1 MHz square wave, with an amplitude of at least 2.4 V_{pp} and an offset of half the amplitude. An arbitrary voltage level is chosen for V_{driver}, and the necessary 9 V are set for V_{logic}.

The resulting wave on each pin of the connector is observed on the oscilloscope. The excitation wave will have the form of the input TTL signal, and the amplitude of V_{driver}. Then, the CU transducer contained in the tank is connected to CU_base, and the power required to drive all elements or a subset of the transducer is monitored.

6.5.2.2 Functional test of the TR baseboard

The electronics of the implant are assessed without the transducer. When a power supply is plugged on the transducer connector, the circuit must rectify the wave supplied and use that power to recharge the battery and start the microprocessor. The excitation is provided by a signal generator plugged on the connector hosting the transducers. On each of the six pins connected to the PCB a resistance of 1.2 kΩ is connected, to model the impedance of the transducer element as characterized by the manufacturer. In reality, the impedance of the element also presents a reactive part of about −1.5 kΩ at 1 MHz (equivalent to a capacitance in series). It is very important to have a high impedance at the input of TRANS, because of the backscattering switch: its power supply being at 3.3 V, it cannot withstand the high voltage obtained by the energization (up to 25 V). For this same reason, the backscattering switches are protected by a series of diodes.

The signal is supplied in parallel to all resistances, and a 1 Ω resistance is connected in series to allow the measurement of the power consumption. The small value of this resistance is negligible with respect to the transducer impedance: the total impedance of the transducer varies between 200 Ω (parallel of six resistances of 1.2 kΩ) and 1.2 kΩ (only one element connected). The error is therefore smaller than 0.5%. The ground of the signal is connected to the appropriate pins on the connector. The power is measured indirectly: the voltage drop across the 1 Ω resistance is measured with a differential probe, while another probe measures the amplitude of the wave injected into the PCB (V_{IN}). Two measurements are relevant at this stage:

Minimum voltage to be provided to the PCB in order to obtain the necessary voltage level to recharge the battery (4.2 V DC) and to switch on the microprocessor (at least 2.7 V DC);

Variation of the voltage level depending on the amount of elements dedicated to energization.

6.5.2.3 *In vitro* energization

Both TRANS and CU_base are now connected to their respective transducers, placed in the test bench. The battery and the microprocessor are connected, but not the receiver CU_RX. Aim of the measurement is to assess the minimum power to be supplied on CU so that its transducer is able to recharge the TR battery and that the microprocessor is switched on. To this aim, the supplied current will be read from the DC power supply.

In addition to these measurements, similar to those performed on TRANS alone, the influence of the alignment of the transducers on the ultrasonic transfer is estimated. Different positions, rotations and tilting of the TR are explored, and different sets of CU transducer elements are used in emission. As a starting position, the transducers are aligned by eye, at a distance of about 11 cm, which is the focal distance according to the characterization performed by the manufacturer.

6.5.2.4 Functional test of the CU receiver

Supplying a modulated electrical wave at the input, the correctness of the demodulation and the minimal/maximal amplitude of the carrier wave are evaluated. The RF_IN input of CU_RX is connected to the signal generator through a 2.5 MHz low pass filter stage. The RSSI wave and the demodulated logic signal are monitored on the oscilloscope. The RSSI level is also checked on a multimeter. It should not exceed 4 V DC, which would indicate a saturation of the demodulator circuit.

6.5.2.5 *In vitro* backscattering

Finally, the CU_RX can be connected to the rest of the setup and the whole energization-backscattering chain can be performed: the power generator feeds the CU_base with an electrical wave and the resulting backscattering signal received by the CU elements dedicated to reception is observed. Like for the energization tests, several positions, rotations and tilting of the TR, and different sets of CU emitting elements are explored. The TRANS elements dedicated to backscattering and those dedicated to energization are defined by the previous tests.

6.5.3 Results

The equipment used for the tests are the following:

- **Waveform generators**: TG4001, HP33120A
- **Modulated signal generator**: Agilent MGX N5181A
- **Power supplies**: ranging 20 V DC, 1 A
- **Oscilloscope**: Tektronix MSO4034
- **Spectrum analyzer**: Agilent E4402B

All measurements *in vitro* are performed using water as a conductive material, no phantom materials are inserted at this stage.

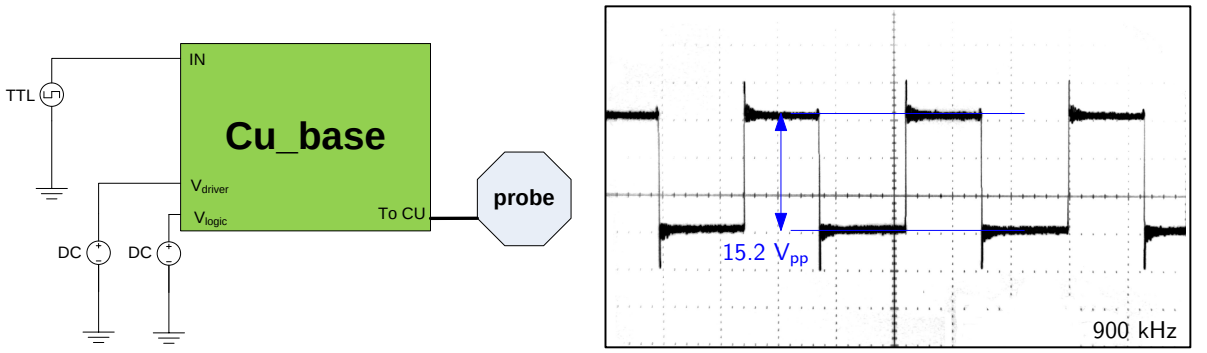

(a) Setup schematic.

(b) Signal emitted on connected CU elements when V_{driver} = 15V.

Figure 6.12: Functional test of CU_base.

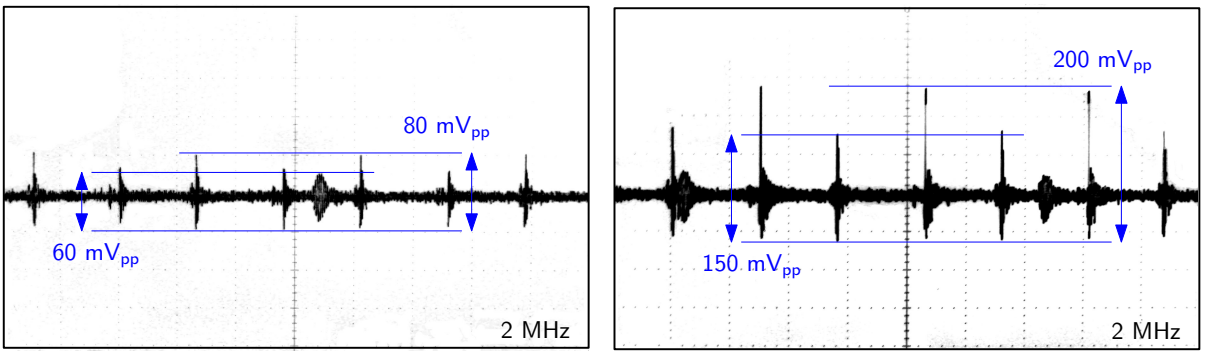

(a) Two adjacent elements are ON.

(b) Six adjacent elements are ON.

Figure 6.13: Crosstalk on CU element #4 dedicated to energization.

6.5.3.1 Functional test of the CU baseboard

At first, the energy transfer on the PCB, without the load of the transducer, is assessed. To this end, a square wave at 900 kHz, 3 V_{pp}, 1.5 V DC offset is applied on the PCB input IN. The level V_{logic} is fixed to 9 V DC and V_{driver} is swept between 0 and 15 V. The wave produced on the enabled transducer elements is, as expected, a square wave at 900 kHz, whose amplitude nicely follows V_{driver} as shown in Figure 6.12.

On the elements switched off, a 0 Volt signal can be observed, as foreseen, but also peaks at various frequencies. There is a clear correlation between the amplitude of the peaks and the state of the adjacent transducer elements. More elements emitting around the element under test result in higher peaks, as well visible in Figure 6.13.

Also on channels dedicated to reception (each 8^{th} element), a square wave at 900 kHz can be observed, which amplitude depends on the state of the other elements: when all elements are switched off, the wave is less than 60 mV_{pp}, while it is about 1.2 V_{pp} when seven energization elements on each side of the observed element are switched on (Figure 6.14).

It can be therefore concluded that a non negligible crosstalk occurs on the CU_base PCB, and that a signal is present on the receiving elements even when no element of the transducer is excited. This

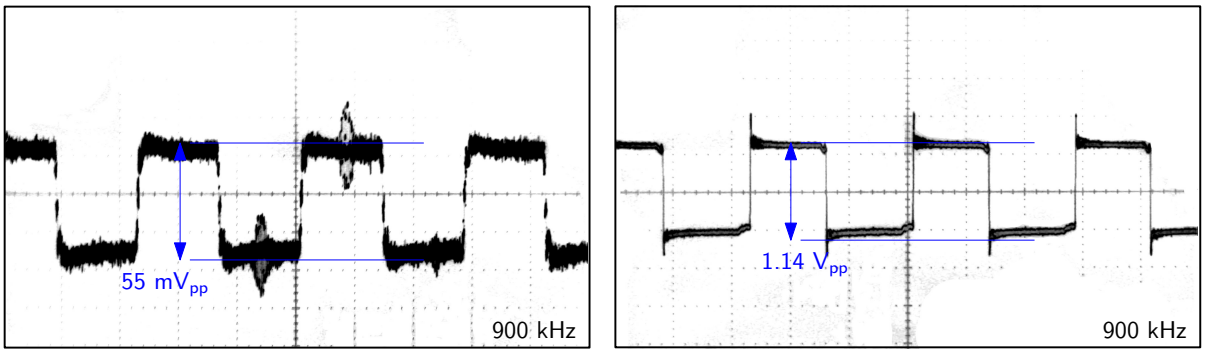

(a) All elements are OFF.

(b) Seven elements on each side of element 8 are switched ON.

Figure 6.14: Crosstalk on CU element #8 dedicated to backscattering.

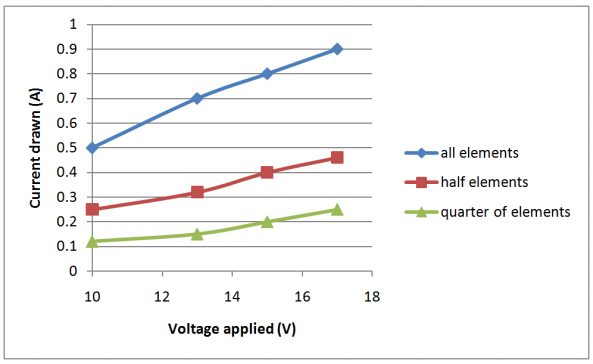

Figure 6.15: Linear increase in power consumed with respect to the amount of elements.

contributes to the saturation of the demodulator (in CU_RX) and should therefore be corrected. The crosstalk level slightly vary according to the position of the element observed: central elements show higher amplitude than side ones, which is very well explained by the quantity of adjacent elements.

In a second step, the transducer is plug to the circuit. Because of the current limitation at 1 A imposed by the commercial power supplies, a voltage of about 17 V DC on V_{driver} when driving all 56 elements cannot be exceeded. The higher the voltage applied, the higher the current drawn by the transducer, which acts like a resistance of about 20 Ω. Figure 6.15 shows the power consumption as a function of the voltage and of the number of elements driven. As expected, the increase is clearly linear. The power provided by V_{logic} is not relevant, due to the low power of the commercial components chosen.

6.5.3.2 Functional test of the TR baseboard

In order to assess the energy transfer inside the implant, a sinusoidal wave of amplitude V_{gen} at 1 MHz is applied through 1.2 kΩ on each input of TRANS and the resulting voltages in the circuit are monitored:

- $\mathbf{V_{in}}$: the amplitude of the electrical wave when connected to the TRANS PCB. A small voltage drop occurs due to the relatively low input impedance of the elements.
- $\mathbf{V_r}$: the rectified voltage, at the input of the regulator. It saturates at 20 V.

Table 6.2: Voltage levels on TRANS when supplying a sinusoidal wave at 1 MHz.

$\mathbf{V_{gen}}$ [V_{pp}]	$\mathbf{V_{in}}$ [V_{pp}]	$\mathbf{V_r}$ [V]	$\mathbf{V_{cc}}$ [V]	$\mathbf{V_{bat}}$ [V]
20	17	8.1	OK	OK
17	14.4	6.9	OK	OK
15	12.8	6.1	OK	OK
13	10.8	5.22	OK	OK
11	9.4	4.4	OK	OK

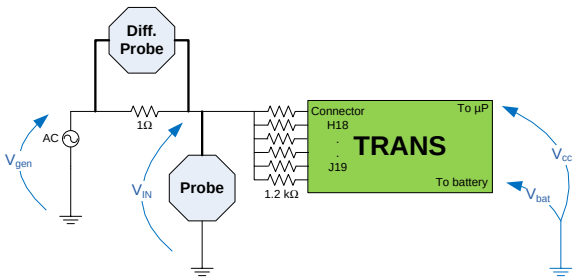

(a) Setup schematic.

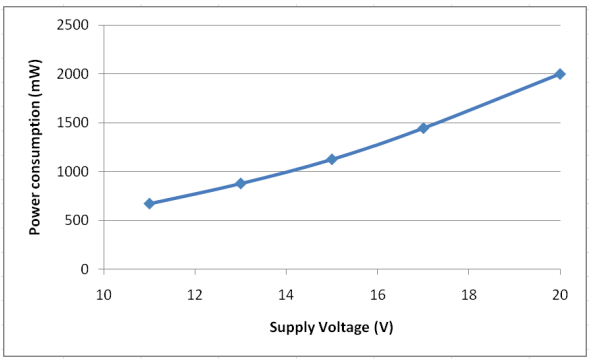

(b) Power consumption of TRANS, with 3 elements dedicated to energization.

Figure 6.16: Functional test of TRANS.

- $\mathbf{V_{cc}}$: the supply voltage for the microprocessor. It is regulated to 3.3 V.
- $\mathbf{V_{bat}}$:the voltage on the battery. It is regulated to 4.2 V.

Table 6.2 shows the different voltages. All measurements have been done without connecting the battery and the microprocessor.

Applying an input amplitude lower than 11 V does not allow obtaining enough rectified voltage to drive the device. Applying a square wave at the input, instead of a sinusoidal wave, gives of course a higher rectified voltage. In a further step, the input amplitude is fixed at 20 V_{pp} and the number of elements dedicated to energization is changed. The elements switched off for energization will be switched on for backscattering and vice-versa. Three TR adjacent elements are dedicated to reception (energization) and the other three are dedicated to emission (backscattering). The power consumed by the circuit in this configuration is shown in Figure 6.16. A part of this power is used to recharge the battery, that is to say it is stored in the device.

6.5.3.3 *In vitro* energization

Finally, TRANS and CU_base can be connected to their respective transducers, and the battery and the microprocessor can be plugged into the system. On the contrary, the receiver CU_RX is not connected. The TR is put in front of the CU and at an approximate distance $x_3 = 11$ cm. This is the focal distance according to the manufacturer datasheets. The transponder is then moved along the three Cartesian axis

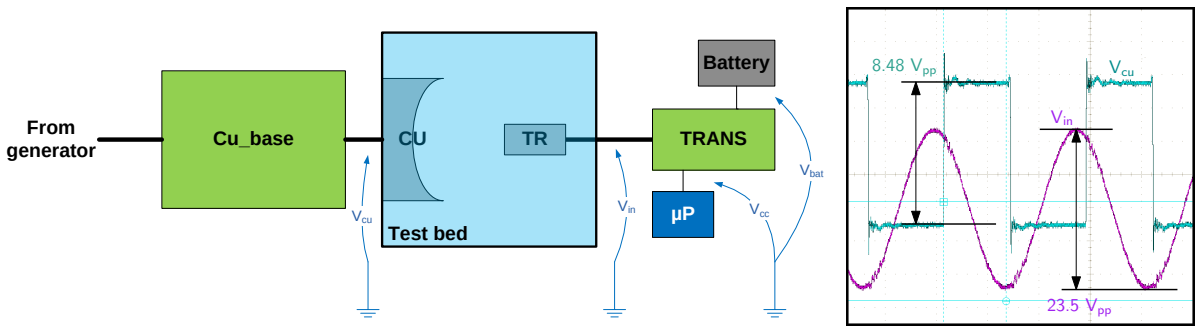

(a) Setup schematic.

(b) Best transfer experienced between CU and TR. Output wave on the CU (turquoise), Input wave on TRANS (violet).

Figure 6.17: *In vitro* energization.

and the rotation axis, in order to obtain the maximum of transfer. Providing $V_{driver} = 9\,\text{V}$ a rectified voltage $V_r > 20\,\text{V}$ was obtained, which is the saturation limit due to the Zener limiting diode in the LTC3588-1 rectifier chip. The supplied voltage must be reduced down to $V_{driver} = 8.5\,\text{V}$ to obtain $V_{IN} = 23.6\,\text{V}_{\text{pp}}$ and therefore $V_r = 19.2\,\text{V}$ (Figure 6.17). This is at a distance $x_3 = 11.2\,\text{cm}$.

6.5.3.4 Misalignment

From the optimal position previously found, on which the highest transfer is achieved, the TR is misaligned first along the x_2 axis (lateral misalignment), then along the propagation axis x_3. A constant CU emission is set, and the rectified voltage on TR is observed. According to the data shown in Figure 6.18, the system can accept a maximal displacement of 20 mm on the x_2 axis and still provide a sufficient transfer to power up the microprocessor. The red box indicates a condition in which no sufficient energy is transferred to achieve the good levels of V_{bat} and V_{cc}. The maximum distance between the transducers for which energy transfer can occur is about 11.15 cm, which is about 0.5 mm from the focal point. On the contrary, placing TR at a distance smaller than the focus always results in a sufficient transfer, because the TR will be in the acoustic beam.

Now, the influence of the amount of emitting elements is observed: the emission of some elements of the CU is disabled, starting from the most peripheral ones. As an effect, the beam will be less focused, i.e., the area of maximal intensity on the focal plan will be larger. A sufficient transfer is possible with as few as 14 elements over the 56 available, as shown on Figure 6.19.

6.5.3.5 Functional test of the CU receiver

Once the energization has been proved, the data communication can be assessed. The input signal is a square wave at 1 MHz modulated by 5 kHz at a modulation depth of 90%. The attenuation of the signal was changed and the resulting RSSI signal was monitored (Figure 6.20). Ideally, its AC part should be as high as possible, in order to be easily recognized by the data slicer, and its DC part should not exceed 4 V, the level of saturation of the CU_RX. According to the measurements shown in Table 6.3, a signal with a level up to −30 dBm can potentially be exploited. Higher amplitude than that will saturate the CU_RX. The minimum amplitude allowed for the signal depends on the demodulator stage.

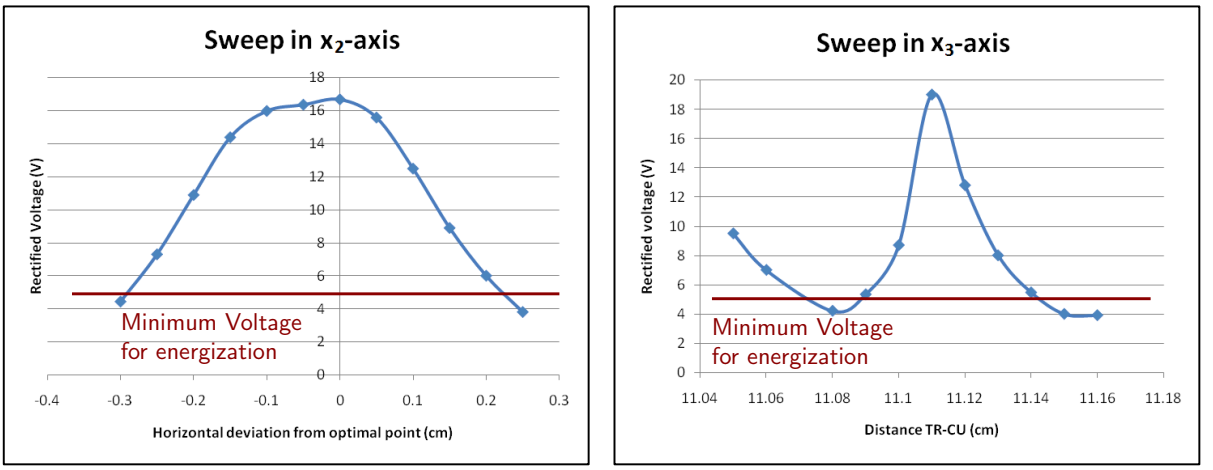

(a) Misalignment along lateral axis.

(b) Misalignment along propagation axis.

Figure 6.18: Displacement of TR from optimal point.

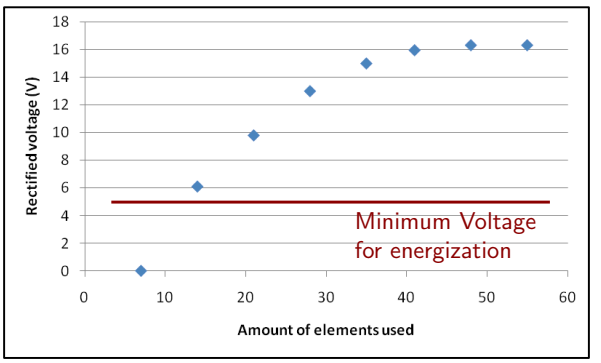

Figure 6.19: Effect of the amount of CU elements emitting on the rectified voltage in the TR.

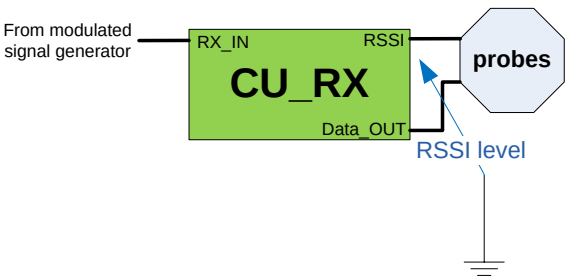

Figure 6.20: Setup schematics for the functional test of CU_RX.

Table 6.3: Efficiency of the CU_RX.

Attenuation [dBm]	**RSSI level AC** [mV_{pp}]	**RSSI level DC** [V]
-70	520	2.8
-60	900	3.13
-50	1080	3.53
-40	1080	4
-30	800	4.2
-25	560	4.34

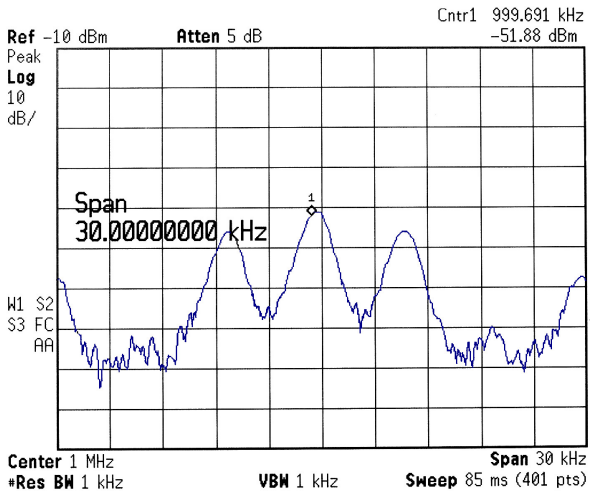

Figure 6.21: Modulated signal at the output of CU_RX.

6.5.3.6 *In vitro* backscattering

The circuit CU_RX can finally be connected to the system tested for the energization test and the backscattering can be assessed.

The excitation applied on the CU is exactly the same used for energization assessment: the TTL signal on CU_base is a square wave at 900 kHz (3 V_{pp}, 1.5 V offset), V_{driver} = 8.5 V, V_{logic} = 9 V. All CU elements are used and the reception of the backscattered wave is enabled only on the middle receiving element (PZ_32). The signal generator drives the backscattering switches with a modulated signal at 5 kHz superposed with a subcarrier at 100 kHz. The incident wave on CU_RX (RF_IN, connector P1) is visualized on the spectrum analyzer.

The signal delivered on the input of CU_RX is shown in Figure 6.21: it has a component at the combined frequency of carrier and subcarrier f_{C+SC} = 1 MHz and two side bands at ±5 kHz. The modulation depth is very high: the difference between the amplitude of the carrier and the amplitude of the modulation signal is only 4 dBm. The signal amplitude (−50 dBm) is acceptable.

6.5.3.7 Misalignment

The displacement along x_2 is repeated and the selection of different amounts of emitting CU elements. The amplitude of both the carrier and its side bands (modulated signal) are monitored on the spectrum

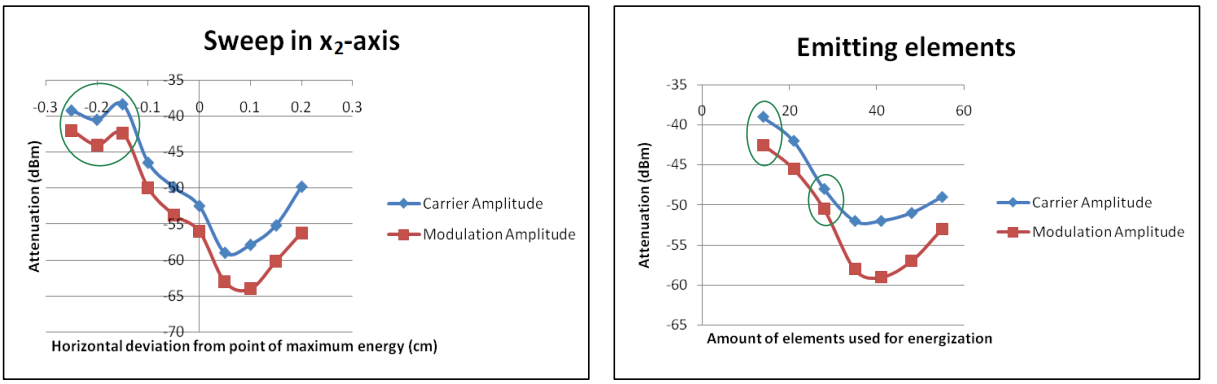

(a) Misalignment along x_2 axis.

(b) Variation of amount of CU elements emitting.

Figure 6.22: Effect of side displacement on data communication.

analyzer. Ideally, both the attenuation and the difference between the two amplitudes should be as small as possible (high RSSI level, high modulation depth). Figure 6.22 shows the effect of a side displacement and of the amount of elements used for emission from CU_base. Green circles indicate the best results concerning communication.

6.6 Final electronics

6.6.1 Electronics description

An improved circuit for the TR has been designed and manufactured, based on preliminary tests *in vitro*. Major advantages are a better charge and discharge management of the local battery, an integrated and stable backscattering technique and a shape adapted to the Kinetra® casing.

On CU side, two major improvements have been performed, namely the Data Slicer and the GUI. Also, the power levels provided by the driver can be adjusted.

Figure 6.23 shows the final CU board and the final TR electronics in the biocompatible casing. The connections between the PCB and the feedthroughs are not performed.

The TR baseboard is composed of different blocs.

Thin film battery: two 0.4 mAh batteries, manufactured by Infinite Power Solutions (IPS).
FRAM: a ferro-electric non-volatile memory (e.g., FM25V10, 128 kB, manufactured by Ramtron).
Transducer modulator: Two backscattering switch ADG719 from Analog Devices Inc. (Norwood, MA, USA), performing dual modulation with a 100 kHz subcarrier.
Voltage multiplier: in order to increase the voltage level coming from the transducer elements, and to overcome the threshold at the input of the battery recharge circuit, a voltage tripler was developed, which needs a minimum input amplitude of 650 mV_{pp} to work (corresponding to two Schottky diode drops). The correct behavior of the stage was verified by simulation: a V_{ac} input level of 1.7 V_p is successfully rectified into a 5.6 V DC V_{trip}.
MAX17710 chip: the power management of the battery occurs through this chip, which was custom designed by Maxim Integrated (San Jose, CA, USA) for the IPS battery chosen. It replaces a big part of the energy harvesting circuit previously designed. It contains an on-chip voltage boost converter, which

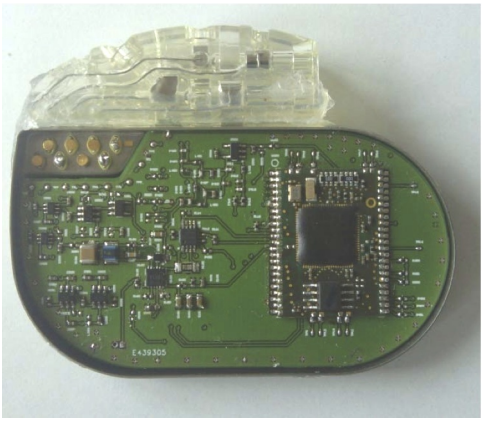

(a) TR electronics in the Kinetra® casing. Microprocessor submodule on the right.

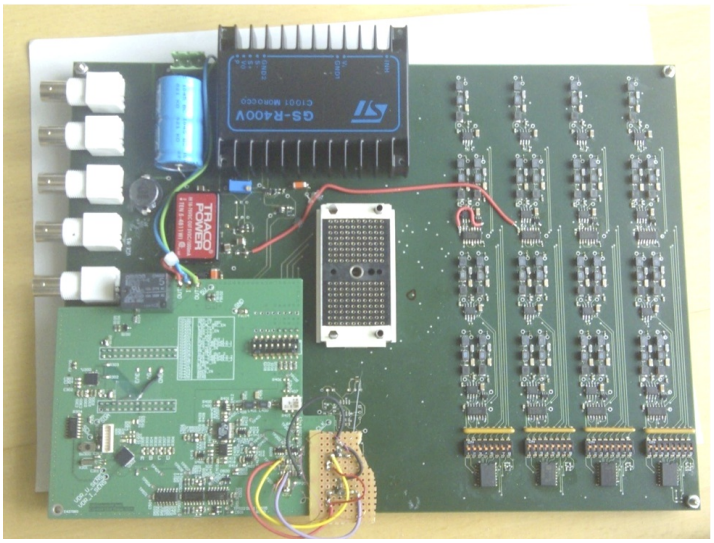

(b) CU electronics.

Figure 6.23: Final CU and TR electronics. Not at scale.

will be used after the tripler. It allows a better management of the recharge of the battery, the control the power consumption of the electronics, and the protection of the battery from deep discharge.

Two submodules complete the baseboard: an **Icycom daughter board**, containing the microprocessor, and an **ADC submodule**, designed to host the custom ADC, which converts the data collected by the sensor leads. The ADC submodule was designed and manufactured, but not yet integrated in the PCB. As no data can be sensed in real time, the Icycom submodule continuously sends a fixed hexadecimal message, i.e., “ABBA DADA ADDA”.

An oscilloscope powered by USB on a laptop is exploited (Picoscope® by Pico Technologies, Cambridgeshire, UK), in order to insulate the system from the AC power line, thus avoiding parasitic signals.

Wires give access to AC signals from 2 transducer channels (backscattering and communication), regulated voltage for Icycom (3.3 V nominal), and V_{chg} voltage (output of voltage booster circuit, input to battery charger).

On CU side, the **Data Slicer** circuit converts the received analog backscattered signal into a tidy square signal representing the signal series of bits. Four threshold levels are programmed, which identify the minimum high level (Lo+), the maximum high level (Hi+), and the minimum and maximum low levels (Lo- and Hi-, respectively). A “peak-to-peak” input signal is interpreted based on the crossing of those levels. The output gets high when the input crosses the Hi+ threshold upwards, and it gets low when the input crosses the Lo- threshold downwards.

In the current application, the thresholds are set on the peak signal amplitude, the top threshold is set at 96%, and the bottom threshold is set at 89%. This ensures good decoding.

6.6.2 Tests performed

With this latest version of TR and CU electronics, both the energy transfer from the CU to the TR and the data transmission from TR to CU are tested. The first assessment is performed in the test bench, then in a surgical facility, in conditions close to real implantation in humans.

6.6.2.1 *In vitro* test

The developed electronics board, containing a power management and a backscattering circuitry, is inserted into the casing and connected to the TR transducer. Among the six transducer elements, one is used for energy harvesting (acoustic wave from CU to TR) and another for backscattering (reflection of the wave from TR to CU). The 14 central elements of a flat, 32-elements transducer are used for emission from the CU, using a carrier at 900 kHz. Pulses of an electrical power equal to 82 mW are injected on each element, for a total 1.15 W electrical power emitted. Given the efficiency of the transducer (58%), it results in 0.67 W acoustic power emitted. Under those conditions, according to the Rayleigh propagation model , the incoming power on the Transponder is equal to 0.64 W, which is 1.8 W/cm^2. Being the CU emission duty cycle 5%, this corresponds to about 0.1 W/cm^2 in average. The tests are performed in a custom testbed, described by Mazzili, Peisino *et al.* [63]. Energization and communication are performed both in water and through the custom phantom material, whose attenuation has been assessed by pulse echo acquisition to be close to the attenuation of a body soft tissue [63].

To avoid ground loops and parasites on the transmission, an oscilloscope powered by USB and connected to a portable PC is used.

6.6.2.2 *In vivo* test

The same casing and the same TR electronics are used for *in vivo* assessment. Tests are performed at the University Hospital of Oslo on a Norwegian pig of about 35 kg. The test underwent usual ethical approval according to the regulation.

An incision is first done in the abdomen (*laparotomy*), the excitation transducer is applied on the abdominal skin, and the Kinetra® is placed at subcutaneous distance (about 1 cm), medium distance (3-5 cm), and longer distances (10 cm).

During the operation, the surgeon tries to keep as much parallelism and alignment as possible between the planes of the two transducers.

In a second step, the demonstrator is placed inside the rib cage (thoracotomy) and the transmission trough the ribs is tested. In this case, the communication and recharging distance is limited to a couple of centimeters. Acoustic gel is copiously used in the cavity to ensure the best possible acoustical contact with the demonstrator.

For the energization assessment, the Control Unit presents the same configuration as for *in vitro* tests: the central 14 channels are used and a pulsed power of 1.8 W on a 5% duty cycle is sent. On TR side, one element is dedicated to reception and energization, and another to backscattering communication.

For the communication assessment, continuous emission from the CU is used, injecting approximately the same amount on average power as in the pulsed case.

In order to protect the CU from over-heating, all the tests are done using acoustic gel, and excitation is always cut before lifting the transducer from the skin. Displacement between two locations is done by sliding the CU, leaving as much as possible the transducer in contact with the skin.

Figure 6.24 visualizes the setup used for the *in vivo* tests and the manual placement of the transducers at a distance of about 4 cm.

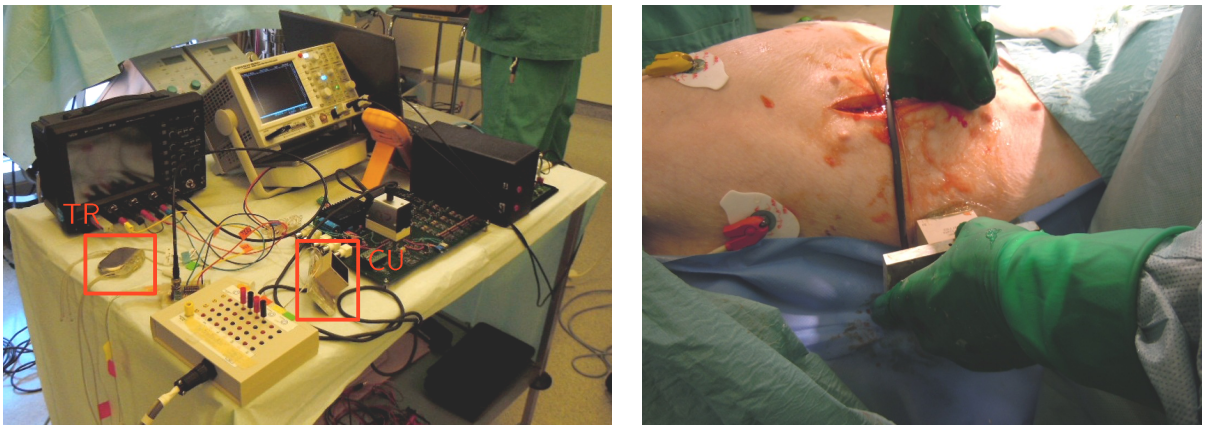

(a) Setup.

(b) Test at ~4 cm.

Figure 6.24: *In vivo* test of the final demonstrator.

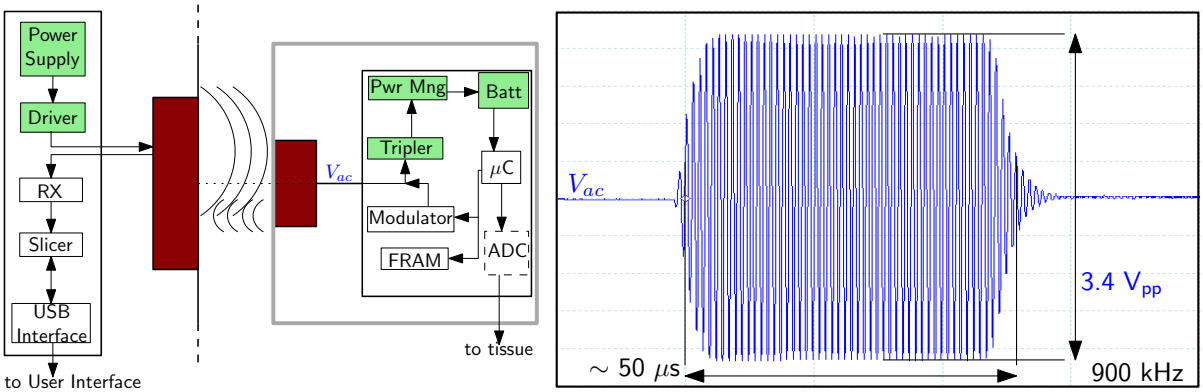

(a) Setup schematic.

(b) Signals obtained.

Figure 6.25: Acoustic pulse received on transducer element.

6.6.3 Results

Using the optimal casing thickness previously determined by simulation (100 µm), the system is assembled and tested *in vitro*. As a first test, the peak response of the system is evaluated, by emitting in burst mode at 5% duty cycle. The TR is placed at about 11 cm distance in water, and the signal received on a single transducer element is monitored. The incoming power intensity is approximately 0.1 W/cm^2. Emitting with the 14 central elements of the CU in pulse mode, a maximum amplitude of 3.4 V_{pp} at about 11 cm (Figure 6.25) can be obtained.

Emitting with two more elements shows no noticeable effect.

For the next tests, continuous mode is always used. The relatively small amplitude received is treated by the voltage multiplier and fed into the booster stage of the battery recharge regulator chip (MAX17710). As expected by simulations, the voltage multiplier proves to be able to rectify the amplitude V_{ac} = 3.4 V_{pp} into a 5.6 V DC level (named V_{trip}), which has previously proven to be sufficient to recharge the battery. Figure 6.26 shows the incoming signal V_{ac} and the rectified voltage V_{trip}.

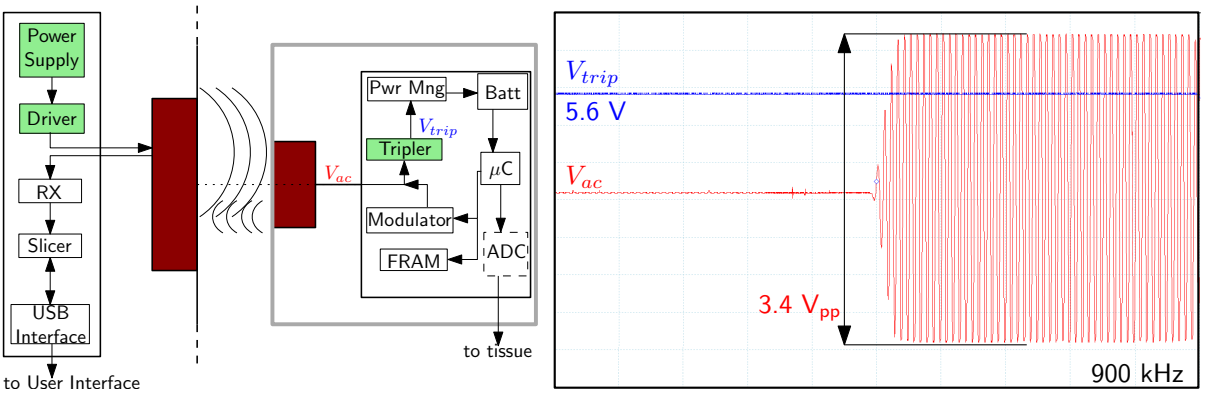

(a) Setup schematic.

(b) Signals obtained.

Figure 6.26: Treatment of the incoming voltage V_{ac} (red) into a DC level V_{trip} (blue).

As a result, current is periodically drawn from the regulator chip and used to recharge the battery. Figure 6.27 shows the behavior of the booster stage when collecting V_{ac} from only piezo element 1, piezo 1 and 2, or piezo 1 to 5. Corresponding to each voltage drop (red) on the buffer capacitor on the booster input, there's current (blue) flowing into the battery and recharging it. The period between peaks depends on the power provided by the transducer elements, while the duration of the peak depends on the battery state only, and the current level injected is fixed. For this reason, continuous mode of CU emission is more efficient than pulse mode, because it allows more frequent peaks, thus quicker recharge of the battery. It can be noticed that using more elements in reception does not necessarily improve the recharge time. In the example shown, using both element 1 and 2 is beneficial, but using elements 1 to 5 is not. This basically depends on the differences between power levels on the elements used.

The energy stored in the battery can be then used to produce a fixed message and accordingly modulate the acoustic wave backscattered to the CU.

Figure 6.28 presents the digital message (blue) produced by the microcontroller and driving the backscattering switch, and the actual backscattered signal (red) as seen on the TR transducer elements. The amplitude of the "high" bit is about 700 $\mathrm{mV_{pp}}$, while the amplitude of the "low" bit is 50 $\mathrm{mV_{pp}}$.

The message is sent through the phantom material developed by INSERM, and the wave on the CU transducer is monitored.

Figure 6.29 shows the message as received on the CU, at different stages of the demodulation. Important to notice are: the turquoise signal, which is the analog signal arriving on the CU transducer elements, and the corresponding green digital signal, fully demodulated by the CU circuit.

The same device assessed *in vitro* is used for *in vivo* tests. The TR is placed at different locations in the pig's body and transmission from and to the CU is assessed. Figure 6.30 shows the incoming acoustic signal V_{ac} (blue) and the voltage V_{chg} at the input of the battery charger (red). Whenever V_{chg} exceeds 4.1 V, its level drops again shortly after.

The backscattered signal is observed on the CU transducers and is shown in Figure 6.31. The amplitude of the "high" bit is about 500 $\mathrm{mV_{pp}}$ and the "low" bit is about 450 $\mathrm{mV_{pp}}$.

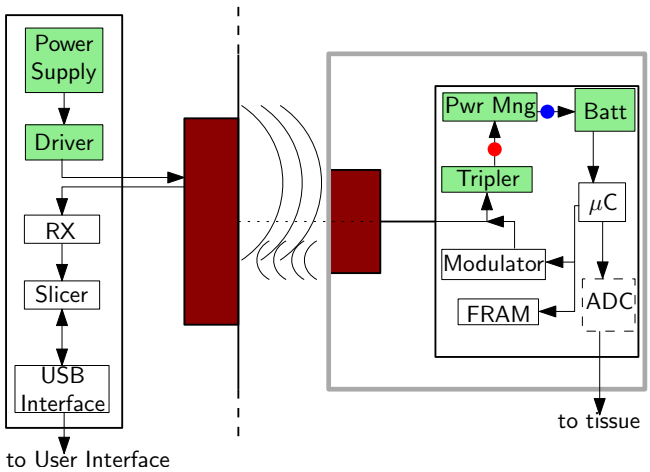

(a) Setup schematic.

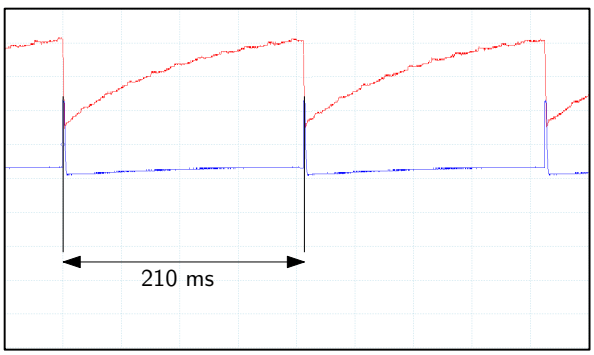

(b) Effect of element 1.

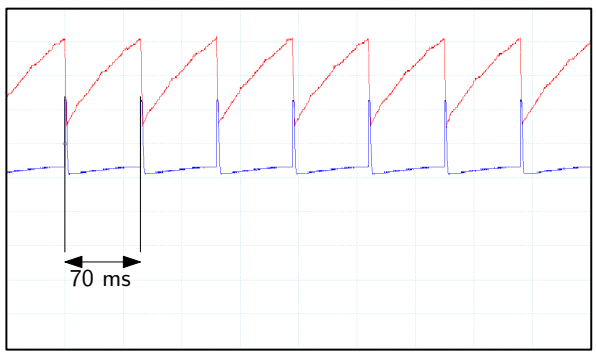

(c) Effect of elements 1 and 2.

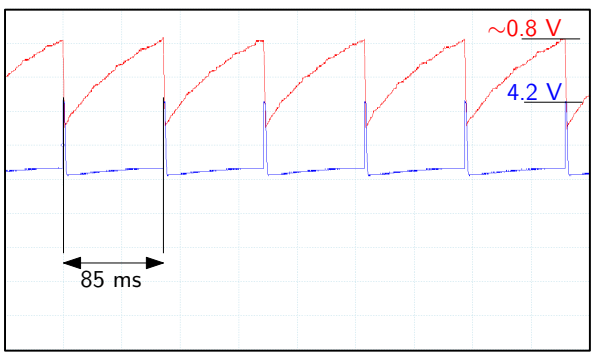

(d) Effect of elements 1 to 5.

Figure 6.27: Battery charging using different sets of piezoelectric elements. Voltage drop on the buffer capacitor on the booster input (red); current flowing into the battery (blue).

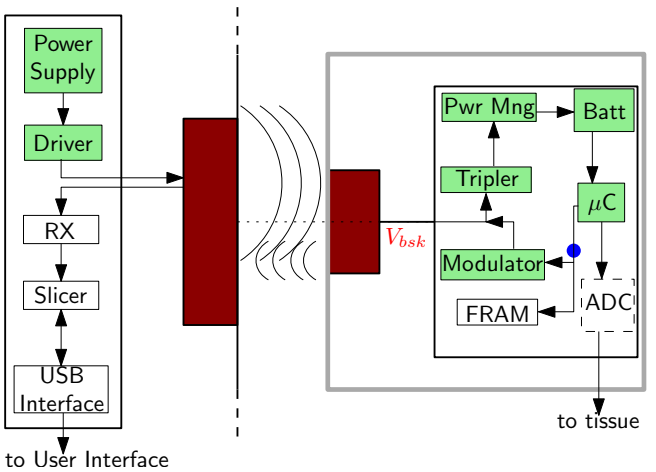

(a) Setup schematic.

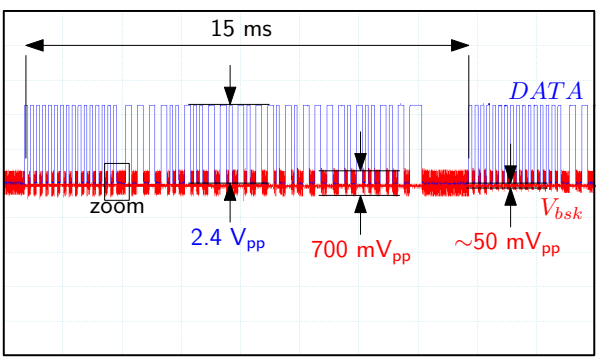

(b) Message produced by the microcontroller (DATA) and sent by backscattering (V_{bsk})

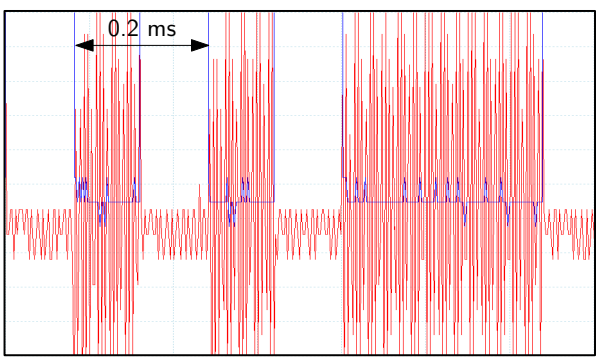

(c) Zoom.

Figure 6.28: Backscattering of a fixed message created by the microcontroller. The analog signal V_{bsk} is observed on one transducer element dedicated to backscattering.

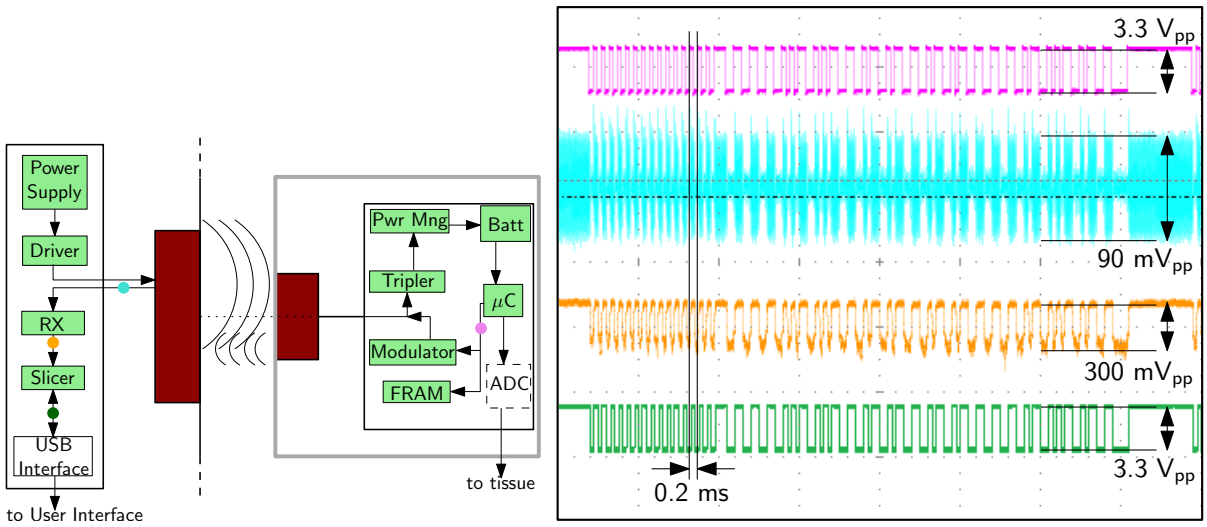

(a) Setup schematic. (b) Signals obtained.

Figure 6.29: Backscattering and demodulation of a message (violet) through a custom phantom material. Incoming wave (turquoise), level recognition (orange), resulting digital signal (green).

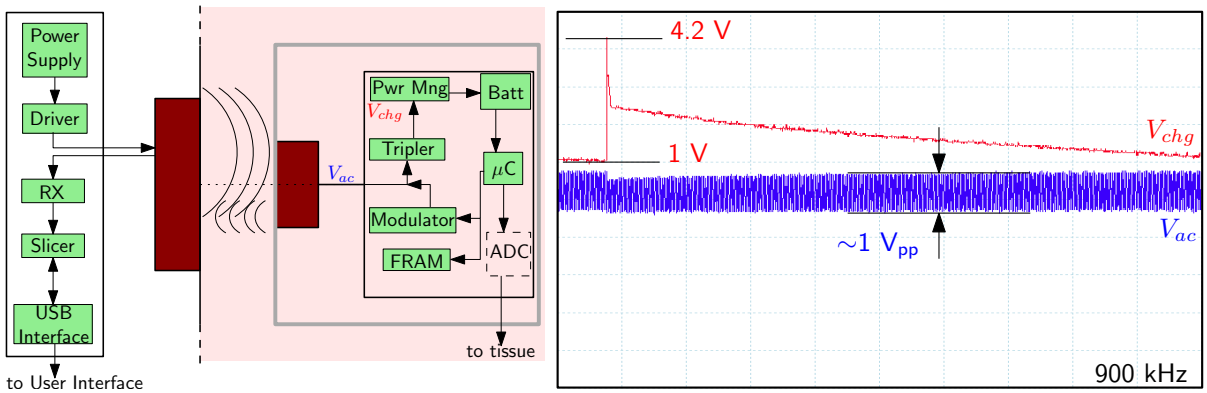

(a) Setup schematic. (b) Signals obtained.

Figure 6.30: Energy harvesting *in vivo* at subcutaneous distance. During V_{chg} peaks (red) the battery is recharged. The corresponding acoustic signal V_{ac} (blue) is also shown.

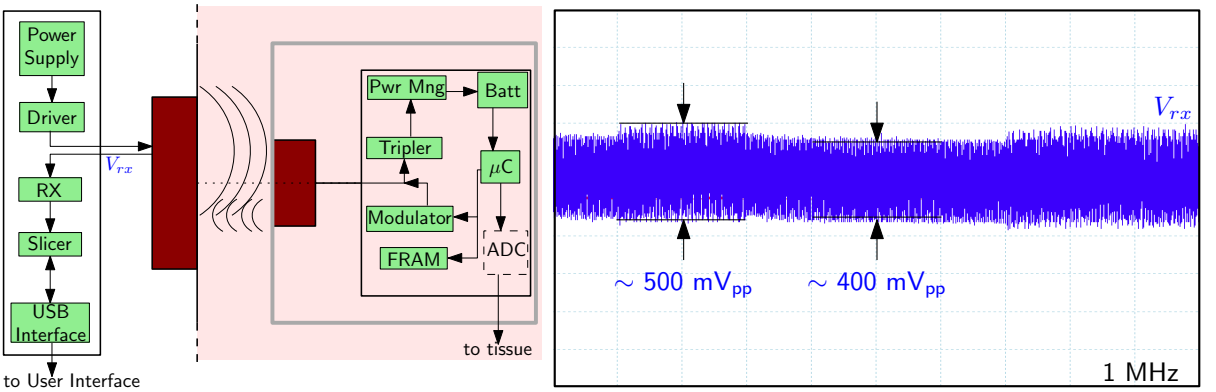

(a) Setup schematic.

(b) Signals obtained.

Figure 6.31: Backscattered acoustic signal from subcutaneous implant, to be demodulated by the CU. The signal is modulated in amplitude.

6.7 Discussion

After refinement of the system electronics, and assessment of the system through *in vitro* and *in vivo* tests, the suitability of the manufactured system can be evaluated.

In particular, it is interesting to assess if energization of TR is possible within the FDA limits, and if energization and communication can be efficiently performed *in vivo*.

6.7.1 Energization simulation and *in vitro* assessment

The energy received by the TR, which is well below the limit of 720 mW/cm^2, proved sufficient to start the battery recharge, to switch on the microprocessor, and thus allow communication between the TR and the CU by backscattering.

It has to be noted that the battery is recharged only during the small periods in which current is drawn from the V_{chg} signal at the input of the booster stage of the power management.

The demodulation strategy on CU is efficient for the backscattered message type received, both in water and through an attenuating phantom.

6.7.2 *In vivo* energization and communication

Energization and communication were tested *in vivo* at about 1 cm, 4 cm, and 10 cm (deep implantation).

From Figure 6.30 it can be seen that the voltage V_{chg} on the buffer cyclically rises to 4.1 V and drops: the battery is indeed absorbing energy in order to recharge.

Energization could be assessed up to 4 cm, while bigger distances resulted in insufficient amplitude of V_{ac}. Good communication between TR and CU was obtained at 1 cm (Figure 6.31).

6.8 Conclusion

The system manufactured and tested within the ULTRAsponder project proved the concept of an energy and data transfer based on ultrasound.

Successful *in vivo* operation could be only assessed in subcutaneous range. This is not sufficient for the applications addressed in the ULTRAsponder project. One of the key reasons for using ultrasound as a carrier was its ability to reach deeply IMDs. Based on the current state of tests, the feasibility of a system based on ultrasonic energy and data transfer cannot be proven.

Longer distances could be achievable sending more energy, up to the FDA limit. To this end, a *more powerful CU transducer* has already been manufactured within the project, but unfortunately not exploited for the tests due to a lack of resources. The electric power delivered by the CU could be automatically adjusted according to a *feedback on the acoustic intensity received* on the TR, in order to send the maximum acoustic power allowed. From the perspective of better power management, the impedance of the TR electronics can be further matched to the transducers, and the microprocessor use can be optimized.

Outlook for the proposed system would include the *integration of the heart impedance sensor* into the implant, in order to address a real application and test the real readings.

Also, the TR electronics must be *miniaturized* and fitted in a custom casing, much smaller than the Kinetra®. In order to do this, a flexible PCB support could be necessary.

From an industrial point of view, the *robustness* of the system needs to be increased, in order to handle real-life conditions.

7 Conclusions

This thesis work describes the contribution of the author to the development of a new generation of Implanted Medical Devices, which addresses a certain amount of technological challenges present in today commercial devices. IMDs are very promising tools for further development of minimally invasive medicine. They allow conceiving new applications and performing therapies better adapted to the patient's needs.

Despite intensive research and development in the field during the last few decades, current IMDs suffer from limitations concerning their size and their interaction with the external world. Several technical challenges still need to be overcome towards a new generation of IMDs.

Within the European FP7 project ULTRAsponder, a generic IMD platform and its external CU were developed, manufactured, and tested. The target implant identified is a trade-off among small size, long-term autonomous operation, and deep implantation capability. Particular focus is put on the device compatibility with MRI procedures and external electromagnetic wave sources (e.g., mobile phones and medical equipment). This generic device can be combined with several sensors and actuators, making it a precious tool for a multitude of applications. The longer-term vision is a BSN, in which several implanted nodes are devoted to different sensing/actuation tasks and a central CU manages the operations. The nodes should work autonomously, but wirelessly connect to the CU on a regular basis for recharging and in order to exchange data.

The main novelties proposed by the project are the exploitation of ultrasonic waves as a carrier for both energy and data transfer, and exploitation of backscattering technique for data communication. The ultrasonic carrier allows reaching deeply implanted devices, outperforming techniques based on electromagnetic waves in case of small transducers with respect to the implantation depth. Moreover, ultrasound is intrinsically compatible with MRI and does not suffer from interference with external radiators. The backscattering method reduces to the minimum the needed power consumption to transmit data from the TR to the CU, because the sent data travels on a carrier generated by the CU, where power consumption is not critical. Also, the proposed system is aimed to be industrially exploited. Therefore, it must comply with current regulation and standards in the medical domain. An important constraint on the proposed device is the exploitation of titanium for the casing: titanium keeps indeed its place as the most suited material for IMD housing, due to its excellent characteristics and biocompatibility.

The contribution of the author to the device design covers different domains. It includes:

- Choice and assessment of components and technologies adapted to the target device: MRI compatible, long-life FRAM memory devices; ultra-thin, long-life, all-solid-state battery, with an integrated power management unit (Chapter 5).
- Development of SPI communication among the microprocessor, the ADC device, and the FRAM memory device (Chapter 5).
- Development of the firmware for the microprocessor on TR side: managing the power received by the CU, creating the message to be sent and driving the TR electronics.
- Design of a testbed for the *in vitro* assessment of the demonstrator (Chapter 6).

- Modeling of the reception of an acoustic power on the receiving transducer, its propagation through the different layers of the transducer sandwich and its translation into electrical power. Assessment of the influence of the titanium casing on the ultrasonic transmission. Simulation of different thicknesses of the titanium layers, and for different geometrical configurations of the transducer. Definition of a suitable titanium thickness for acceptable transmission (Chapter 4).

- Choice of a micro-machining strategy (laser ablation) for the local thinning of the titanium casing, design of the region to be thinned down (Chapter 5).

Together with the design of custom ADC device, microprocessor, transducers, and electronics, which were performed by other consortium members within the project, the author's work led to demonstrators of the intended system. A working frequency of 1 MHz was chosen, because the wavelength in the *mm* range is advantageous for beam shaping, and the relatively high frequency minimizes the biological effects.

Simulations of the titanium barrier and *in vitro* verification showed that ultrasonic transmission through a titanium barrier of 100 µm is feasible.

Tests *in vitro* and *in vivo* have been performed and proved the ability of the system to transfer energy to an implant placed up to 4 cm into soft tissues and to establish data communication with subcutaneous implants. Longer distances may be achievable by sending more energy from the CU, up to the FDA limit.

As an *outlook*, the system manufactured could be optimized in several ways: the electrical impedance of the *TR electronics could be better matched to the transducer*, thus improving the power transfer; better power management could be obtained by optimizing the *use of the microprocessor*; finally, both the TR and the CU should be made more *robust*, and the TR must be *miniaturized*. To this end, a flexible PCB support might be necessary.

The designed ADC and sensor device, which were absent from the demonstrator, should be integrated in the system, in order to substitute the fixed message to send with real sensing data. This would allow assessment of the system on a real application and *tests on some real readings*.

On the theoretical level, the acoustic power transfer between the CU and the TR should be better estimated by simulations and assessed, in order to *refine the CU emission settings*. The electric power delivered by the CU could be even automatically adjusted according to a *feedback on the acoustic intensity* received on the TR, in order to provide at any time the maximum energy allowed by the regulation.

With a refined system, *chronic* in vivo *assessment* could be performed.

Although the absence of a sensor in the implant, and despite the limited spatial range in which the demonstrators proved efficient, the concept of the target system could be proven: energy and data transfer based on ultrasound can be exploited to implement a deep IMD. In particular, an important result emerges from the simplified simulations presented in this thesis work: titanium encapsulation can coexist with ultrasonic propagation, given an appropriate coupling with the piezoelectric element, an appropriate design of the piezocomposite, and a locally thinned layer of titanium. This opens the way to a new generation of long-term biocompatible IMD, based on ultrasonic power transfer and communication.

Bibliography

[1] Food and Drug Administration, "Information for manufacturers seeking marketing clearance of diagnostic ultrasound systems and transducers," *US Food and drug administration, Silver Spring, Md*, 2008. [Online]. Available: http://www.gpo.gov/fdsys/pkg/FR-1997-06-13/pdf/97-15452.pdf

[2] *ASTM F2475 - 11 Standard Guide for Biocompatibility Evaluation of Medical Device Packaging Materials*, American Society for Testing and Materials, 2011.

[3] H. Azhari, *Basics of biomedical ultrasounds for engineers*, IEEE, Ed. John Wiley & sons, INC., 2010.

[4] B. Bannon and E. E. Mild, "Titanium alloys for biomaterial application: An overview," *ASTM Standards and Engineering Digital Library*, January 1983. [Online]. Available: http://65.209.24.102/DOWNLOAD/STP28931S.1102465-1.pdf

[5] F. Barreras and O. Jimenez, "RF coupled, implantable medical device with rechargeable back-up power source." US Patent RE42 682E, 2011. [Online]. Available: http://www.google.com/patents/US5733313

[6] S. P. Beeby, M. J. Tudor, and N. M. White, "Energy harvesting vibration sources for microsystems applications," *Measurement Science and Technology*, vol. 17, pp. 175–195, October 2006. [Online]. Available: http://iopscience.iop.org/0957-0233/17/12/R01/

[7] P. D. Bianco, P. Ducheyne, and J. M. Cuckler, "Determination of in vivo titanium release from a non-articulating commercially pure titanium implant," *ASTM Standards and Engineering Digital Library*, January 1996.

[8] W. G. Bigelow, J. C. Callaghan, and J. A. Hopps, "General hypothermia for experimental intracardiac surgery," *Annals of Surgery*, pp. 531 – 537, September 1950. [Online]. Available: http://www.ncbi.nlm.nih.gov/pmc/articles/PMC1616776/pdf/annsurg01396-0215.pdf

[9] T. C. Bischoff, "Reduction of infection associated with medical device," EU Patent EP2 144 640B1, 2012.

[10] ——, "Element for implantation with medical device," US Patent US8 092 443B2, 2012.

[11] R. C. Bourge, W. T. Abraham, P. B. Adamson, M. F. Aaron, J. M. Aranda Jr, A. Magalski, M. R. Zile, A. L. Smith, F. W. Smart, M. A. O'Shaughnessy, M. L. Jessup, B. Sparks, D. L. Naftel, and L. Warner Stevenson, "Randomized controlled trial of an implantable continuous hemodynamic monitor in patients with advanced heart failure: The COMPASS-HF study," *Journal of the American College of Cardiology*, vol. 51, no. 11, pp. 1073 – 1079, 2008. [Online]. Available: http://www.sciencedirect.com/science/article/pii/S0735109708001356

[12] F. Braunschweig, C. Linde, M. Eriksson, C. Hofman-Bang, and L. Rydén, "Continuous haemodynamic monitoring during withdrawal of diuretics in patients with congestive heart failure," *European Heart Journal*, vol. 23, no. 1, pp. 59–69, 2002. [Online]. Available: http://eurheartj.oxfordjournals.org/content/23/1/59.abstract

[13] H. Brisby, H. Ashley, and A. D. Diwan, "In vivo measurement of facet joint nitric oxide in patients with chronic low back pain," *The Spine Journal*, vol. 32, no. 14, 2007. [Online]. Available: http://journals.lww.com/spinejournal/Fulltext/2007/06150/In_Vivo_Measurement_of_Facet_Joint_Nitric_Oxide_in.5.aspx

[14] R. G. Bryant, "Process for preparing a tough, soluble, aromatic, thermoplastic copolymide," US Patent 5 639 85, 1997.

[15] A. L. Bui and G. C. Fonarow, "Home monitoring for heart failure management," *Journal of the American College of Cardiology*, vol. 59, no. 2, pp. 97–104, 2012. [Online]. Available: http://dx.doi.org/10.1016/j.jacc.2011.09.044

[16] Canadian Heritage Information Network. (2001). [Online]. Available: http://www.museevirtuel-virtualmuseum.ca/edu/ViewLoitDa.do?method=preview&lang=EN&id=4093

[17] D. Cassereau and M. Fink, "Time-reversal of ultrasonic fields. III. theory of the closed time-reversal cavity," *IEEE Transactions on Ultrasonics, Ferroelectrics and Frequency Control*, vol. 39, no. 5, pp. 579–592, September 1992.

[18] *Icycom: A 1V ISM-band RF SoC with integrated DSP for demanding portable applications*, Centre Suisse d'Electronique et Microtechnique SA. [Online]. Available: http://csem.ch/docs/show.aspx/12228/docname/icycom.pdf

[19] S. Chung-Yang and T. Nan-Chyuan, "Human powered MEMS-based energy harvest devices," *Applied Energy*, vol. 93, pp. 390 – 403, 2012. [Online]. Available: http://www.sciencedirect.com/science/article/pii/S0306261911008336

[20] B. Cotté, C. Lafon, J. Chapelon, and C. Dehollain, "Suitable acoustic paths to transfer energy in depth using ultrasound," in *Engineering in Medicine and Biology Society (EMBC) Proceedings*, 2010.

[21] D. Dalecki, "Mechanical bioeffects of ultrasounds," *Annual Review in Biomedical Engineering*, vol. 6, 2004.

[22] A. Denisov and E. Yeatman, "Ultrasonic vs. inductive power delivery for miniature biomedical implants," in *2010 International Conference on Body Sensor Networks*, Department of Electrical and Electronic Engineering. IEEE, 2010. [Online]. Available: http://ieeexplore.ieee.org/xpl/articleDetails.jsp?arnumber=5504736

[23] T. Denning, K. Fu, and T. Kohno, "Absence makes the heart grow fonder: new directions for implantable medical device security," in *Proceedings of the 3rd conference on Hot topics in security*. Berkeley, CA, USA: USENIX Association, 2008, pp. 1–7. [Online]. Available: http://dl.acm.org/citation.cfm?id=1496671.1496676

[24] M. Deterre, E. Lefeuvre, and E. Dufour-Gergam, "An active piezoelectric energy extraction method for pressure energy harvesting," in *Smart Materials and Structures*, vol. 21, no. 8, 2012. [Online]. Available: http://iopscience.iop.org/0964-1726/21/8/085004/

[25] E. Doron and A. Penner, "Acoustic biosensor for monitoring physiological conditions in a body implantation site," US Patent US 6 486 588 B2, 2002.

[26] ——, "Implantable medical device with integrated acoustic transducer," US Patent US 2010/0 004 718 A1, 2009.

[27] C. T. Dotter and M. P. Judkins, "Transluminal treatment of arteriosclerotic obstruction: Description of a new technic and a preliminary report of its application," *Circulation*, vol. 30, pp. 654 – 670, 1964. [Online]. Available: http://circ.ahajournals.org/content/30/5/654

[28] F. A. Duck, *Physical Properties of Tissue: A Comprehensive Reference Book*. Academic Press, 1990.

[29] P. Dumas, J. Poguet, and G. Fleury, "Piezocomposite technology: an innovative approach to the improvement of n.d.t. performance using ultrasounds," in *8th ECNDT*, 2002.

[30] H. Ector and P. Vardas, "Current use of pacemakers, implantable cardioverter defibrillators, and resynchronization devices: data from the registry of the European Heart Rhythm Association," in *European Heart Journal Supplements*, E. S. of Cardiology, Ed., 2007. [Online]. Available: http://eurheartjsupp.oxfordjournals.org/content/9/suppl_I/I44

[31] C. Eingartner, "Current trends in total hip arthroplasty," *Ortopedia, traumatologia, rehabilitacja*, vol. 9, no. 1, pp. 8–14, Jan-Feb 2007.

[32] European Commission, "Council directive of 20 june 1990 on the approximation of the laws of the member states relating to active implantable medical devices," June 1990.

[33] *ETSI EN 301 839-1*, European Telecommunications Standards Institute, 2007. [Online]. Available: http://www.etsi.org/deliver/etsi_en/301800_301899/30183901/01.03.01_60/en_30183901v010301p.pdf

[34] Federal Communications Commission, *47 CFR 95.601-95.673 Subpart E*, 1999. [Online]. Available: http://wireless.fcc.gov/services/index.htm?job=operations&id=medical_implant

[35] K. W. Ferrara, M. A. Borden, and H. Zhang, "Lipid-shelled vehicles: engineering for ultrasound molecular imaging and drug delivery," *Accounts of Chemical Research*, vol. 42, no. 7, pp. 881–92, July 2009.

[36] M. Fink, "Time reversal of ultrasonic fields. I. basic principles," *IEEE Transactions on Ultrasonics, Ferroelectrics and Frequency Control*, vol. 39, no. 5, pp. 555–566, September 1992.

[37] G. Fleury and C. Gondard, "Improvements of ultrasonic inspections through the use of piezo-composite transducers," in *6th European Conference on Non Destructive Testings*, 1994.

[38] P. A. Floor, I. Balasingham, T. Ramstad, E. Meurville, and M. Peisino, "Compression schemes for in-body and on-body UWB sensor networks," in *3rd International Symposium on Applied Sciences in Biomedical and Communication Technologies (ISABEL)*, 2010.

[39] S. Fruitsmaak. (2007, October). [Online]. Available: http://commons.wikimedia.org/wiki/File:St_Jude_Medical_pacemaker_with_ruler.jpg

[40] C. Gabriel and S. Gabriel, *Compilation of the Dielectric Properties of Body Tissues at RF and Microwave Frequencies*. King's College, London, Department of Physics, 1996.

[41] Goodfellow Sàrl. Titanium (Ti) material information. [Online]. Available: http://www.goodfellow.com/E/Titanium.html

[42] J. Grevious and T. Kallmyer, "Universal recharging of an implantable medical device," US Patent WO 2010/047 983 A2, 2010.

[43] D. Halperin, T. S. Heydt-Benjamin, K. Fu, T. Kohno, and W. H. Maisel, "Security and privacy for implantable medical devices," *IEEE Pervasive Computing*, vol. 7, no. 1, pp. 30–39, January 2008. [Online]. Available: http://dx.doi.org/10.1109/MPRV.2008.16

[44] International Agency for Research on Cancer, "IARC monographs on the evaluation of carcinogenic risks to humans," World Health Organization, Tech. Rep., 2012.

[45] *Technical and operating parameters and spectrum use for short-range radiocommunication devices*, International Telecommunication Union. [Online]. Available: www.itu.int/pub/R-REP-SM.2153-2-2011

[46] A. Iribarne, R. Easterwood, E. Y. H. Chan, J. Yang, L. Soni, M. J. Russo, C. R. Smith, and A. M., "The golden age of minimally invasive cardiothoracic surgery: current and future perspectives." *Future Cardiol*, vol. 7, no. 3, pp. 333–346, May 2011.

[47] J. Jimenez, G. Echarri, J. Kast, E. Riekels, and E. Schommer, "Method of charging an implantable medical device," US Patent 8 170 681B2, 2012.

[48] S. Jo, M. Kim, M. Kim, and Y. Kim, "Flexible thermoelectric generator for human body heat energy harvesting," *Electronics Letters*, vol. 48, no. 16, pp. 1013 –1015, February 2012. [Online]. Available: http://ieeexplore.ieee.org/stamp/stamp.jsp?tp=&arnumber=6260067

[49] M. Karamanoglu, M. McGoon, R. P. Frantz, R. L. Benza, R. C. Bourge, R. J. Barst, B. Kjellström, and T. D. Bennett, "Right ventricular pressure waveform and wave reflection analysis in patients with pulmonary arterial hypertension," *CHEST Journal*, vol. 132, no. 1, pp. 37–43, 2007. [Online]. Available: +http://dx.doi.org/10.1378/chest.06-2690

[50] S. Kelly, P. Doyle, A. Priplata, O. Mendoza, and J. Wyatt, "Optimal primary coil size for wireless power telemetry to medical implants," in *Applied Sciences in Biomedical and Communication Technologies (ISABEL), 2010 3rd International Symposium on*, November 2010, pp. 1 –5.

[51] R. Kleinerman, T. B. Whang, R. L. Bard, and E. S. Marmur, "Ultrasound in dermatology: Principles and applications," *Journal of the American Academy of Dermatology*, vol. 67, no. 3, pp. 478–87, September 2012. [Online]. Available: http://dx.doi.org/10.1016/j.jaad.2011.12.016

[52] W. Kong, J. Huang, D. L. Rollins, R. E. Ideker, and W. M. Smith, "A fully implantable multi-channel biotelemetry system for measurement of blood flow and temperature: a first evaluation in the green sturgeon," *Hydrobiologia*, 2008. [Online]. Available: http://dx.doi.org/10.1007/s10750-008-9578-7

[53] G. Kotzar, M. Freas, P. Abel, A. Fleischman, S. Roy, C. Zorman, M. Moran, and J. Melzak, "Evaluation of MEMS materials of construction for implantable medical devices," *Biomaterials*, 2002.

[54] P. Kovacs and J. A. Davidson, "Chemical and electrochemical aspects of the biocompatibility of titanium and its alloys," *ASTM Standards and Engineering Digital Library*, Januar 1996.

[55] R. Krimholtz, D. A. Leedom, and G. L. Mattaei, "New equivalent circuits for elementary piezoelectric transducer," *Electronics Letters*, vol. 6, 1970.

[56] L. T. Kuhn, "Chapter 5 - biomaterials," in *Introduction to Biomedical Engineering (Third Edition)*, 3rd ed. Boston: Academic Press, 2012, pp. 219 – 271. [Online]. Available: http://www.sciencedirect.com/science/article/pii/B9780123749796000058

[57] N. Lee and S. Vasudevan, "Spinal cord stimulation use in patients with failed back surgery syndrome," *Pain Management*, vol. 2, no. 2, pp. 135–140, March 2012. [Online]. Available: http://dx.doi.org/10.2217/pmt.12.3

[58] B. Li, J. Grevious, T. Davis, L. Perz, and C. Paidosh, "Titanium housing for implantable medical device," EU Patent EP 2 117 619B1, 2008.

[59] B. Linke, "Sterilization methods and impact on electronics in medical devices," *EE Times*, 2011. [Online]. Available: http://www.eetimes.com/design/medical-design/4217655/Sterilization-methods-and-impact-on-electronics-in-medical-devices-

[60] M. Long and H. Rack, "Titanium alloys in total joint replacement—a materials science perspective," *Biomaterials*, vol. 19, no. 18, pp. 1621 – 1639, 1998. [Online]. Available: http://www.sciencedirect.com/science/article/pii/S0142961297001464

[61] T. Martinez, "Calcul de l'impédance électrique d'un transducteur électro mécanique à l'aide du modèle KLM (simulation 1D)," 2009, internal document within ULTRAsponder project collaboration.

[62] L. Mateu, C. Codrea, N. Lucas, M. Pollak, and P. Spies, "Human body energy harvesting thermogenerator for sensing applications," in *Sensor Technologies and Applications, 2007. SensorComm 2007. International Conference on*, October 2007, pp. 366 –372. [Online]. Available: http://ieeexplore.ieee.org/xpl/articleDetails.jsp?arnumber=4394949

[63] F. Mazzilli, M. Peisino, R. Mitouassiwou, B. Cotté, P. Thoppay, C. Lafon, P. Favre, E. Meurville, and C. Dehollain, "In-vitro platform to study ultrasound as source for wireless energy transfer and communication for implanted medical devices," in *Engineering in Medicine and Biology Society (EMBC), 2010 Annual International Conference of the IEEE*, September 2010, pp. 3751 –3754.

[64] J. A. McWilliam, "Electrical stimulation of the heart in man," *British Medical Journal*, February 1889.

[65] Medtronic Inc. [Online]. Available: http://www-test.medtronic.eu/your-health/parkinsons-disease/device/our-dbs-therapy-products/kinetra/index.htm

[66] MEMS and Nanotechnology Exchange. Material: Lead zirconate titanate (PZT). [Online]. Available: http://www.memsnet.org/material/leadzirconatetitanatepzt/

[67] C. Ming Li, H. Dong, X. Cao, J. H. T Luong, and X. Zhang, "Implantable electrochemical sensors for biomedical and clinical applications: Progress, problems, and future possibilities." *Current Medicinal Chemistry*, vol. 14, no. 8, pp. 937–951, 2007.

[68] P. Mitcheson, E. Yeatman, G. Rao, A. Holmes, and T. Green, "Energy harvesting from human and machine motion for wireless electronic devices," *Proceedings of the IEEE*, vol. 96, no. 9, pp. 1457–1486, September 2008. [Online]. Available: http://ieeexplore.ieee.org/stamp/stamp.jsp?tp=&arnumber=4618735

[69] Å. Ohlsson, S. Kubo, D. Steinhaus, D. Connelly, S. Adler, C. Bitkover, R. Nordlander, L. Rydén, and T. Bennett, "Continuous ambulatory monitoring of absolute right ventricular pressure and mixed venous oxygen saturation in patients with heart failure using an implantable haemodynamic monitor: results of a 1 year multicentre feasibility study," *European Heart Journal*, vol. 22, no. 11, pp. 942–954, 2001. [Online]. Available: http://eurheartj.oxfordjournals.org/content/22/11/942.abstract

[70] J. J. Pacella and A. R. Carson, "Sonic boon: ultrasound enhances angiogenic cell therapy," *Cardiovasc Res*, vol. 95, no. 4, pp. 401–2, September 2012. [Online]. Available: http://dx.doi.org/10.1093/cvr/cvs244

[71] D. Panescu, "Emerging technologies: Wireless communication systems for implantable medical devices," *Engineering in Medicine and Biology Magazine, IEEE*, vol. 27, no. 2, pp. 96–101, March-April 2008.

[72] T. G. Papaioannou, N. Stergiopulos, and C. Stefanadis, "Bioengineering and clinical perspectives in diagnostic and therapeutic applications of microbubbles," *Current Pharmaceutical Design*, vol. 18, no. 15, pp. 2113 – 2114, 2012.

[73] M. Patel, *Medical Sterilization Methods*, Lemo USA, Inc., December 2003. [Online]. Available: http://www.digikey.com/Web%20Export/Supplier%20Content/lemo-1124/pdf/lemo-rf-medical-steril.pdf?redirected=1

[74] A. Penner, "Method of implanting wireless device within an anatomical cavity during a surgical procedure," US Patent 0 274 565 A1, 2007.

[75] A. Penner and E. Doron, "Apparatus and method using acoustic telemetry for intrabody communications," US Patent US7 198 603B2, 2007.

[76] ——, "Implantable medical device with integrated acoustic transducer," EU Patent EP2 289 392 B1, 2012.

[77] ——, "Acoustic switch and apparatus and methods for using acoustic switches within a body," UN Patent WO/2002/032 502, 2003.

[78] Y. Porat, A. Penner, and E. Doron, "Implantable acoustic bio-sensing system and method," US Patent US6 432 050B1, 2002.

[79] Y. Porat, Y. Tsaliah, and E. Doron, "Piezoelectric transducer," US Patent US6 504 286B1, 2003.

[80] S. Ramakrishna, J. Mayer, E. Wintermantel, and K. W. Leong, "Biomedical applications of polymer-composite materials: a review," *Composites Science and Technology*, vol. 61, no. 9, pp. 1189 – 1224, 2001. [Online]. Available: http://www.sciencedirect.com/science/article/pii/S0266353800002414

[81] *F-RAM Technology Brief*, Ramtron International. [Online]. Available: http://www.ramtron.com/files/tech_papers/Ferro_Tech_Brief.pdf

[82] R. A. M. Receveur, F. W. Lindemans, and N. F. de Rooij, "Microsystem technologies for implantable applications," *Journal of Micromechanics and Microengineering*, vol. 17, no. 5, May 2007.

[83] J. Ritzema-Carter, D. Smyth, R. Troughton, I. Crozier, I. Melton, A. Richards, N. Eigler, J. Whiting, S. Kar, H. Krum, and W. Abraham, "Images in cardiovascular medicine. dynamic myocardial ischemia caused by circumflex artery stenosis detected by a new implantable left atrial pressure monitoring device." *Circulation*, vol. 113, no. 15, pp. e705–6, April 2006. [Online]. Available: http://europepmc.org/abstract/MED/16618824

[84] T. N. Robinson and G. V. Stiegmann, "Minimally invasive surgery," *Endoscopy*, vol. 36, no. 1, pp. 48–51, January 2004. [Online]. Available: http://europepmc.org/abstract/MED/14722855

[85] F. J. O. Rodrigues, J. H. Correia, and P. M. Mendes, "Modeling of a neural electrode with MEMS magnetic sensor for telemetry at low frequencies," in *MicroMechanics Europe 2009*, 2009.

[86] M. G. L. Roes, J. L. Duarte, M. A. M. Hendrix, and E. A. Lomonova, "Acoustic energy and transfer: A review," in *IEEE Transactions on industrial electronics*, IEEE, Ed., vol. 60, no. 1. IEEE, 2013, pp. 242 – 248.

[87] P. Ronan. [Online]. Available: http://fr.wikipedia.org/wiki/Fichier:EM_spectrum.svg

[88] Sanpaz. (2009, August). [Online]. Available: http://en.wikipedia.org/wiki/File:2D_geometric_strain.svg

[89] A. Schmeling, W. Phillips, D. Olson, and O. Jimenez, "External power source, charger and system for an implantable medical device having thermal caracteristics and method therefore," UN Patent WO/2005/039 698, 2005.

[90] T. Schmitz-Rode, U. Schnakenberg, J. G. Pfeffer, W. Piroth, G. vom Bögel, W. Mokwa, and R. W. Günther, "Vascular capsule for telemetric monitoring of blood pressure," *Fortschritte auf dem Gebiete der Röntgenstrahlen und der Nuklearmedizin*, vol. 175, no. 02, pp. 282–286, 2003. [Online]. Available: http://dx.doi.org/10.1055/s-2003-37232

[91] J. H. Schulman, "The feasible FES system: Battery powered BION stimulator," *Proceedings of the IEEE*, vol. 96, no. 7, pp. 1226 –1239, July 2008.

[92] D. Séverac, D. Manic, M. Morgan, C. Henzelin, and E. Le Roux, *Flexible Power Management in the icycom System-On-Chip*, Centre Suisse d'Electronique et Microtechnique SA, 2009. [Online]. Available: http://csem.ch/docs/show.aspx/12648/docname/CSEM-STR09-Page%2029.pdf

[93] O. Sigmund, S. Torquato, and I. A. Aksay, "On the design of 1–3 piezocomposites using topology optimization," *Journal of Materials Research*, vol. 13, pp. 1038–1048, March 1998. [Online]. Available: http://dx.doi.org/10.1557/JMR.1998.0145

[94] J. Smith and J. Henderson, "FDA regulation of implantable sensors: Demonstrating safety and effectiveness for marketing in the u.s." *Sensors Journal, IEEE*, vol. 8, no. 1, pp. 52 –56, January 2008. [Online]. Available: http://ieeexplore.ieee.org/stamp/stamp.jsp?tp=&arnumber=4418373

[95] N. Smith and P. Zhong, "Stone comminution correlates with the average peak pressure incident on a stone during shock wave lithotripsy," *Journal of Biomechanics*, 2012.

[96] O. Soykan, "Power sources for implantable medical devices," *Medical Device Manufacturing & Technology*, pp. 76–79, 2002. [Online]. Available: http://www.touchgroupplc.com/pdf/753/mdev02_p_soykan.pdf

[97] R. Spencer, "Novel methods for the prevention of infection of intravascular devices," *Journal of Hospital Infection*, vol. 43, Supplement 1, no. 0, pp. S127 – S135, 1999, the 4th International Conference of the Hospital Infection Society. [Online]. Available: http://dx.doi.org/10.1016/S0195-6701(99)90075-0

[98] V. Spitzer, M. J. Ackerman, A. L. Scherzinger, and D. Whitlock, "The visible human male: A technical report," *Journal of the American Medical Informatics Association*, vol. 3, pp. 118 – 130, 1996.

[99] W. Stallings, *Data and computer communications (5th ed.)*. Upper Saddle River, NJ, USA: Prentice-Hall, Inc., 1997.

[100] J. Stern, E. K. Heist, L. Murray, C. Alabiad, J. Chung, M. H. Picard, M. J. Semigran, J. N. Ruskin, and J. P. Singh, "Elevated estimated pulmonary artery systolic pressure is associated with an adverse clinical outcome in patients receiving cardiac resynchronization therapy," *Pacing and Clinical Electrophysiology*, vol. 30, no. 5, pp. 603–607, 2007. [Online]. Available: http://dx.doi.org/10.1111/j.1540-8159.2007.00719.x

[101] S. Stoebe, A. Tarr, T. Trache, J.-G. Kluge, D. Pfeiffer, and A. Hagendorff, "Systematic evaluation of current possibilities to determine left ventricular volumes by echocardiography in patients after myocardial infarction," *Open Journal of Medical Imaging*, no. 2, pp. 68–75, June 2012. [Online]. Available: http://www.scirp.org/Journal/PaperDownload.aspx?FileName=OJMI20120200008_48977857.pdf&paperID=19697

[102] *MSP430F551x, MSP430F552x Mixed Signal Microcontroller*, Texas Instruments Inc. [Online]. Available: http://www.ti.com/lit/ds/slas590j/slas590j.pdf

[103] F. Thorey, F. Witte, J. Nellesen, N. Griep-Raming, H. Menzel, G. Gross, A. Hoffmann, J. Seufert, and H. Windhagen, "Improved osseointegration of titanium implants after surface coating with polymers in a rabbit model," *Orthopaede*, vol. 34, no. 11, pp. 1112–1117, November 2005. [Online]. Available: http://dx.doi.org/10.1007/s00132-005-0852-3

[104] B. C. H. Tsui and S. Suresh, "Ultrasound imaging for regional anesthesia in infants, children, and adolescents," *Anesthesiology*, 2010.

[105] M. Turina. (2009, April). [Online]. Available: http://commons.wikimedia.org/wiki/File:First_pacemaker_%28Siemens-Elema_1958%29.jpg

[106] R. Valdez, "Detecting undiagnosed type 2 diabetes: Family history as a risk factor and screening tool," *Journal of Diabetes Science and Technology*, vol. 3, pp. 722 – 726, July 2009.

[107] S. Venkatraman, F. Boey, and L. L. Lao, "Implanted cardiovascular polymers: Natural, synthetic and bio-inspired," *Progress in Polymer Science*, vol. 33, no. 9, pp. 853 – 874, 2008. [Online]. Available: http://www.sciencedirect.com/science/article/pii/S0079670008000543

[108] W. H. Vieira, K. A. Aguiar, K. Moreira da Silva, P. Miranda Canela, F. Santos da Silva, and B. J. Abreu, "Overview of ultrasound usage trends in orthopedic and sports physiotheraphy," *Critical Ultrasound Journal*, vol. 4, no. 1, 2012.

[109] T. Walther, V. Falk, and F. W. Mohr, "Minimally invasive surgery for valve disease," *Current Problems in Cardiology*, vol. 31, no. 6, pp. 399 – 437, 2006. [Online]. Available: http://www.sciencedirect.com/science/article/pii/S0146280606000156

[110] Q. Wang, M. Maillard, U. Schibler, M. Burnier, and F. Gachon, "Cardiac hypertrophy, low blood pressure, and low aldosterone levels in mice devoid of the three circadian par bzip transcription factors dbp, hlf, and tef," *American Journal of Physiology - Regulatory, Integrative and Comparative Physiology*, vol. 299, no. 4, pp. 1013–1019, October 2010. [Online]. Available: http://ajpregu.physiology.org/content/299/4/R1013.short

[111] Q. Wang, H. R. Brunner, and M. Burnier, "Determination of cardiac contractility in awake unsedated mice with a fluid-filled catheter," *American Journal of Physiology - Heart and Circulatory Physiology*, vol. 286, no. 2, pp. 806–814, February 2004. [Online]. Available: http://ajpheart.physiology.org/content/286/2/H806.short

[112] J. Weiland and M. Humayun, "Visual prosthesis," in *Proceedings of the IEEE*. IEEE, 2008.

[113] B. S. Wilson, C. C. Finley, D. T. Lawson, R. D. Wolford, D. K. Eddington, and W. M. Rabinowitz, "Better speech recognition with cochlear implants," *Nature*, vol. 352, no. 6332, pp. 236–238, July 1991. [Online]. Available: http://dx.doi.org/10.1038/352236a0

[114] F. Wu, J.-L. Thomas, and M. Fink, "Time reversal of ultrasonic fields. II. experimental results," *IEEE Transactions on Ultrasonics, Ferroelectrics and Frequency Control*, vol. 39, no. 5, pp. 567–578, September 1992.

[115] T. Yamada, T. Uezono, K. Okada, K. Masu, A. Oki, and Y. Horike, "RF attenuation characteristics for in vivo wireless healthcare chip," *Japanese Journal of Applied Physics*, vol. 44, 2005.

[116] G.-Z. Yang, *Body Sensor Networks*, G.-Z. Yang, Ed. Springer, 2006.

[117] D. C. Yates, A. S. Holmes, and A. J. Burdett, "Optimal transmission frequency for ultralow-power short-range radio links," *IEEE Transactions on circuits and systems*, vol. 51, no. 7, pp. 1405 – 1413, July 2004.

[118] Y. Zhou, F. H. Cocks, G. M. Preminger, and P. Zhong, "The effect of treatment strategy on stone comminution efficiency in shock wave lithotripsy," *The Journal of Urology*, 2004.

[119] J. Zhu, "Optimization of matching layer design for medical ultrasonic transducer," Ph.D. dissertation, Pennsylvania State University, August 2008.

Curriculum Vitæ

Michela PEISINO

Address:	Route du Simplon 14, CH-1094 Paudex
Mobile:	+41 (0)78 873 64 19
Email:	michela.peisino@epfl.ch
Date/place of birth:	1983 in Moncalieri, Italy
Citizenship:	Italian citizenship, Swiss B permit
Personal status:	Single

Education

10/2008–04/2013 (expected) **Ph.D. degree in Manufacturing Systems and Robotics**,
Laboratoire de Production Microtechnique, École Polytechnique Fédérale de Lausanne (EPFL), Lausanne, Switzerland.

Research on deep implanted, long term, autonomous body sensor nodes, energized by ultrasound. Assessment of titanium influence on the acoustic transfer. Design and integration of the demonstrator; Identification of biocompatible, efficient commercial components for demonstrator manufacturing.
Collaboration in the project ULTRAsponder (www.ultrasponder.org) with several industries at European level.

02/2007–08/2007 **"Projet de Fin d'Etudes"** (Master's thesis),
Laboratoire de Microsystèmes 4 (LMIS4), École Polytechnique Fédérale de Lausanne (EPFL), Lausanne, Switzerland. *"Blood pressure sensor for mice."*

Development of a demonstrator of a miniaturized sensor for continuous heart pressure monitoring in mice.

09/2005–08/2007 **"Diplôme d'Ingénieur"** (Master of Science MSc.)
in Micro and Nanotechnologies, *Ecole Nationale Supérieure d'Electronique et de Radioélectricité de Grenoble (ENSERG)*, Grenoble, France.

Tri-national program among Italy (Politecnico di Torino), France (INP Grenoble), and Switzerland (EPFL), with semesters in each location. Main courses in Micro and Nanotechnologies, microelectronics, microsystems.

09/2002–07/2005 **"Laurea"** (Bachelor of Science BSc.)
in "Ingegneria dell'Informazione Franco-Italiana", *Politecnico di Torino*,Turin, Italy.

Bi-national program between Italy (Politecnico di Torino) and France (INP Grenoble), with semesters in each location. Special emphasis on semiconductor technology, integrated circuits, sensors, and microsystem technology.

Work Experience

Fall 2007–Spring 2008 **Internship**,
European Commission, Future and Emerging Technologies (FET), Bruxelles, Belgium.

Assessment of EC funding impact on research centers in Europe by direct survey among research entities. This experience gave me both insight in EC structure and funding process, and an overview on long-term research in Europe.

Summer 2006 **Internship**,
Institut für angewandte Nano- und Optische Technologien (iNano), Hochschule Niederrhein, Krefeld, Germany.

Organization of a grey-room facility for Scanning Electron Microscopy; Development of Fresnel microlenses. I had the opportunity to practically use nano patterning in not optimal conditions.

Language and technical skills

Italian: mother tongue; Proficient in **German**, **French**, and **English** (European level C1).
Computer competences: Macintosh, Windows and Unix environments; Good command of MS Office and OpenOffice; Good knowledge of C and LaTeX; Average knowledge of Java and Visual Basic.
Average knowledge of **engineering and CAD tools**: MATLAB, LabVIEW, Visio, Solidworks, IPE.

Extracurricular activities and soft skills

I have a good ability to **perform in teams**. In particular, I was involved in organizing **social events and representing** Ph.D. students as a member of the **executive board of the EPFL Association of Research Scientists and Lecturers (ACIDE)**, from 2009 to 2013.
I am a well-organized, **analytic** person, with good ability in **leadership and communication**.
Several experiences abroad, starting with an **Exchange year** in Germany during high school, made me **independent** and **open-minded**.
I enjoy exercising my **creativity**, mostly by painting and reading. I am very enthusiastic about **travel and culture**, which has led me to learn constructed language **Esperanto**.
Recent discovery of **Scuba diving** has allowed me to develop my ability to **deal with stress**.

Publications

1. P. A. Floor, I. Balasingham, T. Ramstad, E. Meurville, and **M. Peisino**. *Compression Schemes for In-body and On-body UWB Sensor Networks*. 3rd International Symposium on Applied Sciences in Biomedical and Communication Technologies (ISABEL) , Rome, 2010.

2. F. Mazzilli, **M. Peisino**, R. Mitouassiwou, B. Cotté and P. Thoppay Egambaram et al. *In-Vitro Platform to study Ultrasound as Source for Wireless Energy Transfer and Communication for Implanted Medical Devices*. 32nd Annual International Conference of the IEEE Engineering in Medicine and Biology Society, Buenos Aires, 2010.